HYDROTHERMAL SYNTHESIS AND CHARACTERIZATION OF ETHYLENEDIAMINE-CONTAINING MOLYBDENUM OXIDES

A Thesis Submitted to
the Graduate School of Engineering and Sciences of
İzmir Institute of Technology
in Partial Fulfillment of the Requirements for the Degree of

MASTER OF SCIENCE

in Chemistry

by
Özgül GÜN

June 2006
İZMİR

We approve the thesis of **Özgül GÜN**

Date of Signature

……. **19 June 2006**
Assist. Prof. Dr. Mehtap EANES
Supervisor
Department of Chemistry
İzmir Institute of Technology

…… **19 June 2006**
Prof. Dr. Işıl TOPALOĞLU SÖZÜER
Department of Chemistry
İzmir Institute of Technology

…… **19 June 2006**
Assist. Prof. Dr. A. Sedat ÇELEBİ
Department of Chemistry
Ege University

…….... **19 June 2006**
Assoc. Prof. Dr. Ahmet E. EROĞLU
Head of Department
İzmir Institute of Technology

……..
Assoc. Prof. Dr. Semahat ÖZDEMİR
Head of the Graduate School

ACKNOWLEDGEMENTS

I would like to express my thanks to my research advisor, Assist. Prof. Mehtap EANES, for her support and guidance during my master research program. I would also thank to Don Van DERVEER from Clemson University for single X-ray analysis.

Finally, I wish to express my thanks to all of my friends in IYTE for their help and also special thanks to my family and my friend Hasan GÖK for their love, patience, and support.

ABSTRACT

HYDROTHERMAL SYNTHESIS AND CHARACTERIZATION OF ETHYLENEDIAMINE-CONTAINING MOLYBDENUM OXIDES

Recently, hydrothermal synthesis and characterization of organic-inorganic hybrid materials has attracted great attention.

A novel organic-inorganic hybrid material, $[Cu(en)MoO_4]$, was hydrothermally synthesized as blue crystals. A mixture of $Na_2MoO_4 \cdot 2H_2O$, $CuCl_2 \cdot 2H_2O$, NaCl, ethylenediamine and water was loaded into a 23 mL autoclave and heated at 170°C for 72 h. The compound crystallizes in the space group P2(1)/c of the monoclinic system with four formula units in a cell of dimensions a = 7.6743(15) Å, b = 9.4364(19) Å, c = 9.9538(2) Å, β = 72.266(3)°, V = 686.6(2) $Å^3$. The structure is composed of $\{MoO_4\}$ tetrahedra and $\{CuN_2O_4\}$ octahedra. Each pair of copper octahedra forms a binuclear edge-sharing unit through a $\{Cu_2O_2\}$ interaction. The binuclear octahedral units are interconnected through the bridging $\{MoO_4\}$ yielding a layer structure.

Purple crystals of a known hybrid material, $[Cu(en)_2]_2[Mo_8O_{26}]$, was hydrothermally obtained under different reaction conditions. A mixture of $Na_2MoO_4 \cdot 2H_2O$, $CuCl_2 \cdot 2H_2O$, NH_4Cl, ethylenediamine and water was loaded into the autoclave and heated at 170°C for 72 h. $[Cu(en)_2]_2[Mo_8O_{26}]$ crystallizes in the space group Pbca of the orthorhombic system with eight formula units in a cell of dimensions a = 13.516(3) Å, b = 15.548(3) Å, c = 16.725(3) Å, V = 3514.7(12) $Å^3$. The structure consists of γ-$[Mo_8O_{26}]^{4-}$ linked through $[Cu(en)_2]^{2+}$ groups. Each γ-$[Mo_8O_{26}]^{4-}$ unit forms covalent interactions with two $[Cu(en)_2]^{2+}$ units.

Green and black crystals were obtained from the reaction of $(NH_4)_6Mo_7O_{24} \cdot 4H_2O$, $CuCl_2 \cdot 2H_2O$, $H_2C_2O_4 \cdot 2H_2O$ and H_2O with different ratios. Via the reaction of $(NH_4)_6Mo_7O_{24} \cdot 4H_2O$, KVO_3, $Zn(C_2H_3O_2)_2$, NaCl, ethylenediamine and H_2O, yellow crystals were obtained.

ÖZET

ETİLENDİAMİN İÇEREN MOLİBDEN OKSİTLERİN HİDROTERMAL SENTEZİ VE KARAKTERİZASYONU

Son zamanlarda organik-inorganik melez materyallerinin hidrotermal sentezi ve karakterizasyonu büyük ölçüde ilgi çekmektedir.

Yeni bir organik-inorganik melez materyali olan [Cu(en)MoO_4] hidrotermal yöntemle mavi kristal olarak sentezlenmiştir. $Na_2MoO_4 \cdot 2H_2O$, $CuCl_2 \cdot 2H_2O$, NaCl, etilendiamin ve su karışımı 23 mL otoklavlara konuldu ve 170°C'de 72 saat boyunca ısıtıldı. Bileşik a = 7.6743(15) Å, b = 9.4364(19) Å, c = 9.9538(2) Å, β = 72.266(3)°, V = 686.6(2) $Å^3$ birim hücre boyutlarında, dört formül birimi içeren monoklinik sistemin P2(1)/c uzay grubunda kristallenir. Yapı {MoO_4} düzgün dörtyüzlü ve {CuN_2O_4} düzgün sekizyüzlülerinden oluşmaktadır. Her bir düzgün sekizyüzlü bakır çifti {Cu_2O_2} etkileşimi ile köşe paylaşımlı iki çekirdekli birim oluşturur. Bu iki çekirdekli düzgün sekizyüzlü birimler köprü yapan {MoO_4} ile tabakalı bir yapı oluşturacak bir şekilde birbirine bağlanır.

Bilinen melez materyali olan $[Cu(en)_2]_2[Mo_8O_{26}]$'nin mor kristalleri hidrotermal olarak farklı reaksiyon koşullarında elde edilmiştir. $Na_2MoO_4 \cdot 2H_2O$, $CuCl_2 \cdot 2H_2O$, NH_4Cl, etilendiamin ve su karışımı otoklava konuldu ve 170°C'de 72 saat boyunca ısıtıldı. $[Cu(en)_2]_2[Mo_8O_{26}]$, a = 13.516(3) Å, b = 15.548(3) Å, c = 16.725(3) Å, V = 3514.7(12) $Å^3$ birim hücre boyutlarında, sekiz formül birimi içeren ortorombik sistemin Pbca uzay grubunda kristallenir. Yapı $[Cu(en)_2]^{2+}$ grupları ile bağlanmış γ-$[Mo_8O_{26}]^{4-}$ 'den oluşur. Her bir γ-$[Mo_8O_{26}]^{4-}$ birimi iki $[Cu(en)_2]^{2+}$ birimi ile kovalent etkileşim oluşturur.

Yeşil ve siyah kristaller $(NH_4)_6Mo_7O_{24} \cdot 4H_2O$, $CuCl_2 \cdot 2H_2O$, $H_2C_2O_4 \cdot 2H_2O$ ve H_2O karışımının farklı oranlarda kullanılmasından oluşmuştur. $(NH_4)_6Mo_7O_{24} \cdot 4H_2O$, KVO_3, $Zn(C_2H_3O_2)_2$, NaCl, etilendiamin ve H_2O'nun reaksiyonu ile sarı kristaller elde edilmiştir.

TABLE OF CONTENTS

LIST OF FIGURES

LIST OF TABLES

CHAPTER 1

INTRODUCTION

Various methods are available for synthesizing solids, the method adopted depending on the form of the desired product. Crystalline solids may take the form of one of the following:

- **a.** A single crystal that is pure and free from defects,
- **b.** A single crystal in which its structure has been modified by the creation of defects,
- **c.** A powder (i.e. a large number of small crystals),
- **d.** A polycrystalline solid piece e.g. a pellet or a ceramic tube, in which there are a large number of crystals in various orientations, or
- **e.** A thin film.

The above classes of solids each have their own special preparative methods. Furthermore, the solid may be prepared in different forms, including single crystal, powder, solid piece, etc. Most of the preparative methods that are used are unique to solid state chemistry and are not encountered in other branches of chemistry (West 1996).

A large variety of inorganic solids have been synthesized by the reaction of a solid with another solid, a liquid (melt) or a gas, usually at high temperatures. It is difficult to determine what physical phases are involved in a given reaction. In many reactions that start with solid compounds, a liquid phase (melt) is formed at the reaction temperature therefore, many 'solid-solid' reactions are actually 'solid-liquid' reactions (Schubert and Hüsing 2000).

The most common method for the preparation of inorganic solid materials is the direct reaction of the component materials in the solid state at high temperatures. Solids do not usually react together at room temperature and usually require much higher temperatures, often 1000 to 1500°C, in order for reaction to occur.

Solid state reactions take place with great difficulty and only at high temperatures because of the considerable differences in structure between reactants and product. A significant amount of structural reorganization is required for forming the

product which means that bonds must be broken and reformed and atoms must migrate, perhaps over considerable distances. This diffusion makes the reactions slow unless very high temperatures are used (Schubert and Hüsing 2000). Most thermodynamically stable compounds are prepared at high temperatures. The synthesis of new compounds is difficult at high temperatures since thermodynamically stable known phases can not be avoided (Kanatzidis 1990). The synthesis of new kinetically stable or metastable compounds, which require lower temperatures in their synthesis, may be possible if the proper reaction conditions are found.

Two solids may not react even if thermodynamic considerations favor product formation. It is necessary to maximize some factors such as (a) the area of contact between the reacting solids and hence their surface areas, (b) the rate of nucleation of the product phase, and (c) the rates of diffusion of ions through the various phases and especially through the product phase so as to reduce the time required for solids to react together.

The surface of a given amount of solid varies, depending on whether it is in the form of a fine powder, coarse powder, or a single crystal. The surface area of any solid increases greatly with decreasing particle size. The total area of contact between the grains of the reacting solids depends on the total surface area of the grains; therefore, the surface area of reacting solids has a great influence on reaction rates.

Nucleation of the product and its subsequent growth are the important stages in the reaction of two solids to form a product. If there is a structural similarity between the product and one or both of the reactants, nucleation is facilitated. The similarity between the product and the reactants reduces the amount of structural reorganization which is necessary for nucleation to occur (West 1996).

The thermal reaction of two crystals of compounds A and B which are in intimate contact across one face can be considered in order to understand the difference between reactions in solution and in the solid state. In the first stage, the reaction occurs at the points of contact between A and B when no melt is formed during the reaction. Later, the constituents diffuse through the product phase. In the second stage, the nuclei of the product phase C forms at the interface between A and B. A high degree of structural reorganization may cause this stage to be difficult. A product layer is formed after nucleation of product C. There are two reaction interfaces at this stage: one between A and C, and another between C and B. For further reaction, counter diffusion

of ions from A and B must occur through the product layer C towards the new reaction interfaces.

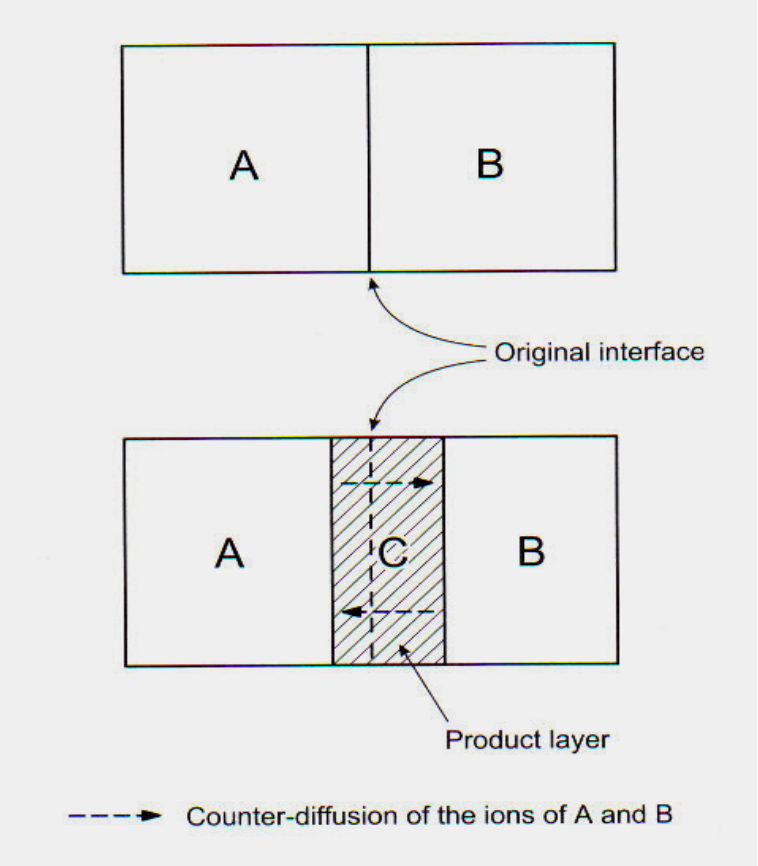

Figure 1.1. Reaction of two crystals (A and B) sharing one face
(Source: Schubert and Hüsing 2000)

The progress in the reaction causes the product layer to become thicker which results in increasingly longer diffusion paths and slower reaction rates, because the product layer between the reacting particles acts as a barrier. It is difficult for ions to move to adjacent sites because they are normally regarded as being trapped in their respective lattice sites. The ions have sufficient energy to diffuse through the crystal lattice only at very high temperatures. Correspondingly, in general, two-thirds of the melting temperature of one component is required to activate diffusion and hence to enable the solid-state reaction.

The perovskite barium titanate ($BaTiO_3$) formation by solid state reaction of BaO and TiO_2 may be given as an example to illustrate this point. The formation of $BaTiO_3$ takes place in three stages:

1. Initially BaO reacts with the outer surface regions of TiO_2 grains to form nuclei and a surface layer. At this step reorganization of the oxide lattice at the $TiO_2/BaTiO_3$ interface is required.
2. Further reaction of BaO and the formed $BaTiO_3$ causes the formation of the intermediate Ba-rich phase Ba_2TiO_4 which is necessary for the migration of the Ba^{2+} ions.
3. Ba^{2+} ions from the Ba-rich phase Ba_2TiO_4 migrate into the TiO_2 to form $BaTiO_3$ (Schubert and Hüsing 2000).

1.1. Synthesis of Inorganic Materials

A number of different ways are available for preparing new kinetically stable solid state compounds at low temperatures. The most common methods are the vapor phase transport method, the use of liquid salts as solvents, the sol-gel method, and the solvothermal synthesis (hydrothermal synthesis) method.

1.1.1. Vapor Phase Transport Method

This method is most often used for the purification of solids, for the synthesis of new compounds or for the growth of single crystals. Generally, the method consists of a sealed tube (silica glass) which contains the reactants, A, at one end and either under vacuum or more usually with an atmosphere of a gaseous transporting agent, B. The tube is put inside a furnace such that a temperature gradient exists inside the tube. Typically, there is 50°C temperature change along the length of the tube (West 1996).

The principle is that reactant A reacts with a gaseous agent (B) in order to form a gaseous product (AB) which subsequently decomposes at the end of the tube to redeposit the crystals of A. When the product deposits at the end of the reaction, the carrier gas diffuses back to the solid reactant. Halogens, HCl, HF, and sometimes oxygen or hydrogen gases are used as a carrier gas.

The vapor phase transport method is faster than solid state reactions because the mass transport which is always necessary for reaction or recrystallization is rate-limiting and it is faster through the gas phase than through solids (van der Put 1998).

In Figure 1.2 the vapor phase transport method for the growth of magnetite crystals is shown. At a high temperature, powder reacts with a reactive gas (HCl) to form volatile compounds. These decompose at a lower temperature in another part of the closed reactor. HCl is formed there and diffuses back to react again with powder.

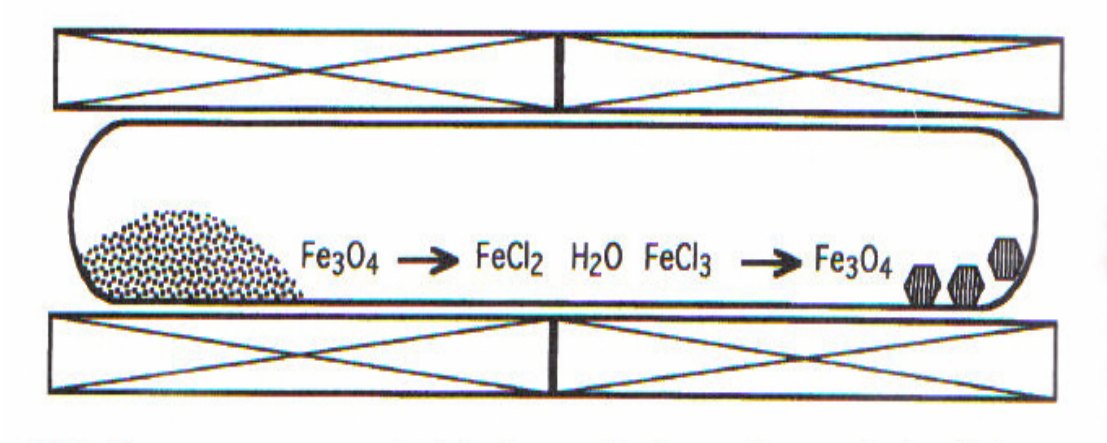

Figure 1.2. The vapor phase transport method for the growth of magnetite crystals (Source: van der Put 1998)

1.1.2. Liquid Salts as Solvents

Melts are high temperature liquids whereas aqueous solutions are liquids at low temperatures. On melting together the solid starting materials, homogenization takes place and recrystallization occurs on subsequent cooling of the melt. In the presence of the liquid phase and in the absence of too many crystal nuclei, large crystals can readily grow. Therefore, crystallization of melts is an important method for growing single crystals.

Knowledge of the relevant phase diagram is required in order to use melt crystallization methods because the phase diagram provides a diagrammatic representation of conditions such as temperature and composition (West 1996).

Molten salts can be used as solvents because they have some properties including the following which make them attractive for use in inorganic synthesis (Mamantov and Marassi 1987, O'Donnell 1993).

a. The dissolving capacity of the molten salts is large: they can dissolve metals, nonmetals, covalent compounds, metal oxides, other salts, water and many gases.

b. They can be used over wide temperature ranges: 100-1000°C.

c. Their acidity and oxidation/reduction properties can be adapted to the required values with the composition of mixtures of molten salts.

d. They have very high electrical and thermal conductivity.

e. The conversion efficiency in syntheses of molten salts is very high.

Molten salts are useful as solvents in chemical synthesis, electrolysis, soldering, enameling, de-enameling, metal recycling and preparation, coal gasification, and desulfuration. They are also reactants and catalysts for heat storage and heat transfer. The reaction is carried out in fluxes and the solvent can participate in the reaction. $BaTiO_3$ is synthesized in molten TiO_2 as a solvent and $Bi_8(AlCl_4)_2$ can only be synthesized in a very acidic cryolite ($NaAlCl_4$).

Followings are examples of chemical syntheses in a flux:

a. The synthesis of hydrides.

b. The synthesis of halides from oxides in liquids salts.

c. The synthesis of single crystals of oxides, as summarized in Table 1.1 (van der Put 1998).

Table 1.1. Process conditions for growth of single crystals from solutions[a]

(Source: van der Put 1998)

Compound	Solvent	Conditions
$Y_3Fe_5O_{12}$ (YIG)	PbO	T_o =1300°C, CR=3deg/h
$Y_3Al_5O_{12}$ (YAG)	PbO/PbF_2	T_o =1500°C, CR=4deg/h
$BaTiO_3$	TiO_2	T_o =1200°C, CR=0.3deg/h
$MgFe_2O_4$	PbP_2O_7	T_o =1310°C, CR=4deg/h
YVO_4	V_2O_5	T_o =1200°C, CR=3deg/h
$BeAl_2Si_6O_{16}$ (beryl)	Li_2O/MoO_3	T_o =975°C, CR=6deg/h
Al_2O_3; $YCrO_3$; TiO_2	BiF_3 / B_2O_3; PbF_2	T_o =1300°C, evaporation

[a]T_o is the temperature at the beginning of the process; CR = cooling rate.

1.1.3. Sol-Gel Method

The sol-gel method is very useful for preparing oxides since the technique makes it possible to form crystals of widely different morphologies and particle sizes (Brinker and Scherer 1990, Klein 1988). In this process water or alcohol is used as a solvent at or near room temperature and ambient pressure (van der Put 1998). The solid products can be obtained by gelation rather than by crystallization or precipitation. The sol-gel method is the creation of an oxide network by progressive polycondensation reactions of molecular precursors in a liquid medium, or is a method to form materials via a sol, gelation of the sol and finally removal of the solvent. This method is considered to be the chimie douce or soft chemical approach to the synthesis of metastable oxide materials.

A sol, which can be amorphous or crystalline, is a stable suspension of colloidal solid particles or polymers in a liquid. It is different from aerosols which are suspensions of particles or droplets in a gas phase.

A gel consists of a porous, three-dimensionally continuous solid network. It surrounds and supports a continuous liquid phase which is considered as a wet gel. The sol particles are connected by covalent bonds, van der Waals forces, or hydrogen bonds. In most sol-gel systems the creation of the gels (gelation) results in formation of covalent bonds and is irreversible. However, gel formation may be reversible due to the presence of other types of bonding during gelation (Schubert and Hüsing 2000).

Very small solid particles are precipitated as a colloidal sol from an aqueous or alcoholic solution of suitable molecules. The particles in the sol agglomerate to a hydrogel or alcogel which can be shaped or processed. The gel can be dried to form a xerogel or the solvent can be supercritically evacuated to form an aerogel. The oxides of silicon, germanium, aluminum, and the other metals can be synthesized via this method (van der Put 1998).

Figure 1.3 presents a scheme of the different processing routes leading from the sol to a variety of materials.

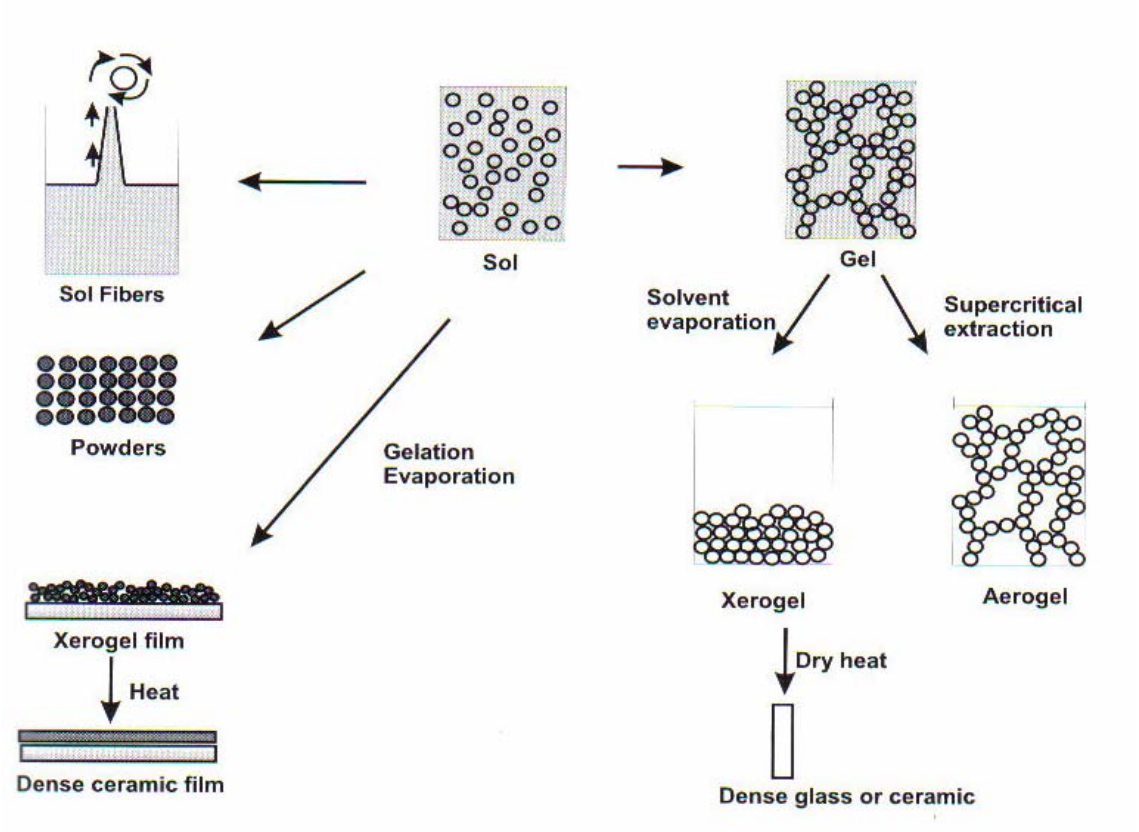

Figure 1.3. Sol-gel processing options
(Source: Schubert and Hüsing 2000)

1.1.4. Solvothermal Synthesis

Many inorganic phases are unstable under traditional solid state synthesis conditions that are performed at high temperatures. Solvothermal processes occur in a liquid medium above the boiling point and 1 bar. Water (hydrothermal synthesis) and ammonia (ammonothermal synthesis) are the most important solvothermal reaction media (Schubert and Hüsing 2000). Substances which are insoluble under ambient conditions are dissolved and the crystalline phase is formed.

Although water is the most important solvothermal reaction medium, other solvents can also be used. The purpose behind using different types of solvents in the chemical reactions is to bring down the pressure-temperature required. (Byrappa and Yoshimura 2001). Other solvents have to be used in cases in which the solubilities are

not high enough in water, or in which the product reacts with water (Schubert and Hüsing 2000).

1.1.4.1. Hydrothermal Technology

Most solvothermal syntheses are carried out in water, and hence are termed hydrothermal. Our interest is in the preparation of new organic-inorganic hybrid materials as single crystals via the hydrothermal method. In cases where suitable crystal sizes for X-ray diffraction were not obtained, further hydrothermal crystal growth procedures were applied.

1.1.4.1.1. History of Hydrothermal Synthesis

The hydrothermal term was first used by the British Geologist, Sir Roderick Murchison (1792-1871), to describe the action of water at elevated temperature and pressure. Hydrothermal reactions make changes in the earth's crust leading to the formation of rocks and minerals (Murchison 1840). Many oxidic gem stones have been formed hydrothermally in nature. An understanding of the mineral formation in nature in the presence of water under elevated temperature and pressure conditions led to the development of the hydrothermal technique. The laboratory simulations of the natural conditions existing under the earth's crust have helped earth scientists to determine complex geological processes in the formation of rocks, minerals, and ore deposits.

The first successful commercial application of hydrothermal technology began with mineral extraction or ore beneficiation. The use of NaOH to leach bauxite (aluminum ore) was invented in 1892 by Karl Josef Bayer (Goranson 1931). Today over 90 million tons of bauxite ore is treated annually by this process (Habashi 1994). Ilmenite, wolframite, cassiterite, laterites, a host of uranium ores, sulphides of gold, copper, nickel, zinc, arsenic, and antimony are treated by this process in order to extract the metal.

During World War II, the demand for the large quartz crystals forced many scientists in Europe and North America to grow large size crystals. The success in the growth of quartz crystals has provided further developments for hydrothermal crystal growth (Nacken 1950).

Today, the hydrothermal technique is used in several branches of science and technology. There are different kinds of hydrothermal techniques such as hydrothermal synthesis, hydrothermal growth, hydrothermal alteration, hydrothermal treatment, hydrothermal dehydration, hydrothermal decomposition, hydrothermal extraction, hydrothermal sintering, and so on (Byrappa and Yoshimura 2001).

1.1.4.1.2. Definition of Hydrothermal Synthesis

The term hydrothermal refers to any heterogeneous reaction in the presence of aqueous solvents or mineralizers under high pressure and temperature conditions in order to dissolve and recrystallize materials which are relatively insoluble under ordinary conditions (Byrappa and Yoshimura 2001). According to Rabenau hydrothermal synthesis involves heterogeneous reactions in aqueous media above 100°C and 1 bar (Rabenau 1985). Roy states that hydrothermal synthesis uses water as a catalyst and as a component of solid phases syntheses at elevated temperature (>100°C) and pressure (greater than a few atmospheres) (Roy 1994). According to Morey and Niggli in the hydrothermal method the reactants are subjected to the action of water, at temperatures generally above the critical temperature of water (~370°C) in closed bombs, and therefore, under the corresponding high pressures developed by such conditions (Morey 1913). Although the majority of scientists think of hydrothermal synthesis as taking place above 100°C temperature and above 1 atm, there is no definite lower limit for temperature and pressure conditions.

Under hydrothermal conditions the reactants go into solution as complexes under the action of mineralizers or solvents, hence, one may expect the conditions of chemical transport reactions. Due to the specific physical properties, like high solvation power, high compressibility, and mass transport of these solvents, unique benefits and applications can be shown in the following:

a. Synthesis of new phases or stabilization of new complexes.

b. Crystal growth of several inorganic compounds.

c. Preparation of finely divided materials and microcrystallites with well-defined size and morphology for specific applications.

d. Leaching of ores in metal extraction.

e. Decomposition, alteration, corrosion, and etching (Byrappa and Yoshimura 2001).

Water is the most important solvent for most ionic compounds (salts). The properties of water under hydrothermal conditions are very different from water at standard conditions. It can dissolve nonionic covalent compounds (insoluble oxides) at high pressures and at temperatures above its boiling point at 1 bar pressure (hydrothermal conditions) (van der Put 1998). However, some compounds do not show high solubility for water even at supercritical temperature, and hence the size of the obtained crystals or minerals in all the early hydrothermal experiments did not exceed thousandths or hundredths of a millimeter. Therefore, in the 19^{th} century the search for other suitable mineralizers began (Byrappa and Yoshimura 2001).

A mineralizer is added to the aqueous solution to speed up crystallization. It increases the solubility of the solute through the formation of soluble species which would not normally be present in water. The hydroxides of the alkali metals, silicates, germanates, or elemental metals, alkali salts of weak acids, (e.g. Na_2CO_3, Na_3BO_3, Na_2S), or the chlorides of alkali metals are used as mineralizers.

One of the most important advantages of using water is the environmental benefit. It is nontoxic, nonflammable, noncarcinogenic, and nonmutogenic. It is cheaper than other solvents (Eanes 2000).

Water serves as the solvent and the pressure transmitting medium in hydrothermal syntheses. The PVT-data (pressure, volume, temperature) and the physico-chemical properties of water at high temperatures and pressures are of significant importance. The ion product of water increases with higher pressure and temperature, the viscosity decreases with increasing temperatures (making diffusion processes to be easier and causing mobility to increase), and the polarity, i.e., the dielectric constant, decreases with higher temperatures, but increases with increasing pressures. The low viscosity and high mobility of supercritical water allows it to be excellent reaction media for the synthesis of metastable phases and the growth of good quality single crystals.

Hydrothermal reactions are carried out in closed vessels; therefore, the pressure-temperature relations of water at constant volume are very important. Figure 1.4 shows the volume-temperature diagram of water.

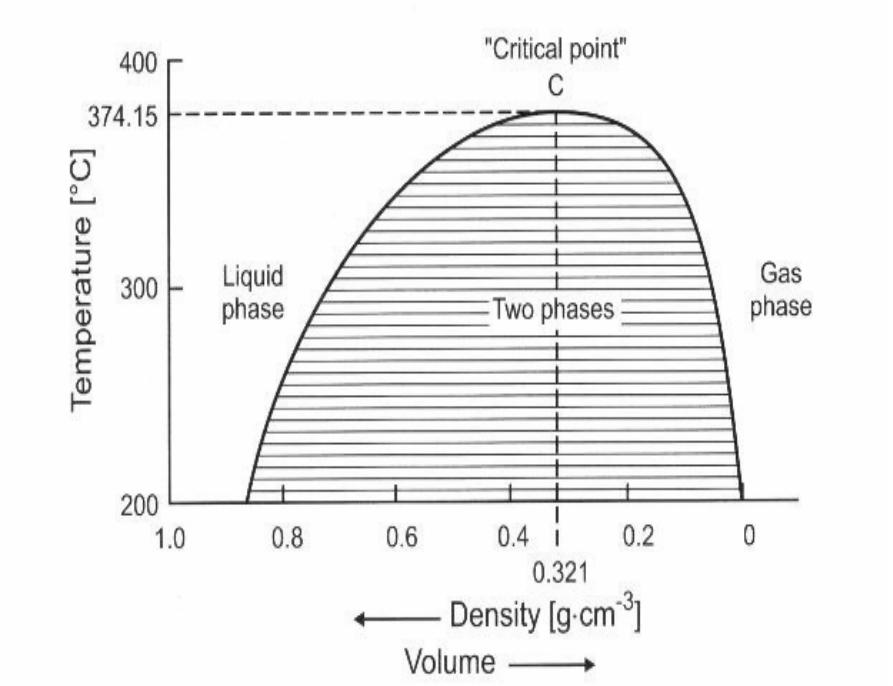

Figure 1.4. Volume (density)-temperature dependence of water
(Source: Schubert and Hüsing 2000)

At a given temperature the density of the liquid phase and the gas phase is given by the two intersections of a horizontal line through the two-phase region with the equilibrium curve. For instance, at 300°C, the density is 0.75 g/cm^3 for the liquid phase and 0.05 g/cm^3 for the gas phase. With higher temperatures the density of the liquid water decreases, while the density of the gas phase increases as liquid becomes vapor. The densities of both phases, as are all other properties, are the same at the critical point C. It can be concluded that the difference between liquid and gaseous water has disappeared. Above the critical temperature there is only one phase which is called the supercritical or fluid phase.

The corresponding pressure-temperature diagram is more useful for practical applications. The curve between the triple point (Tr), at which gas, liquid and solid phase is exist, and the critical point (C) is the saturated steam curve. The liquid and the gaseous phase coexist at the saturated steam curve. Liquid water is absent and the vapor phase is not saturated at pressures below this curve. Above this curve liquid water is under compression and the vapor phase is absent. The solid lines in figure 1.5 are used to calculate the pressure which is developed in a vessel after it has been partially filled with water, after closing and heating to a certain temperature.

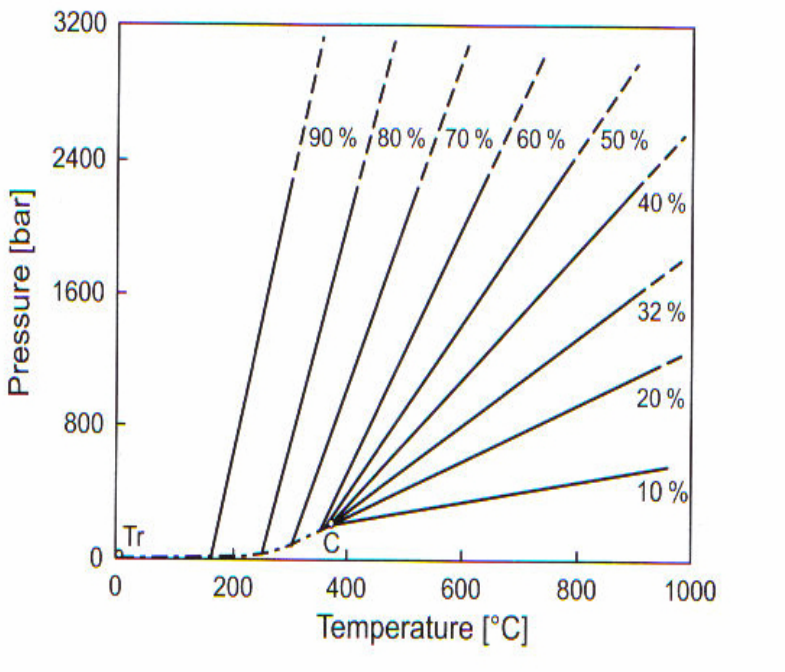

Figure 1.5. Pressure/temperature dependence of water for different degrees of filling of the reaction vessel

(Source: Schubert and Hüsing 2000)

A typical hydrothermal procedure is as follows: The precursor substance (nutrient) is put at the bottom of the reaction vessel. The reaction vessel is filled to the desired degree with the solvent (water and mineralizer). This slurry is heated to the desired reaction temperature. At this temperature the nutrient materials react and/or transform, primarily through dissolution and precipitation, to the stable compound. After cooling the autoclave, the product is isolated by filtration and washed in order to obtain the pure product (Schubert and Hüsing 2000). In most hydrothermal experiments, the pressure is determined by degree of filling and the temperature. Hydrothermal crystallization is made possible with the vessel filled to 32% total volume and more successfully above 65% with pressures of 200-3000 bar.

The hydrothermal method has several advantages over traditional solid state reactions. For instance, compounds which have elements with an unusual oxidation state may be synthesized by the hydrothermal method (Rabenau 1985). Another important advantage is that this method is useful for the synthesis of low temperature phases and metastable compounds. Hydrothermal reactions do not require much time compared to traditional methods. Although a solid state reaction may be done in a few weeks, the hydrothermal reaction can be performed in a few days.

1.2. Crystal Growth

Crystal growth is an important process producing suitable crystals for single X-ray diffraction measurements. For collecting X-ray diffraction data, the crystal must possess uniform internal structure and must be of proper size and shape (Dunitz 1964).

Crystallization includes two processes: nucleation (the formation of a crystalline nucleus) and crystal growth. The nucleus may be either homogeneous, i.e. formed through the interactions between the solute particles in the solution (called unassisted nucleation), or heterogeneous, i.e. formed at a pre-existing surface such as impurity, crucible wall, etc. (referred to assisted nucleation). If no crystalline nuclei are present, crystal growth can not occur.

The temperature dependence on crystal growth rate and nucleation rate are very similar to each other. Crystals can grow at any temperature below T_m (melting temperature) so long as a crystalline nucleus (homogeneous or heterogeneous) is available. As for nucleation, if the viscosity of the melt (η) is low, the growth rate will tend to be large. When the temperature decreases, the rapid increase in viscosity will stop crystal growth. In such cases, there would be a maximum in the resulting curve of the crystal growth rate as a function of temperature.

Nucleation and crystal growth occur simultaneously during cooling of a melt. If there are a sufficient number of nuclei, crystals will grow upon cooling a melt below its melting temperature. If ΔT is small, a large number of nuclei will be produced at a temperature at which crystal growth is optimal. On the other hand, if ΔT is large (the maximum of crystal growth is at much higher temperature than the maximum of nucleation), nuclei will be formed, but they can not grow since the kinetic barrier at this temperature (higher viscosity) inhibits crystal growth. Under these conditions the melt will form a glass (Schubert and Hüsing 2000).

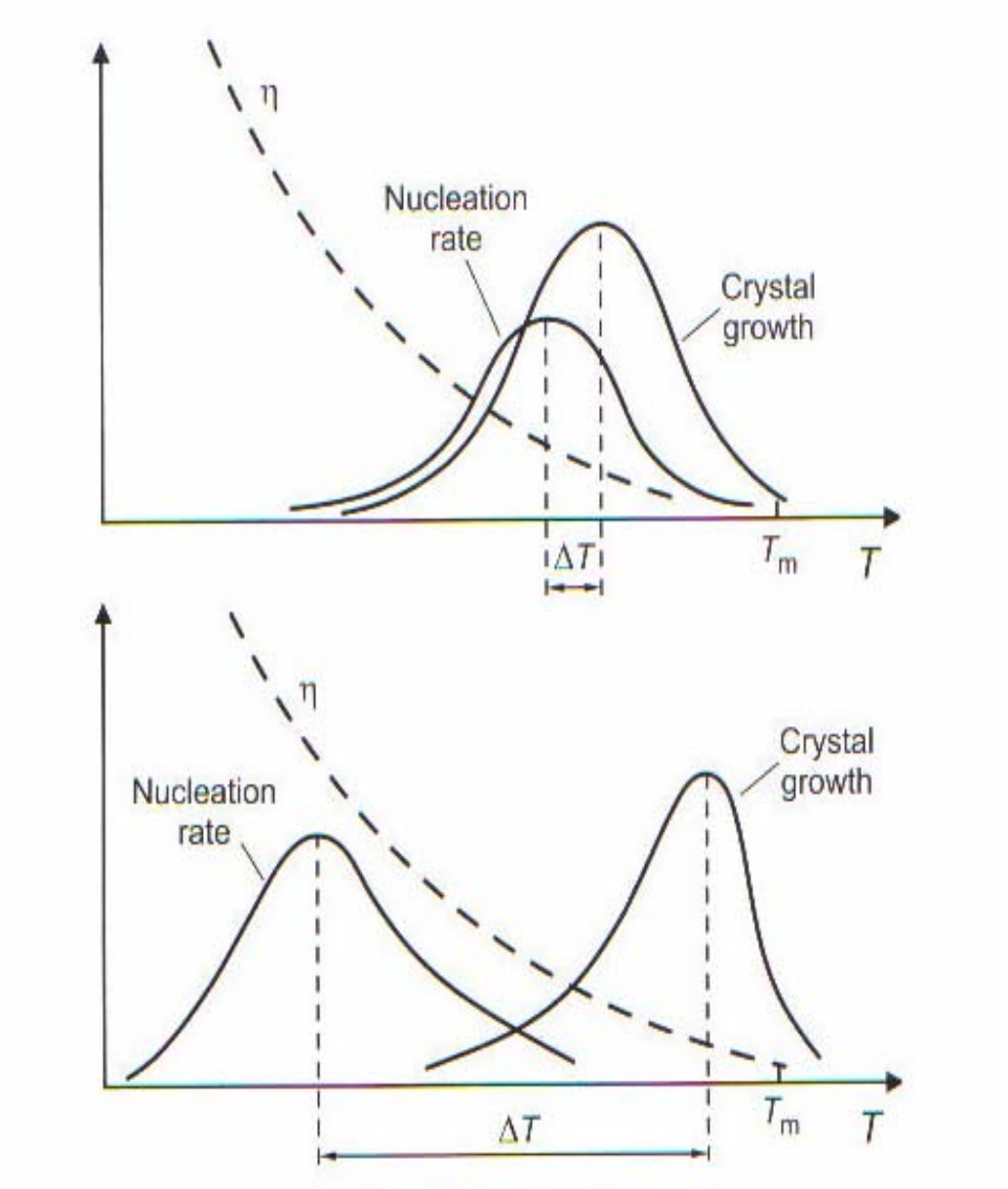

Figure 1.6. The different relation between nucleation rate and crystal growth in a crystallizing system (upper diagram) and glass-forming system (lower diagram)

(Source: Schubert and Hüsing 2000)

Crystals may be grown from vapor, liquid or solid phases. Optimum conditions are available for each crystalline substance for satisfactory crystal growth. The various techniques have certain advantages and disadvantages; these are summarized in Table 1.2.

Table 1.2. Comparison of crystal growth methods
(Source: West 1996)

Method	Advantages	Disadvantages
Melt growth (Czochralski, Bridgman-Stockbarger, Verneuil)	Rapid growth rates, giving large crystals; simple apparatus	Crystal quality may be poor with inhomogeneities and large defect concentrations
Solution growth (water crystallization, flux growth, hydrothermal method)	Isothermal conditions with slow rates give quality crystals of low defect concentration	Slow growth rates; problems of contamination by container or flux

1.2.1. Hydrothermal Crystal Growth

The hydrothermal method of crystal growth is very important in developing larger, purer, and dislocation-free single crystals. This method has been widely accepted since the 1960s and practically all inorganic species such as oxides, silicates, germanates, phosphates, chalcogenides, carbonates have been obtained by this method. Piezoelectric, magnetic, optic, ceramic and a host of other materials both as single crystals and polycrystalline materials are prepared by the hydrothermal crystal growth method. The hydrothermal technique offers several advantages over conventional techniques:

a. Compounds with elements in oxidation states which are difficult to obtain, especially important for transitional metal compounds, may be obtained in a closed system by the hydrothermal method.

b. The hydrothermal method is also useful for the so-called low temperature phases, e.g., α-quartz, α-berlinite, and others.

c. The hydrothermal method is unique for the synthesis of metastable compounds, such as subiodides of tellurium, Te_2I (Byrappa and Yoshimura 2001).

For a typical hydrothermal growth procedure the precursor substance (nutrient) is put at the bottom of the reaction vessel which is filled to the desired level with solvent (water and mineralizer). A baffle (perforated metal disc with defined openings in the

middle) is necessary in order to separate the growth zone of the single crystals from the zone in which the precursor dissolves. Seed crystals which are cut with defined crystallographic orientation are hung into the growth zone to facilitate nucleation.

Because of the high temperatures and pressures incurred during the hydrothermal process, a special design is required for the reaction vessel. Thick walled glass tubes can be used for temperatures up to 300°C and 10 bar. However, a steel tube that is closed at one end is usually used.

The reaction vessel is placed into the oven in which the nutrient section is heated more than the growth zone ($T_1 < T_2$). With increasing temperature, the substance at the bottom part of the reaction vessel dissolves and is transported into the cooler growth zone by convection. Due to its lower temperature, the solution is supersaturated in the growth zone and crystal growth occurs at the single crystal nuclei (Schubert and Hüsing 2000).

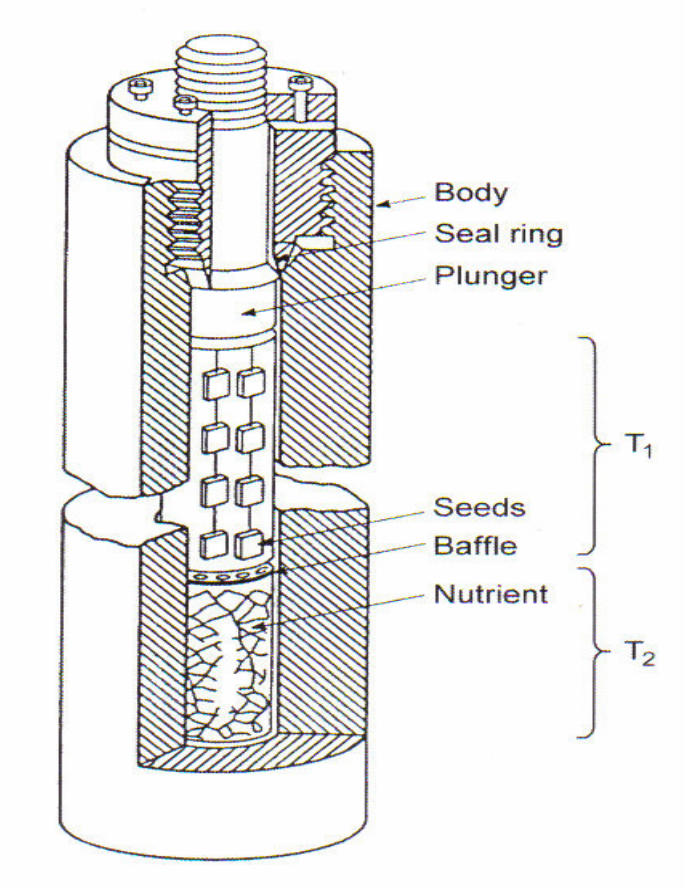

Figure 1.7. Scheme of an autoclave for hydrothermal single crystal growth (Source: Schubert and Hüsing 2000)

For the growth of single crystals by the hydrothermal method a mineralizer is usually added in order to speed up crystallization. The mineralizer increases the solubility of the solute through the formation of soluble species which would not normally be present in the water. For example, the solubility of quartz in water at 400°C and 2 kbar is too small to permit the recrystallization of quartz, in a temperature gradient, within a reasonable amount of time. However, with the addition NaOH as a mineralizer, large quartz crystals may be grown (West 1996).

CHAPTER 2

EXPERIMENTAL METHOD

2.1. Reaction Autoclaves

PTFE (polytetrafluoroethylene)-lined acid digestion bombs purchased from Parr Instrument Company (Illinois, USA) were used as reaction autoclaves. PTFE is used for lining these acid digestion bombs since Teflon is an inert material. The maximum operating temperature is 250°C and the maximum pressure is 1800 psi for the autoclaves which are used in our experiments.

The pressure generated within these bombs depends on the nature of the materials, the filling level and the amount of heat applied to promote the reaction. If the bomb is heated above its maximum temperature limit, the vapor pressure of the materials in the bomb increases exponentially with temperature and the strength of the materials from which the bomb is made falls off again exponentially. When a water based solution is heated to 250°C, it expands to fill a space approximately 25% larger than its standard state volume. If there is not sufficient vapor space in the bomb to accommodate this expansion, tremendous hydrostatic pressure will destroy the bomb.

Most inorganic digestions proceed smoothly without unusual hazards, using not more than 1.0 gram of sample in a 23 mL bomb. The bomb must never be completely filled as there must always be vapor space above the surface of the charge. The total volume of the charge must never exceed 66% of the capacity of the cup when working with inorganic materials.

Many organic materials may be treated satisfactorily in these digestion bombs with careful attentions. In all cases the sample size and the amount of oxidant must be carefully controlled. The dry weight of organic matter must not exceed 0.1 gram in a 23 mL bomb. In all operations the temperature and the pressure must be held within prescribed limits.

Table 2.1. Pressure developed at constant volume by 10 mL of aqua regia in a 23 mL space

(Source: Parr Company 1999)

Temperature (°C)	Pressure (psi)
106	305
155	705
162	765
202	1375
221	1670
236	1960
258	2505

Perchloric acid should not be used in these bombs due to its unpredictable behavior when heated in a closed vessel. Other reactions which are highly exothermic or which may be expected to release large volumes of gas should be avoided (Parr Company 1999).

Parr metal-jacketed acid digestion bombs can be heated in ovens, water baths, sand baths, oil baths, mantles or block heaters. At the end of a run the bomb must be cooled to the touch before removing the PTFE cup. Cooling must proceed slowly (Parr Company 1999).

In our laboratory 23 mL Teflon lined acid digestion bombs (Parr Instruments, model 4749) were used as reaction autoclaves. Schematic representation of model 4749 is shown in Figure 2.1. The sample and the digestion media were added to the Teflon cup. After adding, the Teflon cup was placed into the bomb body. Then, the corrosion disc (thinner, next to the Teflon cover) and the rupture disc (thicker, on the outside of the sandwich) were placed on top of the liner. After that, the spring with upper and lower pressure plates was added. After adding the spring, the screw cap was attached and turned down firmly by hand. The bomb was placed into a Carbolite CWF 1100 furnace for 1-3 day at 170-200°C. Finally, the autoclave was allowed to cool in the furnace.

Table 2.2. Bombs parts list

(Source: Parr Company 1999)

Part No	Description
241AC	Spring
264AC2	Hook Spanner
276AC	Bomb Body (23 mL)
276AC2	Bomb Body (45 mL)
277AC	Bottom Disc
278AC	Screw Cap
A280AC	PTFE Cup with Cover (23 mL)
282AC	Pressure Plate, lower
283AC	Pressure Plate, upper
A284AC	Tumbling Ring
A285AC	Holding Fixture
286AC	Corrosion Disc, .002
287AC	Rupture Disc, .003

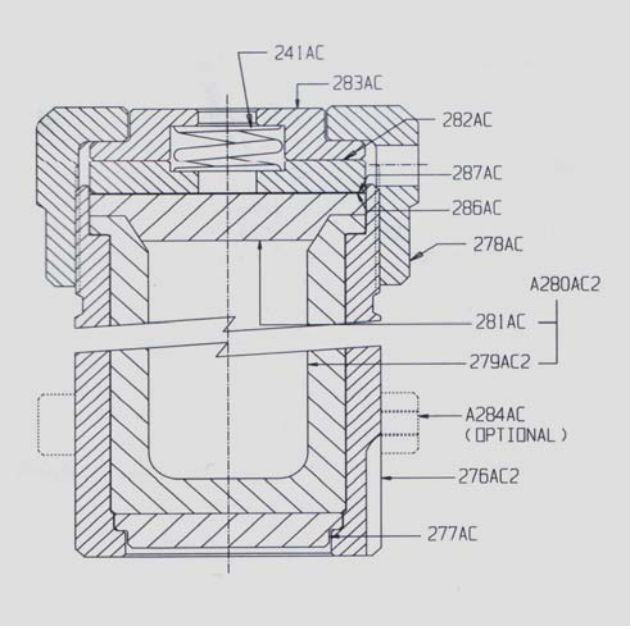

Figure 2.1. Schematic representation of an autoclave

(Source: Parr Company 1999)

Figure 2.2. PTFE cup with cover, acid digestion bomb body, screw cap, pressure plate (upper), pressure plate (lower), corrosion and rupture discs, spring (from left to right)

Figure 2.3. Carbolite CWF 1100 furnace

After the cooling step, the obtained product was washed several times with distilled water in order to remove the excess solvent from the crystals. The obtained single crystals were selected under the J.P. Selecta Zoom Stereo Microscope for further analysis. The selected single crystal was mounted with epoxy in a capillary for analysis by X-ray single crystal diffractometry.

Figure 2.4. J.P. Selecta Zoom Stereo Microscope

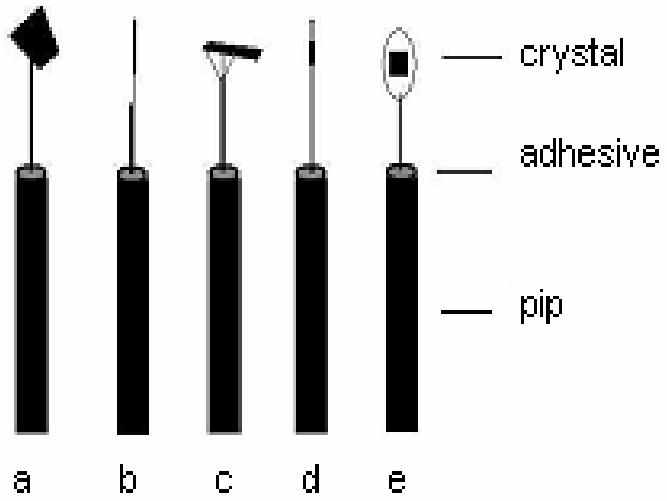

Figure 2.5. Some ways to mount crystals: a) on a glass fiber; b) on a two stage fiber; c) on a fiber topped with several lengths of glass wool; d) within a capillary tube; e) in a solvent loop

2.2. Characterization of Inorganic Solids

Characterization methods are classified into two main categories, depending on whether the substance is molecular or non-molecular. Identification is usually accomplished by some combination of spectroscopic methods and chemical analysis for the molecular substances. However, for the non-molecular and crystalline substances identification is carried out by X-ray powder diffraction and by chemical analysis. Each crystalline solid has its own characteristic X-ray powder pattern (fingerprint) for its identification. The powder patterns of most known inorganic solids are included in an updated library of powder diffraction patterns.

When the substance has been identified, the next stage is to determine its structure. If the substance is crystalline, X-ray crystallography can be used in order to determine the structure.

Different techniques are used in combination for complete characterization, because there is not a single technique which is capable of providing complete characterization of a solid. The physical techniques which may be used to characterize solids are classified into three main categories: diffraction, microscopic and spectroscopic techniques. Furthermore, other techniques such as thermal analysis, magnetic and physical property measurements may be used (West 1996).

Table 2.3. Characterization of solids and techniques available
(Source: West 1996)

	Bond Type	Electronic Structure	Elemental Analysis	Polycrystalline Texture	Surface Structure	Crystal Defects	Local Structure, CN etc	Crystal Structure	Unit Cell, Space Group	Amorphous or Crystalline	Phase Identification
X-ray Diffraction	(x)			(x)		(x)	(x)	x	x	x	x
Electron Microscopy			x	x	x	x		x	x	x	x
Optical Microscopy				x	(x)	(x)				x	x
IR Spectroscopy	(x)		(x)		x		x				x

2.2.1. Diffraction Techniques

Diffraction techniques have been used to solve more crystalline structures than all the other techniques put together. They are able to determine the precise atomic positions, and the bond lengths and angles of molecules within a single crystal.

2.2.1.1. X-ray Powder Diffraction

A finely ground crystalline powder contains a large number of small crystals (crystallites) which are oriented randomly. If such a substance is put in the path of a monochromatic X-ray beam, diffraction will occur from planes in those crystallites which are oriented at the correct angle to fulfill the Bragg condition. These diffracted beams make an angle of 2θ with the incident beam. The reflections lie on the surface of cones whose semi-apex angles are equal to 2θ since the crystallites can lie in all directions while still maintaining the Bragg condition. A flat film which is placed in front of the powder sample records a photograph consisting of concentric rings (Smart and Moore 1996).

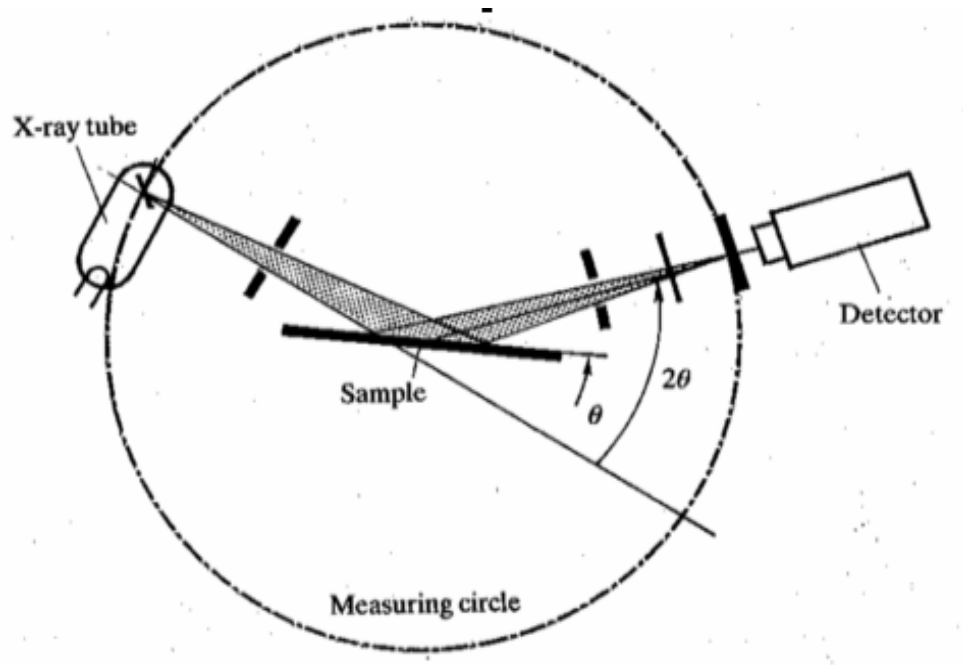

Figure 2.6. Diagram of a powder diffractometer
(Source: Smart and Moore 1996)

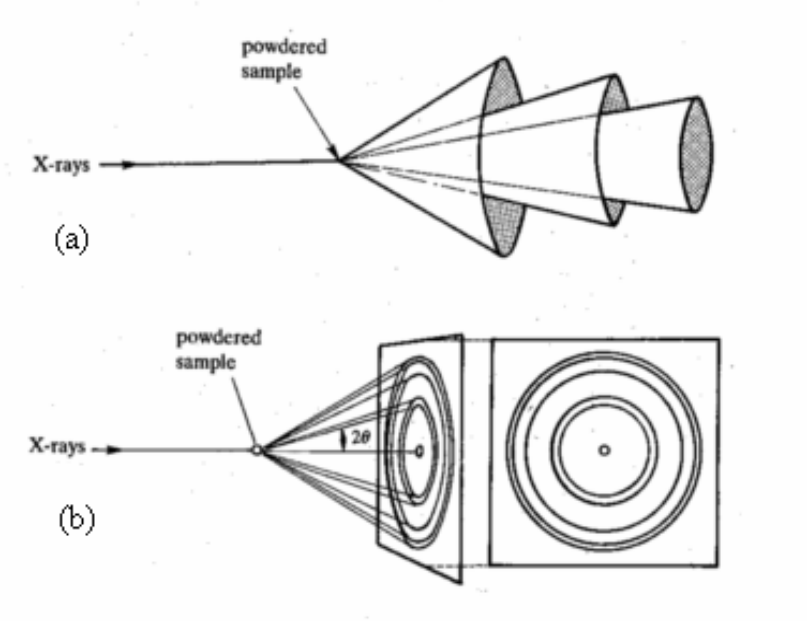

Figure 2.7. (a) Cones produced by a powder diffraction experiment (b) producing a powder photograph

(Source: Smart and Moore 1996)

An X-ray powder diffraction pattern is a set of lines or peaks which have different intensity and position (d-spacing or Bragg angle, θ), on either a strip of photographic film or on a length of chart paper. The line positions are fixed and characteristic for a given substance. The intensities can vary depending on the method of the sample preparation and the instrumental conditions (West 1996).

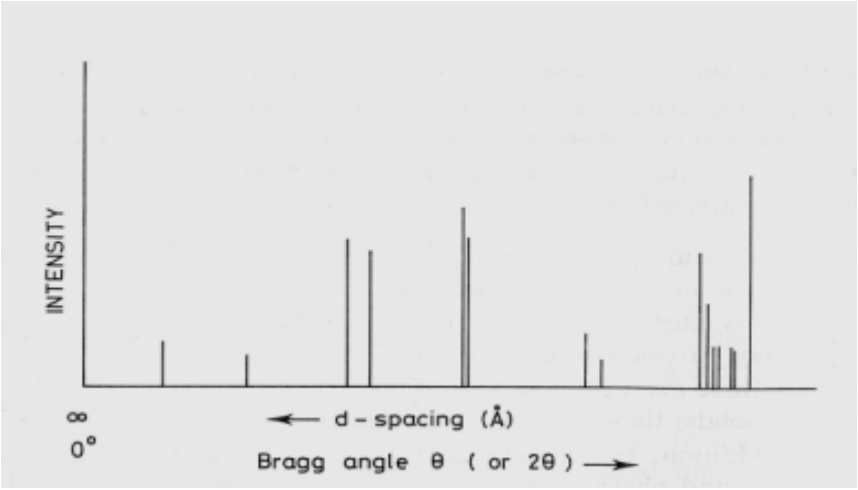

Figure 2.8. Schematic X-ray powder diffraction pattern

(Source: West 1996)

Each crystalline substance has its own characteristic powder diffraction pattern. There is a regularly updated library of powder diffraction patterns which is known as the JCPDS -Joint Committee for Powder Diffraction Standards- file (formerly known as the ASTM File) (Smart and Moore 1996). The file contains over 35000 inorganic substances.

In our laboratory X-ray powder diffraction patterns were obtained by using a Philips X'Pert Pro X-ray Diffractometer. Samples were placed on a zero background silicon sample holder. Data were collected by using CuKα (λ=1.5406 Å) radiation at settings of -45 kV and 40 mA for 30 minutes. The scan rate was 0.1°/sec and the data was collected for 2θ values of 4° to 70°.

2.2.1.2. Single Crystal X-ray Diffraction

Diffraction patterns can be collected from one single crystal instead of the randomly oriented crystals that are found in a powder. From a single crystal the position and intensity of the hkl reflections can be measured accurately and from this data the space group of the crystal and the precise atomic positions can be determined. This method can be performed with speed and accuracy, and it is one of the most powerful structural techniques available to a chemist.

Single crystal X-ray diffraction data is collected using a computer-controlled diffractometer, which measures the Bragg angle (θ), and the intensity (I) for each hkl reflection.

A single crystal is mounted vertically on a goniometer so that it can be rotated about one of the crystallographic axes. The diffraction from each plane will lie on the surface of a set of cones, as described before. Each plane is brought into the diffraction condition by rotating the crystal. The reflections can be recorded on a film which is wrapped around the rotating crystal.

Finally the intensity of each reflection is measured. This measurement provides all the data necessary to solve the crystal structure (Smart and Moore 1996).

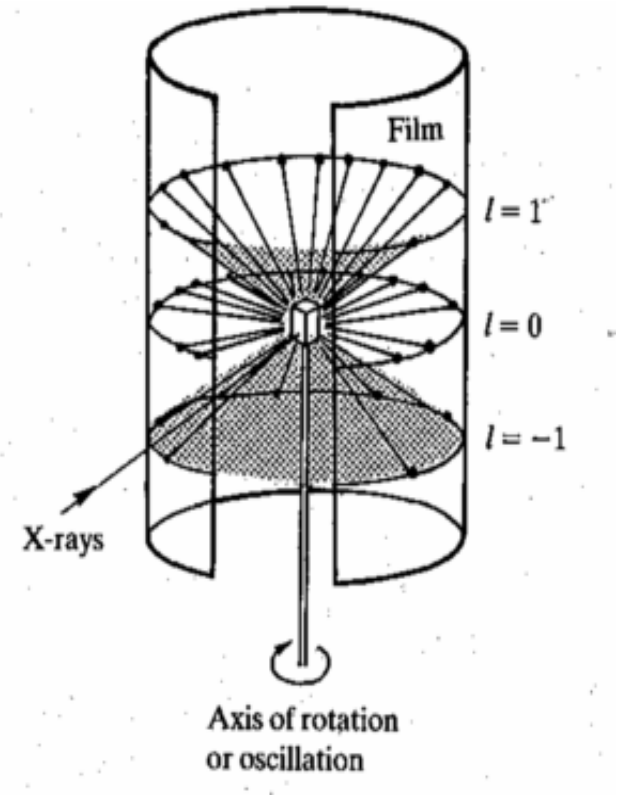

Figure 2.9. Cones of diffracted rays produced by a single crystal
(Source: Smart and Moore 1996)

For single crystal X-ray diffraction a single crystal was mounted in epoxy, and placed in capillary. Single crystal X-ray diffraction data were collected on a Rigaku AFC8 diffractometer equipped with a Mercury CCD area detector. Monochromatic MoKα (λ=0.71073 Å) radiation was used. The structure was solved by direct methods with the SHELXS program.

2.2.2. Microscopic Techniques

As a first step in examining a solid, it is important to have a look at it under magnification. Materials which visually appear to be similar may look quite different under the microscope.

Microscopes can be classified into two classes: optical and electron. Particles down to a few micrometers in diameter can be seen with optical microscopes. It is essential to use electron microscopy for submicrometer-sized particles.

2.2.2.1. Electron Microscopy

Electron microscopy can provide structural information over a wide range of magnification. Scanning electron microscopy (SEM) has many advantages over optical microscopy. For example the texture, topography and surface features of solid pieces can be studied, features up to tens of micrometers in size may be seen and, due to the depth of focus of SEM instruments, the resulting pictures have a definite three-dimensional quality.

Electron microscopy use two types of instruments in which the sample can be viewed in transmission mode (the beam of light or electrons passes through the sample) or in reflection mode (the beam of light or electrons is reflected off the sample surface). With reflection instruments, the sample is coated with a thin layer of metal. SEM is the main reflection instrument.

Elemental analysis can be done by some SEM instruments. Electrons from the electron gun are focused to a small spot on the surface of the sample. The electron beam is scanned systematically over the sample. Both X-rays (used for chemical analysis) and secondary electrons (used to build up an image of the sample surface) are emitted by the sample. The resolution of SEM is between 100 Å and 10 μm (West 1996).

A Philips XL 30S FEG Scanning Electron Microscope was used for the SEM/EDX analysis of our synthesized compounds. The accelerating voltage was 5 kV, spot was 3, and magnification was 1200. The detector type was Secondary Electron (SE) or Through the Lens (TLD). The EDX analysis results were represented as a spectrum. In this graphical representation the x axis represents the energy level (identifies the elements) and the y axis provides the number of counts of each element detected.

2.2.3. Spectroscopic Techniques

Spectroscopy is the study of the interaction between radiation and matter (Brisdon 1998). Many different spectroscopic techniques are available but all work on the same basic principle. Under certain conditions materials can absorb and emit energy. Although the energy can take various forms, it is usually in the form of electromagnetic radiation. The experimental results (spectra) is the plot of intensity of

absorption or emission (y axis) as a function of energy (x axis) which is expressed in terms of frequency or wavelength.

Although diffraction is concerned with long range order, spectroscopy gives information on local order. As a result, spectroscopic measurements on solids complement the results obtained from X-ray diffraction (West 1996).

2.2.3.1. Infrared Spectroscopy

Atoms in solids vibrate at frequencies of 10^{12} to 10^{13} Hz. Vibrational modes, which involve pairs or groups of bonded atoms, may be excited to higher energy states by absorption of radiation of appropriate frequencies (West 1996).

The principle of the IR experiment is to pass IR radiation through a thin sample of compound and to measure which energies of the applied IR radiation are transmitted by the sample (Brisdon 1998). IR spectrum is the plot of intensity of absorption (IR) as a function of frequency or wavenumber. In inorganic solids, IR spectra is used for straightforward identification of covalently bonded linkages such as hydroxyl groups, trapped water and oxyanions, carbonate, nitrate, sulphate, etc. (West 1996).

The IR absorption spectra of single crystals and KBr pellets were studied in the range of 4000-400 cm^{-1} by using an FTIR spectrometer (Nicolet Magna-IR 550). In order to prepare the pellet, a few milligrams of sample was mixed with KBr in an approximately 1:30 ratio. The sample-KBr mixture was ground by using mortar and pestle and placed inside a die. After placing the die, it was held in a hydraulic press for 2 minutes under 7000-psi pressure. Then the pellets were placed inside the spectrometer port for the measurements. Resolution was optimized to 8 cm^{-1} and 64 scans. Samples were typically run in transmittance mode.

2.2.4. Thermogravimetric Analysis (TGA)

In thermogravimetric analysis the change in weight of a sample in a controlled atmosphere is recorded continuously as a function of temperature or time. A plot of mass or mass percent as a function of time is called a thermogram, or a thermal decomposition curve.

The temperature range for thermogravimetric analysis is from ambient to 1500°C. The heating and cooling rates may be selected from somewhat greater than zero to as high as 200°C/min. Nitrogen or argon is usually used to prevent oxidation of the sample.

Thermogravimetric methods are limited to decomposition and oxidation reactions and to some physical processes such as vaporization, sublimation, and desorption (Skoog and Leary 1992).

For thermogravimetric analysis 10-25 mg powder samples were placed in a platinum pan. The samples were analyzed with a Shimadzu TGA-51 at 5°C/min from room temperature to 1000°C. The analyses were done under nitrogen flow of 40 mL/min.

CHAPTER 3

METAL OXIDES

3.1. Polyoxometalates

Polyoxometalates are the polyoxoanions of the early transition metals (V, Nb, Ta, Mo, W) (Pope and Müller 2001). Although the chemistry of polyoxometalates (heteropoly acids and heteropoly salts), started with Berzelius in 1826, it is still a rapidly developing field interconnected with other disciplines (Kozhevnikov 2002).

Generally, there are two types of polyoxometalates based on their chemical composition-isopolyanions and heteropolyanions.

$[M_mO_y]^{p-}$ *Isopoly anions* (contain Mo,W,or V in its maximum oxidation states)

$[X_xM_mO_y]^{q-}$ ($x \leq m$) *Heteropoly anions* (contain at least one p- or d-block element as the heteroatom)

M is the addenda atom and X is the heteroatom (called the central atom when located in the center of the polyanion). Addenda atoms occupy a metal-oxygen polyhedron MO_x and form the essential part of the building blocks. Molybdenum or tungsten are the most commonly used addenda atoms, followed by vanadium or niobium which are less frequently used, or mixtures of these elements in their highest oxidation states (d^0, d^1) can be used. Almost all elements of the periodic table may act as heteroatoms in heteropoly anions, the most typical ones being P^{5+}, As^{5+}, Si^{4+}, Ge^{4+}, B^{3+}, etc. Molybdenum(VI) and tungsten(VI) are the best polyoxometalate formers due to their favorable combination of ionic radius and charge and the accessibility of empty d orbitals for metal-oxygen π bonding (Souchay 1969, Pope 1983).

3.1.1. Historical Background

The chemistry of polyoxometalates started in 1826 when Berzelius discovered the first heteropoly salt, ammonium 12-molybdophosphate (Kozhevnikov 2002). By

1908, approximately 750 heteropoly compounds had been discovered. The structure of polyoxometalates had remained a mystery for more than a century since their discovery. The structures based on sharing metal-oxygen polyhedra were proposed by Werner, Miolati, Rosenheim and Pauling (Rosenheim 1921, Pauling 1929).

By the early 1970s, the polyoxometalate chemistry had been greatly expanded. This period is associated with the work of many groups, including Souchay (France), Ripan (Rumania), Spitsyn (USSR) and Baker (USA) (Kozhevnikov 2002). In the 1980-90s, the number of groups increased enormously with expanding applications of polyoxometalates.

The application of modern characterization techniques led to a better understanding of the structural principles of polyoxometalates and their properties. However, much work remains in this field, because many questions about the structural principles, mechanisms of synthesis and reactivity of polyoxometalates are still unanswered (Kozhevnikov 2002).

3.1.2. Structures of Polyoxometalates

Many structural types and stoichiometries of polyoxometalates are known to date. The minimum degree of condensation of addenda atoms is in the range of 2-6 (Pope 1983). The maximum can be as high as a few hundred.

The variety of polyoxometalate structures start from a few highly symmetrical parent polyanions and then many other polyoxometalate structures can be considered as their derivatives. There are three such parent structures with a tetrahedron, an octahedron, and an icosahedron as their central polyhedron XO_n (n= 4, 6 or 12) which determines the symmetry of the whole polyanion (Kozhevnikov 2002).

3.1.3. Crystal Structure of Heteropoly Compounds

Solid heteropoly compounds generally form ionic crystals (Backer and Glick 1998). These compounds frequently have large interstices between the large heteropoly anions. Such large interstices can accommodate a large amount of water of crystallization and the countercations. These hydrogen-bonded water molecules can be

easily and reversibly removed from the solid by heating to 100-150°C. The extent of hydration can change the crystal structure of heteropoly compounds. For instance, 12-tungstophosphoric acid shows different packing arrangements when the water of hydration is lost (Table 3.1) (Kozhevnikov 2002).

Table 3.1. Crystal structures of 12-tungstophosphoric acid hydrates
(Source: Brown et al. 1977, Noe-Spirlet and Bushing. 1978, Fournier et al. 1992)

Hydrate	**Space group**
$H_3[PW_{12}O_{40}]\cdot 29H_2O$	Cubic Fd3m
$H_3[PW_{12}O_{40}]\cdot 21H_2O$	Orthorhombic Pcca
$H_3[PW_{12}O_{40}]\cdot 14H_2O$	Triclinic P1
$H_3[PW_{12}O_{40}]\cdot 6H_2O$	Cubic Pn3m

In general, polyoxometalate anion surfaces contain both terminal (M=O) and bridging (M─O─M) oxygen atoms. All experimental evidence and recent density functional calculations agree that the bridging oxygens carry a greater negative charge and are protonated in preference to terminal oxygens (Bardin et al. 1998).

The lattice energies (anion cation attractions) of the crystals of heteropoly compounds are very low. The anionic charge is delocalized over a several atoms, hence greatly decreasing electrostatic attractions. The exterior of heteropoly anions consists of oxygens which are strongly polarized towards the addenda, thus nonpolarizable in other directions. These nonbasic oxygens may not form hydrogen bonds of normal strength (Baker and Glick 1998). Therefore, heteropoly anions are weakly solvated in solution. Although the metal oxides have rigid network structures, the crystal structures of heteropoly compounds are quite mobile.

A special structural classification which recognizes the importance of structural flexibility of solid heteropoly compounds was advanced by Misono et al. (Okuhara et al. 1996, Misono 2001). This structural hierarchy is schematically shown in Figure 3.1.

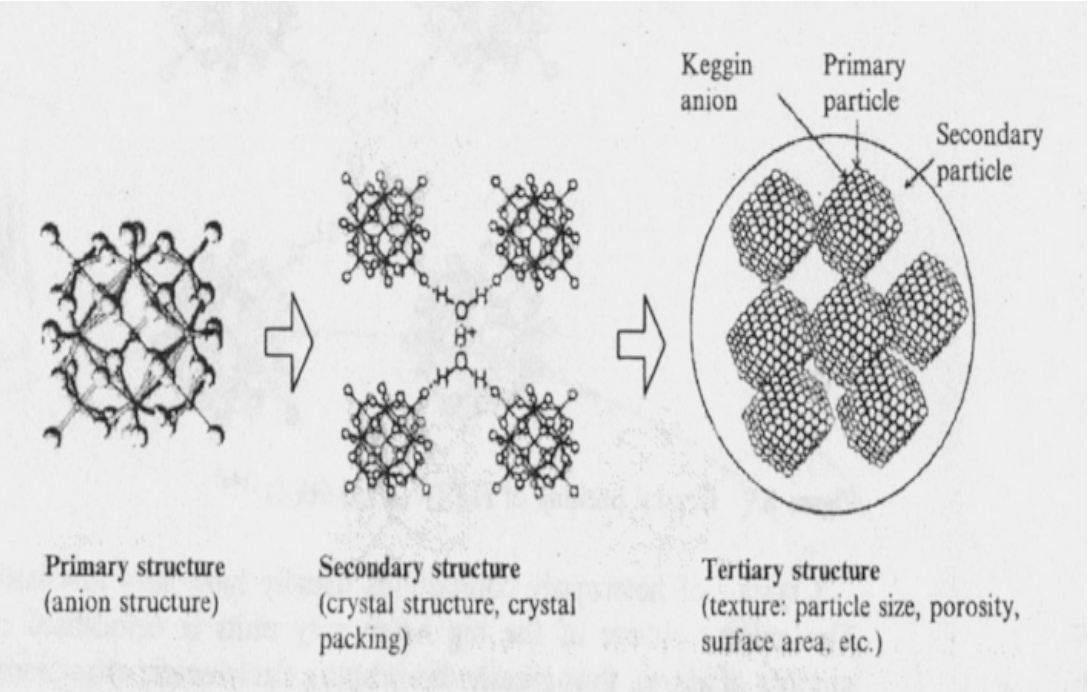

Figure 3.1. Structural hierarchy of heteropoly compounds
(Source: Okuhara et al. 1996)

3.1.4. Applications of Polyoxometalates

Although there are numerous applications of polyoxometalates, catalysis is by far the most important. Over 80% of the patent applications dealing with polyoxometalates are related to catalysis (Katsoulis 1998). In industry polyoxometalates can be used as catalysts for several large-scale chemical processes. Due to their enormous versatility polyoxometalates may be used for clean synthesis of fine and specialty chemicals (Kozhevnikov 2002).

3.1.4.1. Catalysis by Polyoxometalates

Heteropoly compounds have many advantages as catalysts due to their multifunctionality and structural mobility. They have very strong Brønsted acidity, and they are efficient oxidants, exhibiting fast reversible multielectron redox transformations under mild conditions. Their acid-base and redox properties may be varied by changing the chemical composition.

Heteropoly compounds are acid, redox, and bifunctional (acid and redox) catalysts due to their unique properties. The catalytic reactions may be done in homogeneous or in heterogeneous (gas-solid, liquid-solid or biphasic liquid-liquid) systems (Kozhevnikov 2002).

3.1.4.2. Catalysis by Polyoxometalates in Industry

Heteropoly compounds can be used as catalysts in many industrial processes. Japan is the world leader in their commercialization. The first successful industrial application of heteropoly acids as a homogeneous catalyst for the hydration of propene (the Tokuyama process) was shown in 1972. After this application many new large-scale processes in which heteropoly acids or their salts were used as acid or oxidation catalysts have been commercialized. The liquid-phase hydration of butenes, the vapor-phase oxidation of methacrolein to methacrylic acid and of ethylene to acetic acid, and the gas-phase synthesis of ethyl acetate from ethanol and acetic acid can be given as an example of this application (Izumi 1997).

3.1.4.3. Other Applications of Polyoxometalates

There are various applications of polyoxometalates based on their unique physicochemical properties which are illustrated in Table 3.2.

Catalysis is the most important application of polyoxometalates. Other uses such as chemical and biochemical analysis, new materials with advanced characteristics, medicine, etc. are shown in Table 3.3.

Table 3.2. Physicochemical properties of polyoxometalates utilized in various applications

(Source: Katsoulis 1998)

Mixed oxide like
Discrete ionic structure
Nanosized anions (diameter, 0.6-4 nm)
Large anion charge (from -3 to greater than -14)
High molecular weight
Incorporate over 70 elements inside heteropoly anions
High conductivity of solids
Strong Brønsted acidity
Multielectron redox agents
Photoreducible / oxidizable
Color of oxidized forms different from color of reduced forms
High solubility of heteropoly acids in H_2O and polar organic solvents
Transferability of heteropoly anions into nonpolar solvents

Table 3.3. Main applications of polyoxometalates

(Source: Katsoulis 1998, Pope 1983)

Catalysis
Analytical Chemistry
Corrosion resistant coatings
Separations, processing radioactive waste, and sorbents of gases
Membranes
Sensors
Cation exchangers
Dyes and pigments
Electrooptics
Electrochemistry, electrodes, fuel cells, and capacitors
Medicine

3.2. Organic-Inorganic Hybrid Materials

The design of the structures of metal oxide based solid phases remains a challenge in solid state chemistry. The ability to synthesize inorganic materials by rational design remains elusive. The existence of naturally occurring, structurally complex minerals demonstrates that hydrothermal synthesis may provide a low temperature pathway to produce open-framework and layered metastable structures. Therefore, combination of the hydrothermal technique with the introduction of organic components that can act as charge compensating groups, space-filling units, structure directing agents, templates, tethers between functional groups, or conventional ligands in the preparation of inorganic/organic composites is used as a synthesis scheme (Hagrman P.J. et al. 2001).

Generally there is a correlation between the complexity of the structure of a material and its functionality (Stupp and Braun 1997). Thus, many of the naturally occurring oxides contain mixtures of inorganic oxides coexisting with organic molecules. Organic components can dramatically influence the microstructures of inorganic oxides, hence providing a method for the design of novel materials (Hagrman P.J. et al. 1999). The first systematic development of materials in which organic molecules were used to influence the growth of inorganic oxides is the work of Barrer on synthetic zeolites (Barrer 1982).

Organic components influence the nucleation and growth of the inorganic oxide. There is a synergistic interaction between the organic and inorganic components that allows the structural information from the organic molecule to the inorganic framework. Also there is a shift from the thermodynamic to kinetic domain, such that equilibrium phases are replaced by structurally more complex metastable phases. Traditional solid state conditions will not retain the structural elements of the organic component. As a result, hydrothermal synthesis is a powerful method for preparation of organic-inorganic hybrid materials with retention of the structural elements of the reactants in the final products (Hagrman P.J. et al. 1999).

The organic compound may adopt various roles depending on its structure, charge, and the presence of a secondary transition or post-transition metal cation, in addition to the molybdenum component. The most common role of the organonitrogen compound is as a charge-compensating, space filing and structure directing cation

(Mann et al. 1997). They also function as a ligand bound directly to the molybdenum oxide structure as a terminal group or as a linker or pillar (Hagrman P.J. et al. 2000, Zapf et al. 1997a). Finally, the organic moiety can act as a ligand that is bound to a secondary metal site (M'). In Figure 3.2 schematic representations of various modes of involvement of organonitrogen components in molybdenum oxide materials is illustrated. In this figure organonitrogen component act (a) as a counter cation, (b) as a ligand to the $Mo_xO_y^{n-}$ substructure, (c) as a ligand to a secondary metal M' in a coordination complex cation, (d) as a ligand to a secondary metal M' which is incorporated into a bimetallic oxide substructure, and (e) as a ligand and a bridging unit in a secondary metal-ligand network.

In general, organonitrogen ligands are introduced as part of the reaction during the reaction. Organic-inorganic hybrid molybdates that contain carboxyl are rarely reported, because carboxyl containing ligands possess more negative charges and it is difficult to meet the charge balance with the polyanions (Yuan et al. 2003, Tao et al. 2001). As a result it is a great challenge to incorporate carboxyl containing ligands into the molybdate scaffolding.

The structural information is stored in the synthetic building blocks and the final architecture is obtained from the synergistic interactions of the components (Janiak 1997). Although the metal ligand interactions require coordinate covalent bonding, the ultimate architectures of the hybrid materials may also reflect multipoint hydrogen-bonding, the interplay of hydrophobic-hydrophilic interactions and ionic interactions between component substructures (Hagrman P.J. et al. 2001).

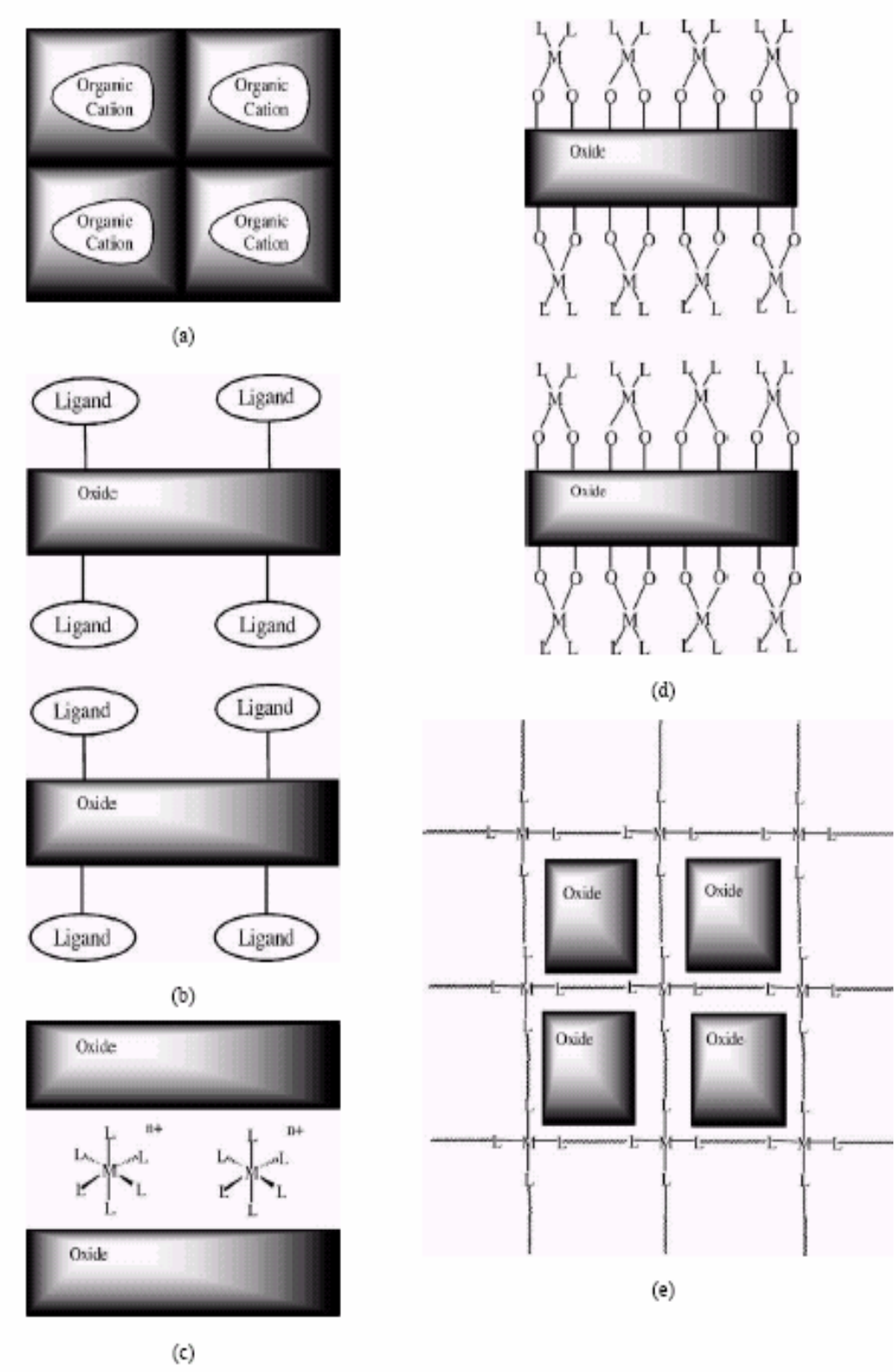

Figure 3.2. Schematic representations of various modes of involvement of organonitrogen components in molybdenum oxide materials

(Source: Zapf et al. 1997b, Zapf et al. 1998a)

3.2.1. Organonitrogen Templated Molybdenum Oxides

In our laboratory synthetic conditions are employed for the preparation of organodiamine templated molybdenum oxides. Molybdenum oxides are generally negatively charged species and may be present as polyanions, chains, two-dimensional networks, or three-dimensional frameworks.

Figure 3.3 illustrates the five common isomers of $[Mo_8O_{26}]^{4-}$. The α, β, and γ isomers have been isolated in a number of salts (Pope 1983, Inoue and Yamase 1995) while the δ-form has been reported as the (α-δ) or (β-δ) intermediate structure. The ε-form is unique to the heterometal-diamine molybdenum oxide materials. The isomer structures differ in number, types and fusion modes of molybdenum polyhedra. These isomeric forms are conceptually and chemically interrelated by minimal bond breaking through lengthening of axial interactions and polyhedral rotations. The occurrence of a particular isomer in hydrothermal synthesis is not predictable (Hagrman P.J. et al. 1999).

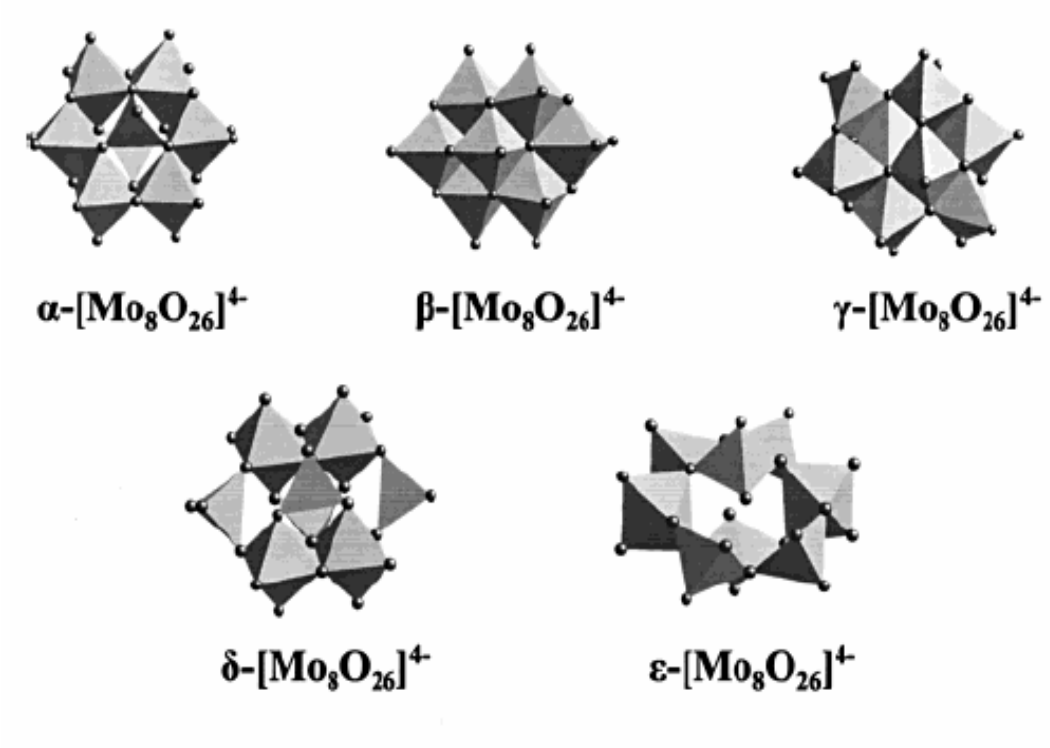

Figure 3.3. Polyhedral representations of the common isomeric structures of $[Mo_8O_{26}]^{4-}$ (Source: Hagrman P.J. and Zubieta 1999)

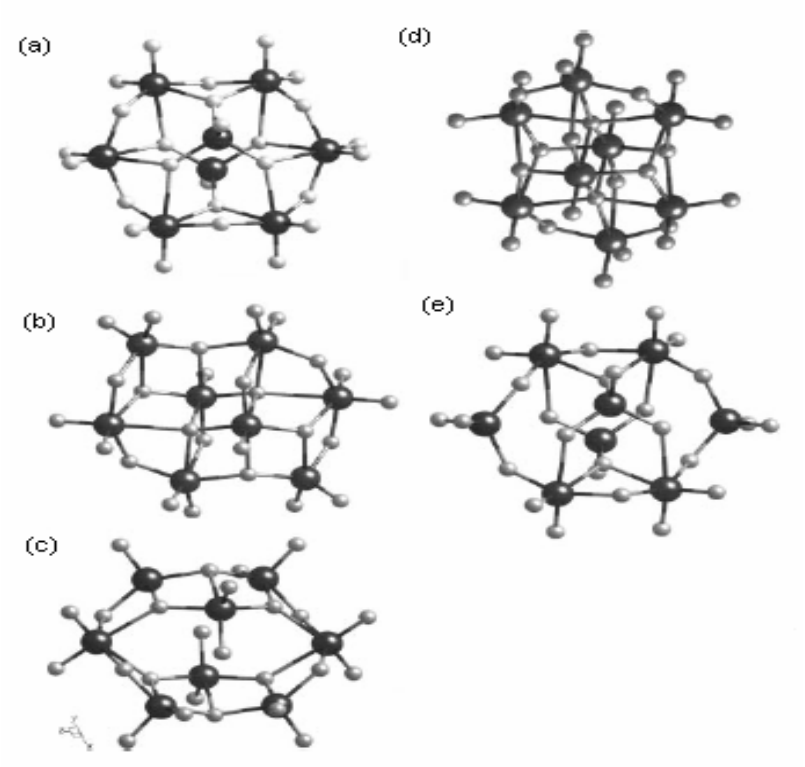

Figure 3.4. The structures of the a) α, b) β, c) γ, d) δ, and e) ε forms of $[Mo_8O_{26}]^{4-}$
(Source: Hagrman P.J. et al. 1999)

In the synthesis of new molybdenum oxide materials, the molecular polyoxomolybdate clusters are linked either through direct coordination into oxo-bridged arrays of clusters or through secondary metal centers acting as inorganic bridging groups. The polyoxomolybdate anion and a coordination complex cation (a secondary transition metal/ligand subunit) are the essential building blocks (Hagrman D. et al. 1997, Kitamura et al. 1997).

In certain cases, a heterometallic component can be introduced either to provide charge compensation or as part of the inorganic bimetallic oxide framework itself. The secondary metal-ligand component is a molecular subunit that coordinates to the peripheral oxo-groups of the polyoxomolybdate clusters as a bridging group. The architecture of the resultant solid reflects the preferred coordination geometry of the secondary metal, the available coordination sites at the secondary metal-ligand subunit, and the number of points of attachment engaged on the oxide cluster (Hagrman P.J. et al. 2001).

Figure 3.5 illustrates the schematic representations of various modes of linking of secondary metal-ligand subunits and polyoxomolybdate clusters based on available attachment points; (a) A rod-like coordination complex polymer cation combining with an oxide subunit to form a one-dimensional composite. In this case, the secondary metal center exhibits a preference for diagonal coordination. (b) The structural consequences of introducing a ligand capable of bridging three metal centers. The rigid ligand backbone directs the donor groups at 120°. The cavity dimensions may be manipulated by adjusting the tether lengths between the donor groups L. (c) A rod-like complex polymer cation as for (a) but with a metal center favoring a square planar coordination geometry. (d) A molecular secondary metal–ligand complex combining with an oxide subunit. (e) Same as for (d) but with a secondary metal–ligand complex capable of four points, rather than two points of attachment to the oxide. (f) Same as for (d) but with an oxide subunit favoring fourfold, rather than twofold, attachment.

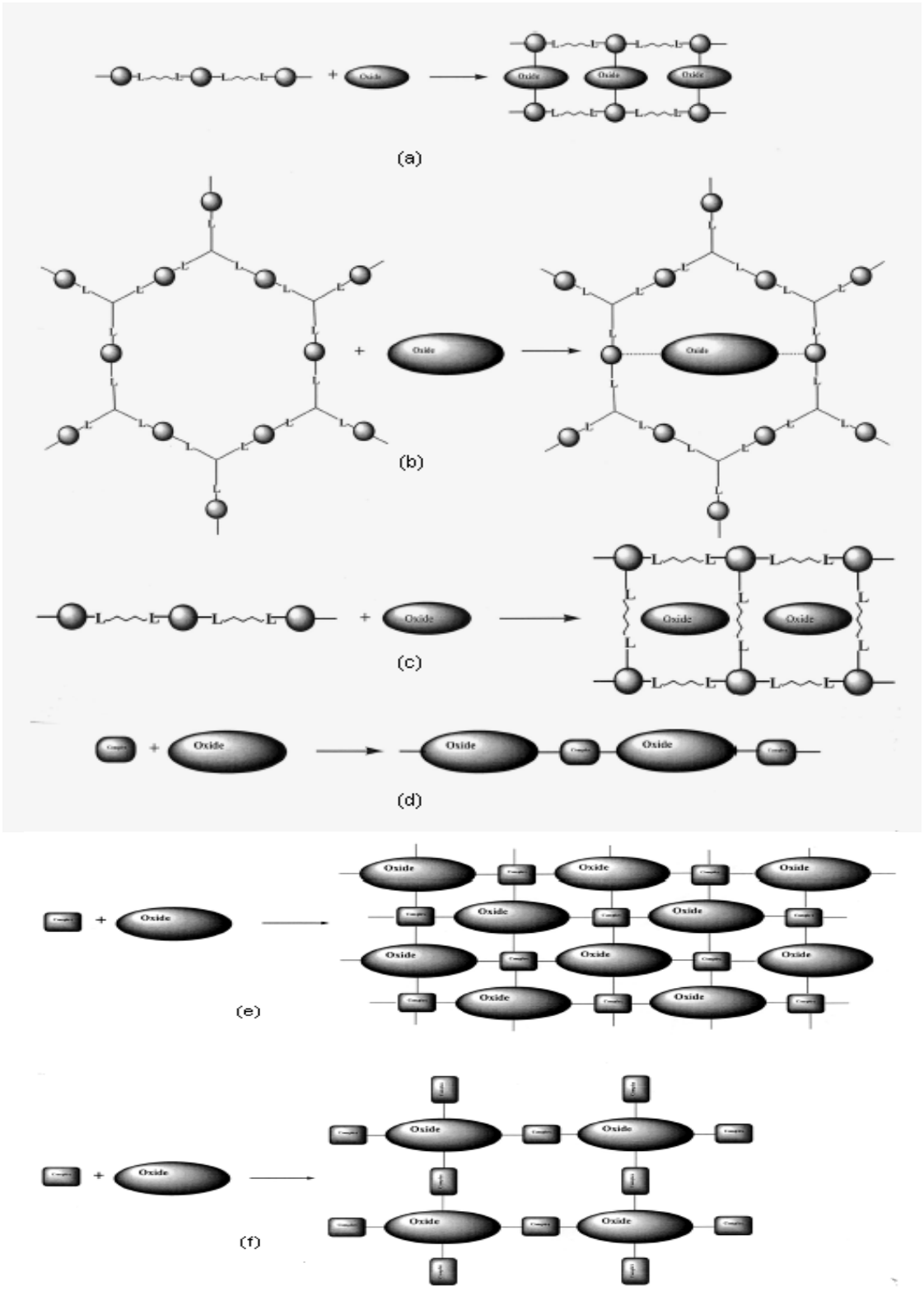

Figure 3.5. The schematic representations of various modes of linking of secondary metal-ligand subunits and polyoxomolybdate clusters based on available attachment points

(Source: Hagrman D. et al. 2000)

The cationic component needs not to be restricted to molecular subunits. The ligand may be introduced as a one-, two- or three-dimensional substructure. As shown in Figure 3.6, the rod-like bridging ligand in combination with the coordination preferences of the secondary metal site may offer different cationic polymer scaffoldings for the oxide substructures. The ligand forms a scaffold or the transmission of metal-based structure in one-, two- or three-dimensions (Chesnut et al. 1999).

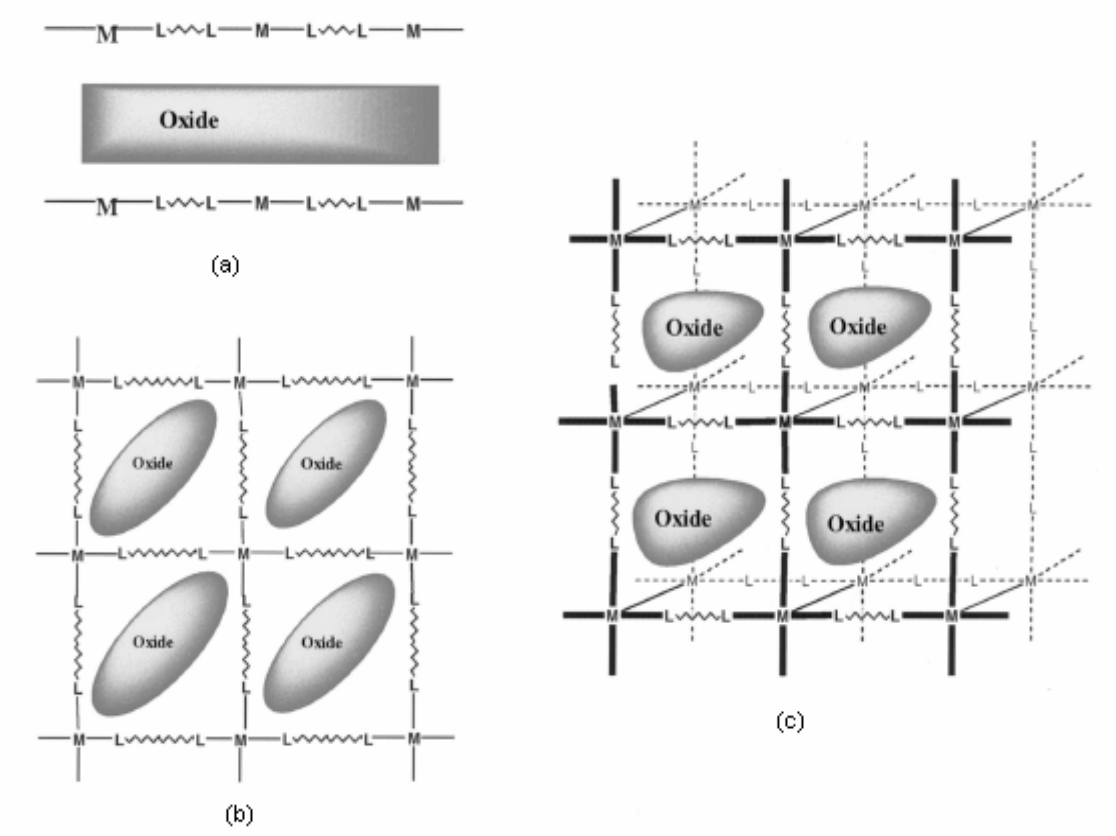

Figure 3.6. Schematic views of metal oxide substructures entrained in one-, two-, and three-dimensional coordination complex cation polymers
(Source: Chesnut et al. 1999)

Under specific conditions of pH and concentration, the polyoxometalate anions may form spontaneously. Hence, the importance lies in the ligand geometry and the type of the secondary metal center. Variation of the secondary metal site may offer different coordination preferences and several photochemical, electrochemical and reaction properties (Hagrman P.J. et al. 1999).

CHAPTER 4

MOLYBDENUM OXIDES

4.1. Introduction

A new class of materials in which an organic component has an important role in influencing the inorganic molybdenum oxide microstructure is called as organodiamine-templated molybdenum oxides. One strategy for the syntheses of novel organic-inorganic hybrid materials is to introduce a secondary transition metal cation and an organic component, which functions as a ligand, into the molybdenum oxide solids (Lu et al. 2002). The interaction within organic-inorganic hybrid materials derives from the nature of the interface between the organic component and the inorganic oxide (Hagrman D. et al. 1998a). Organic component in these types of materials may function as ligand covalently linked to the inorganic backbone of the solid (Hagrman P.J. and Zubieta 1999). The organic component also adopts the role of charge compensating and space-filling counterion for the negatively charged metal oxide skeleton. There are varieties of structural roles of the organic components of the molybdenum oxide class, including templating, tethering of functional groups, and passivation of metal coordination spheres to produce low-dimensional materials (Hagrman P.J. et al. 1999).

It is clear that even minor changes in hydrothermal reaction conditions give rise to structural diversity. Zubieta and other researches have reported different types of molybdenum oxide subunits such as $\{MoO_4\}^{2-}$, $\{Mo_2O_7\}^{2-}$, $\{Mo_3O_{10}\}^{2-}$, $\{Mo_4O_{13}\}^{2-}$, $\{Mo_6O_{19}\}^{2-}$, $\{Mo_8O_{26}\}^{2-}$, $\{Mo_8O_{28}\}^{6-}$, $\{Mo_{14}O_{45}\}^{6-}$, and $\{Mo_{15}O_{47}\}^{4-}$, in which $\{MoO_4\}$, $\{MoO_6\}$ or $\{MoO_5\}$ polyhedra connect together via corner-, edge-, or face-sharing modes (Hagrman P.J. et al. 1999).

Organodiamine templated molybdenum oxides have been divided into three subclasses according to the role of the organodiamine as a protonated cation, as a ligand to a molybdenum site of the oxide array, or as a ligand to a heterometallic site which may be part of a cationic coordination polymer or simply a mononuclear site associated with the molybdenum oxide array (Hagrman P.J. et al. 1999).

4.1.1. Organoammonium-Molybdenum Oxide Phases

Materials in which the organic subunit serves as organoammonium cation have 1D structures. The only example of a 2D organically templated molybdenum oxide of this subclass is represented in Figure 4.1 (Zapf et al. 1997c). Edge- and corner-sharing $\{MoO_6\}$ octahedras produce a stepped 2D motif. In this structure the molybdenum oxide layers are separated by $(4,4'\text{-}H_2bpy)^{2+}$ cations and H_2O molecules of crystallization. Each Mo in $\{MoO_6\}$ has three triply bridging, two doubly bridging and one terminal oxo group. The organic cations and the water molecules are placed in the interlamellar region and participate in strong multipoint hydrogen bonding to each other and to the terminal oxo groups of the layer. This structure is a good example of the role of organic cations in influencing oxide structure (Zapf et al. 1997c).

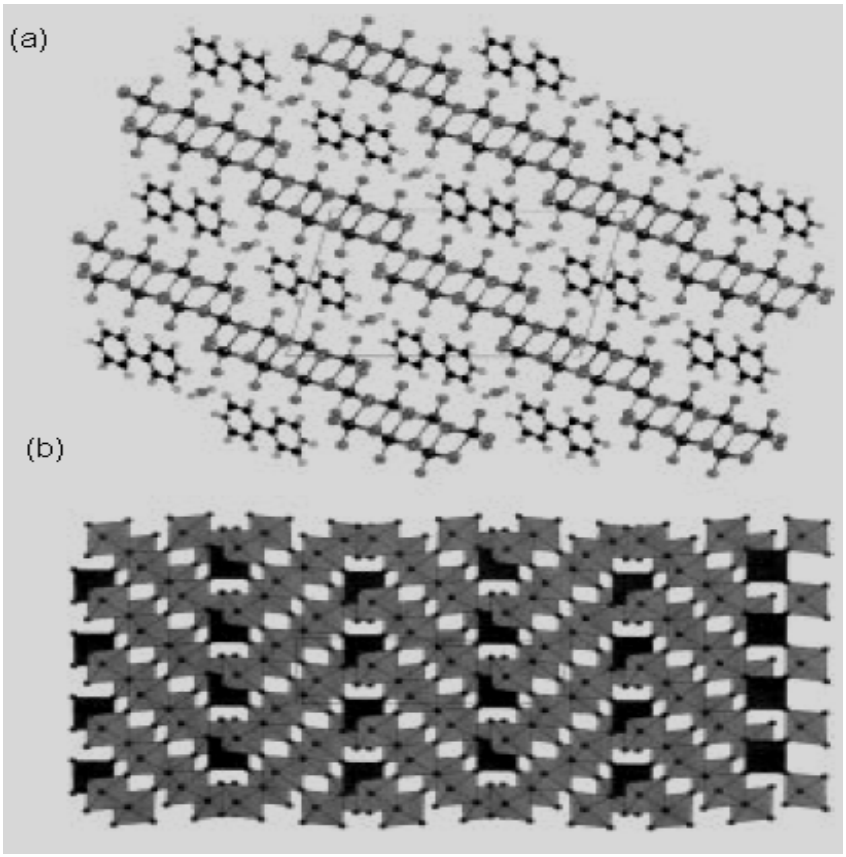

Figure 4.1. a) The stepped layer structure of $[4,4'\text{-}H_2bpy][Mo_7O_{22}]\cdot H_2O$ b) A view normal to the oxide layer. The darkened polyhedra indicate the positions of the dislocations that give rise to the steps

(Source: Zapf et al. 1997c)

4.1.2. Organodiamines as Ligands to the Molybdenum Oxide Array

The rodlike 4,4'-bipyridine group may serve as a ligand, rather than as a cationic component which is illustrated in Figure 4.1. $[MoO_3(4,4'\text{-bpy})_{0.5}]$ was synthesized by raising the pH of the reaction to prevent protonation of the pyridyl nitrogens (Hagrman P.J. et al. 1999). In this structure the layers of corner-sharing $\{MoO_5\}$ square pyramids are linked through 4,4'-bipyridyl groups into a 3D covalently bonded framework. This structure can be described in terms of alternating inorganic metal oxide layers and aromatic organic layers. The distorted $\{MoO_5N\}$ at each molybdenum site is defined by a terminal oxo group, four asymmetrically bridging oxo groups, and a pyridyl nitrogen donor which are the typical 2 short- 2 intermediate-2 long bond length geometry common to molybdenum oxides (Hagrman P.J. et al. 1999).

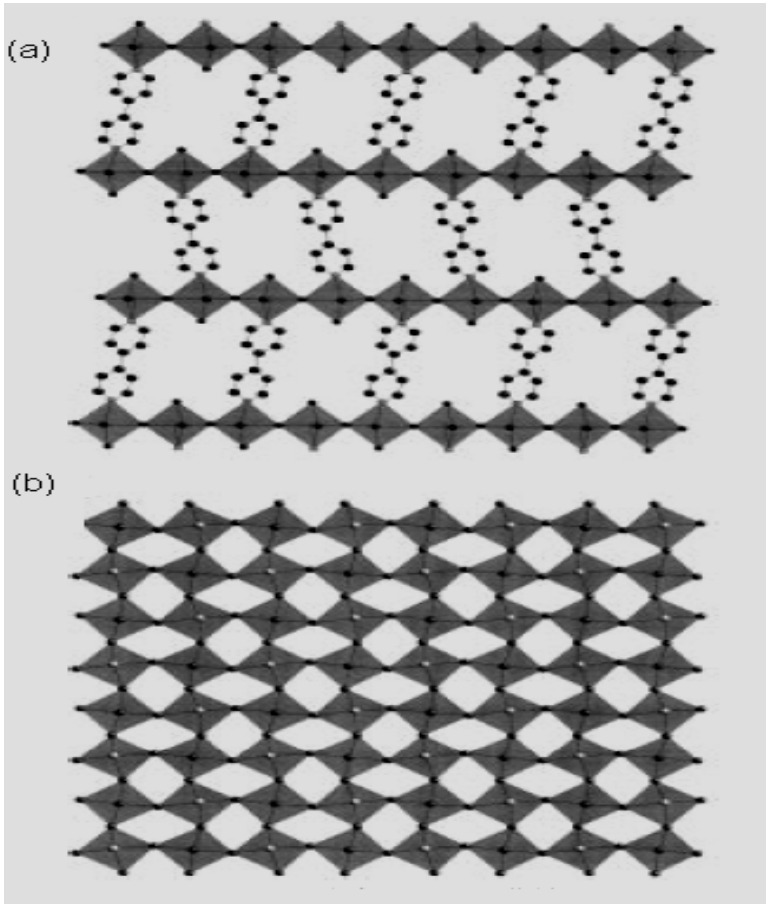

Figure 4.2. The structure of $[MoO_3(4,4'\text{-bpy})_{0.5}]$ a) showing the linking of layers by 4,4'-bpy ligands b) a view normal to the layer
(Source: Hagrman P.J. et al. 1999)

4.1.3. Molybdenum Oxide Phases Containing Organodiamine-Ligated Heterometals

In this classification three subgroups are identified according to the dimensionality of the molybdenum array and to the dimensionality of the M'-Mo-O array. In the first class, discrete molybdenum oxide polyanion clusters are linked by heterometal-diamine coordination complexes or polymers into higher dimensionals. In the second class, one-dimensional molybdenum oxide chains are linked by heterometal-diamine coordination polymers into complex structures. In the third class, one-, two-, and three-dimensional arrays of mixed molybdenum oxide-heterometal-diamine polyhedras join together (Hagrman P.J. et al. 1999).

4.1.3.1. Solids Constructed from Discrete Molybdenum Oxide Clusters

The structure of $[\{Cu(pca)\}_2Mo_8O_{26}]$ is a two dimensional network and contains β-$[Mo_8O_{26}]$ cluster, linked through $\{Cu(pca)\}^{2+}$ subunits. Each molybdate cluster is linked through six (Mo=O) molybdenyl oxo-groups to four $\{CuN_3O_3\}$ octahedras. The metal-oxygen connectivity pattern produces 24-membered $\{Cu_4Mo_8O_{12}\}$ rings (Rarig and Zubieta 2002).

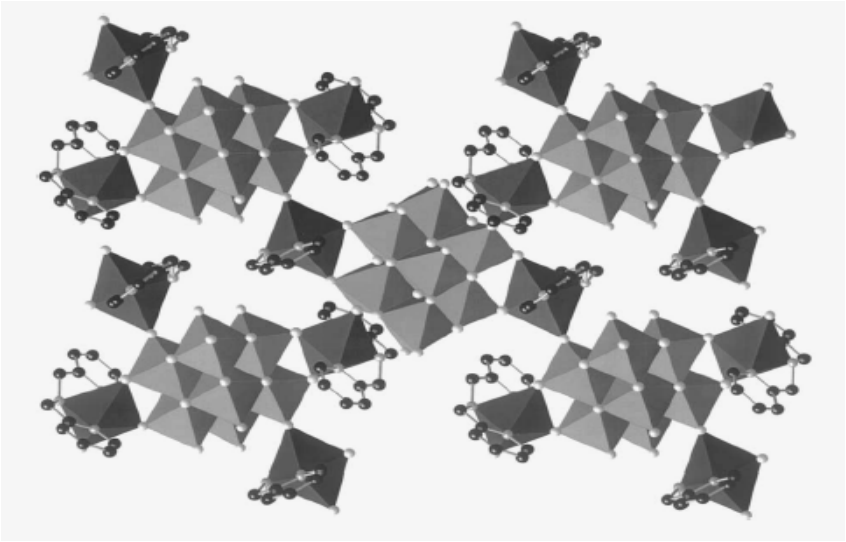

Figure 4.3. A view of network structure of $[\{Cu(pca)\}_2Mo_8O_{26}]$
(Source: Rarig and Zubieta 2002)

4.1.3.2. Solids Exhibiting One-Dimensional Molybdenum Oxide Arrays

The structure of $[Cu_2(pyrd)Mo_3O_{10}]$ can be given as an example of this subclass. The structure is constructed from $\{MoO_6\}$ octahedra and $\{CuO_3N\}$ tetrahedra. In this structure 1D chains of edge-sharing $\{MoO_6\}$ octahedras are linked through $\{Cu_2(pyrd)\}$ groups into a 3D covalent framework. As shown in Figure 4.4, $\{MoO_6\}$ octahedra forms a chain of edge-sharing polyhedra (Hagrman D. et al. 1998b).

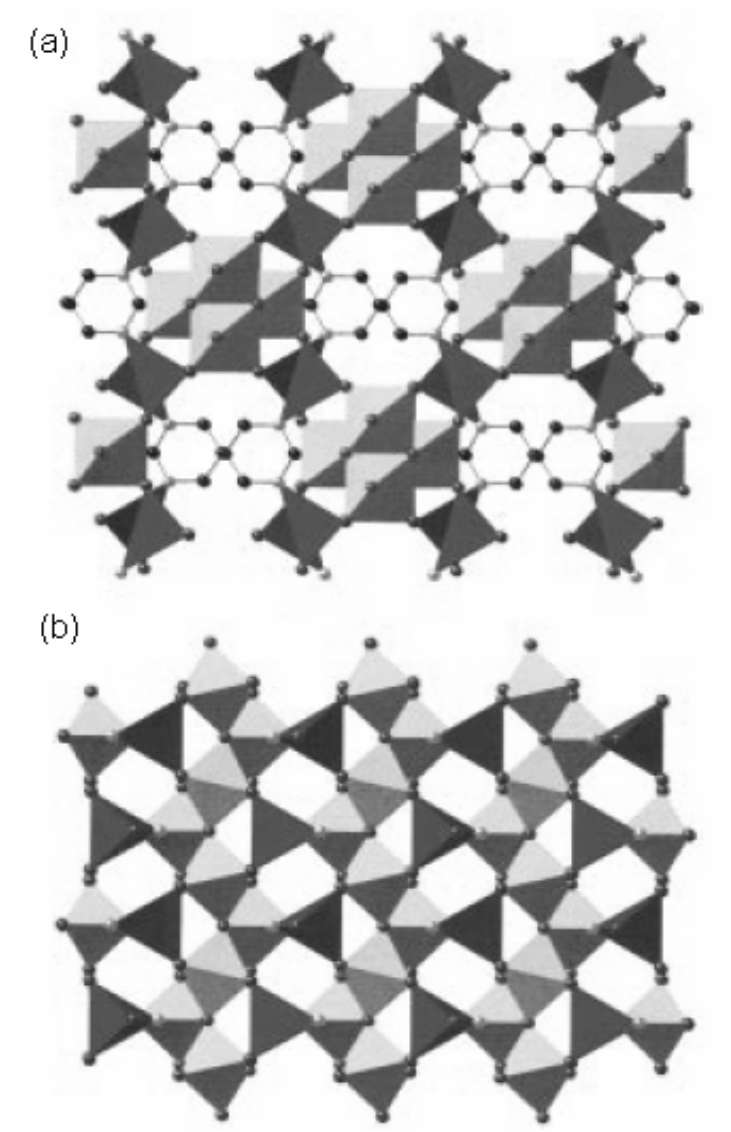

Figure 4.4. a) A view of the structure of $[Cu_2(pyrd)Mo_3O_{10}]$ to show the channels occupied by the pyrimidine groups. b) The linking of $\{Mo_3O_{10}\}^{2-}$ chains by $\{Cu(pyrd)\}$ bridges

(Source: Hagrman D. et al. 1998b)

4.1.3.3. Solids Constructed from Isolated $[MoO_4]^{2-}$ and $[Mo_2O_7]^{2-}$ Units Fused to Bridging Heterometal-Diamine Units

These types of solids are distinguished by the absence of Mo-O-Mo bridging interactions or limitation to a single Mo-O-Mo bridge unit and the structure grows through M'-O-Mo linkages (Hagrman P.J. et al. 1999).

As shown in Figure 4.5 2D $\{CuMoO_4\}$ subunits are linked by bpa ligands into a 3D covalent framework. The inorganic layer is constructed from $\{MoO_4\}$ tetrahedra and $\{CuO_5N\}$ octahedra. These polyhedras form double chains linked through {Cu-O-Mo} bridges into a 2D network.

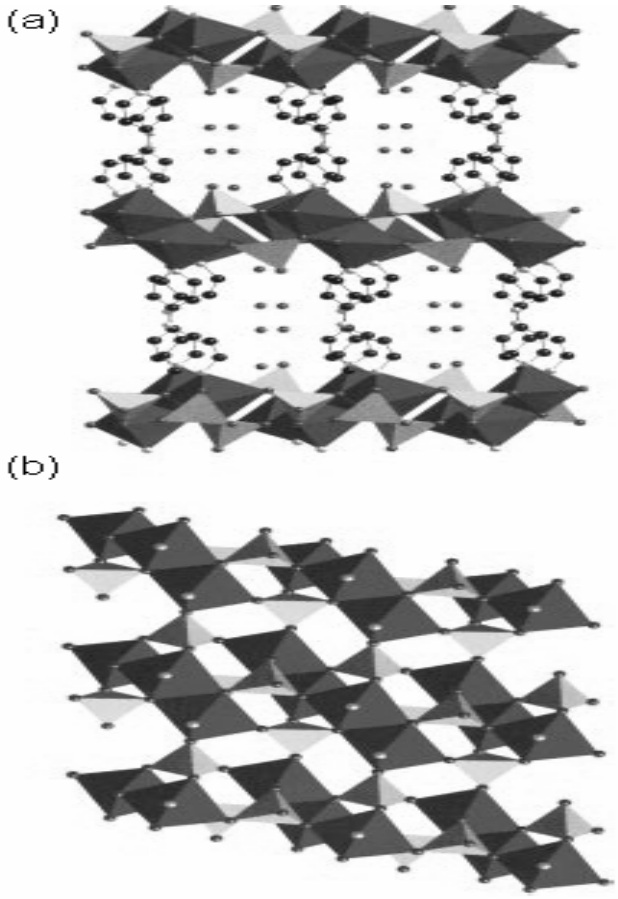

Figure 4.5. a) A view of the covalently linked three-dimensional structure of ($[Cu(bpa)_{0.5}(MoO_4)]$), showing the ligand bridging of $\{CuMoO_4\}$ layers b) The $\{CuMoO_4\}$ layer structure of the compound

(Source: Hagrman D. et al. 1998b)

Representative examples known up to date of this subclass includes [Cu(3,3'-bpy)$_{0.5}$MoO$_4$], [Cu(4,4'-bpy)$_{0.5}$MoO$_4$]·1,5H$_2$O (Rarig et al. 2002), [Cu(4,4'-bpy)]$_2$MoO$_4$·2H$_2$O (Lu et al. 2002), [Cu(4,4'-bpy)MoO$_4$] (Fang et al. 2006), [Cu(dpe)MoO$_4$] (Hagrman D. et al. 1998c), [Cu(bpa)$_{0.5}$MoO$_4$], [Cu(pyz)$_{0.5}$MoO$_4$] (Hagrman D. et al.1998a), [Cu(o-phen)MoO$_4$]·H$_2$O (Hagrman P.J. and Zubieta 1999), [Cu(3,4'-bpy)MoO$_4$] (Rarig et al. 2002), [Cu(terpy)MoO$_4$]·3H$_2$O (Hagrman P.J. and Zubieta 2000) and [Cu$_2$(bisterpy)(MoO$_4$)$_2$] (Koo et al. 2003). A novel compound of this subclass [Cu(en)MoO$_4$] has been synthesized in our laboratory.

In general, the structures of organodiamine-templated molybdenum oxides exhibit one- and two-dimensional structures and this observation is consisted with the general occurrence of low-dimensional structures in the inorganic molybdenum oxide chemistry. Although the number of examples is too limited for general conclusions, it can be said that organodiammonium cations with alkyl backbones favor 1D structures, while those with aromatic linkers favor layered network structures (Hagrman P.J. et al. 1999).

Organodiamine groups that are directly binded to the molybdenum oxide skeleton passivate the oxide surface, which result in low-dimensionality oxide substructures. Chelating bipyridyl ligands (2,2'-bpy) block two coordination sites of the same metal center and passivate the metal toward oxide bridging in more than 1D. When the ligand geometry allow a bridging modality on the nitrogen donors, more complex structures such as the hydrogen-bonded sheetlike structures ([Mo$_4$O$_{13}$(Hbpa)$_2$]) (Zapf et al. 1998b) and the 2D molybdenum oxide structures ([MoO$_3$(4,4'-bpy)$_{0.5}$] (Hagrman P.J. et al. 1999) are observed.

A primitive degree of design and predictability have been achieved for the synthesis of organodiamine-templated molybdenum oxides materials. Such composite materials are complex and this complexity limits the degree of predictability.

Many chemical possibilities such as the roles of ligand geometries and heterometal coordination preferences, pH value, stoichiometries, temperature, and filling volume are important in the evolution of organodiamine-templated molybdenum oxides (Hagrman P.J. et al. 1999).

4.2. Experimental Procedure

The aim of this thesis was to synthesize novel metal oxide compounds, which include molybdenum oxide, secondary transition metal and organic component, as single crystal by hydrothermal method. After the synthesis procedures, the structures of the obtained crystals were solved by SHELX software by using the data which were obtained from the single crystal x-ray diffractometer.

Up to now various organodiamine ligands have been introduced into the copper molybdate family, such as 3,3'-bipyridine (3,3'-bpy), 4,4'-bipyridine (4,4'-bpy), 3,4'-bipyridine (3,4'-bpy), o-phenanthroline (o-phen), 1,2-trans-(4-pyridyl)ethene (dpe), bipyridylamine (bpa), and pyrazine (pyz). Ethylenediamine (en) was rarely introduced into copper molybdate family. To our knowledge $[Cu(en)_2]_2[Mo_8O_{26}]$ (DeBord et al. 1997) is the only reported example which was also synthesized in our laboratory under different synthesis conditions. In this study the second example of the ethylenediamine containing copper molybdate, $[Cu(en)MoO_4]$, was also reported.

4.2.1. Synthesis and Characterization of $[Cu(en)MoO_4]$

The novel compound $[Cu(en)MoO_4]$ (en:ethylenediamine, $NH_2CH_2CH_2NH_2$) was synthesized in aqueous solution and the structure of this compound was solved using SHELX software. In this section the synthesis and structural characterization of $[Cu(en)MoO_4]$ were reported.

4.2.1.1. Synthesis of the Novel Compound $[Cu(en)MoO_4]$

Blue rod-like single crystals of $[Cu(en)MoO_4]$ were obtained from the reaction of $Na_2MoO_4{\cdot}2H_2O$ (1 mmol, 0.2420 g), $CuCl_2{\cdot}2H_2O$ (2 mmol, 0.3410 g), NaCl (1 mmol, 0.0585 g), ethylenediamine (3 mmol, 0.2 mL) and H_2O (500 mmol, 9 mL). $Na_2MoO_4{\cdot}2H_2O$ (Carlo Erba, 99.5%), $CuCl_2{\cdot}2H_2O$ (Sigma, 99.6%), NaCl (Merck, >99%) and ethylenediamine (Merck, >99%) were used without further purification.

The reaction mixture was loaded into a 23 mL Teflon-lined autoclave. Nine mL (40% fill) of distilled water was added to the mixture to obtain hydrothermal synthesis

conditions. The Teflon-lined autoclave was placed into an acid digestion bomb and then put into the oven. The reaction was heated at 170°C for 3 days and then slowly cooled to room temperature.

After cooling, the product was filtered, washed with distilled water and acetone several times, and then dried in air at room temperature. Blue rod-like crystals were obtained in approximately 90% yield as reaction products. The reactants were mixed in a (1:2:1:3:500) mole ratio.

$$Na_2MoO_4{\cdot}2H_2O + CuCl_2{\cdot}2H_2O + NaCl + NH_2CH_2CH_2NH_2 + H_2O \xrightarrow[3\ \text{days}]{170°C} [Cu(en)MoO_4]$$

Similar reactions were tried with different mole ratios such as: (1:2:2:3:500), (2:2:2:3:500), (1:2:0:3:500). The same product with different yields was obtained by these reactions. The best yield was obtained from the reaction with (1:2:1:3:500) mole ratios.

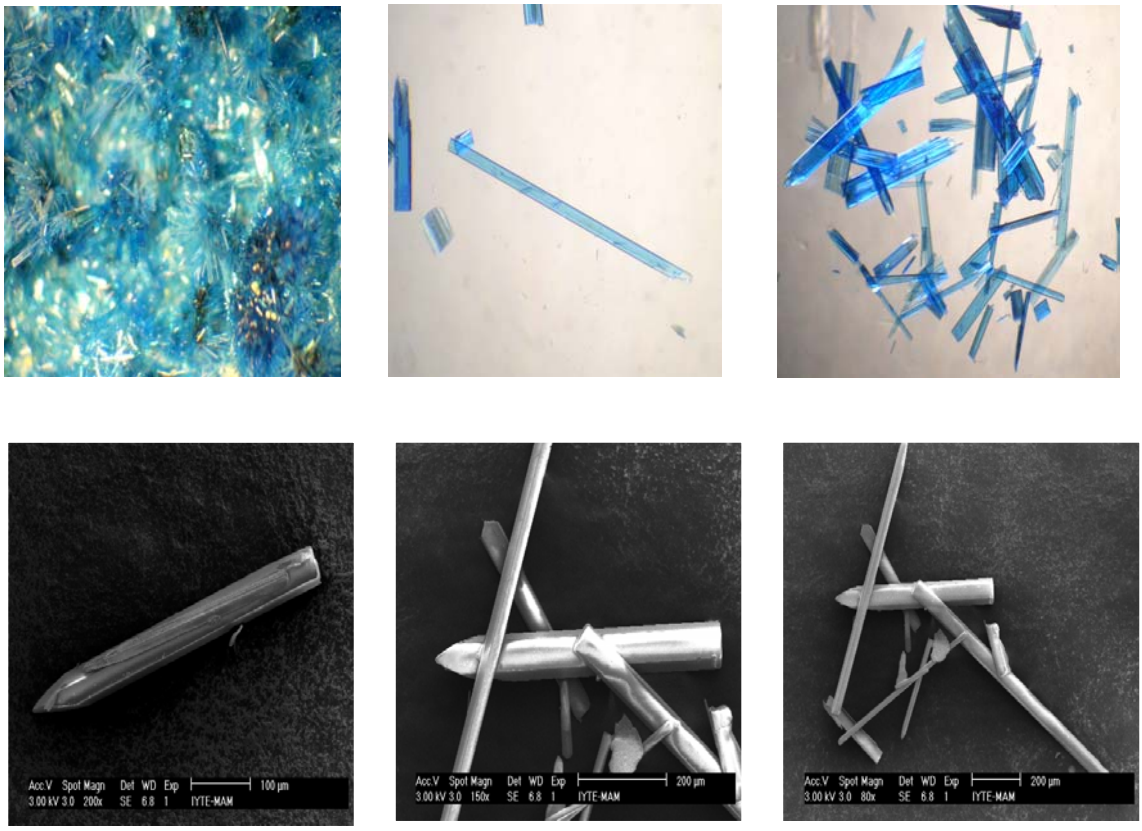

Figure 4.6. Stereomicroscope and SEM images of $[Cu(en)MoO_4]$

The SEM/EDX results of the blue rod-like crystals are illustrated in Figure 4.7. According to these results, the obtained product contained molybdenum, copper, oxygen, carbon and nitrogen elements in the atomic percentages of 6.23%, 6.73%, 28.95%, 36.99%, and 20.44%, respectively.

Table 4.1. EDX results of [Cu(en)MoO_4]

Element	**Weight %**	**Atomic %**
Molybdenum	26.66	6.23
Copper	19.07	6.73
Oxygen	20.67	28.95
Carbon	19.82	36.99
Nitrogen	12.77	20.44

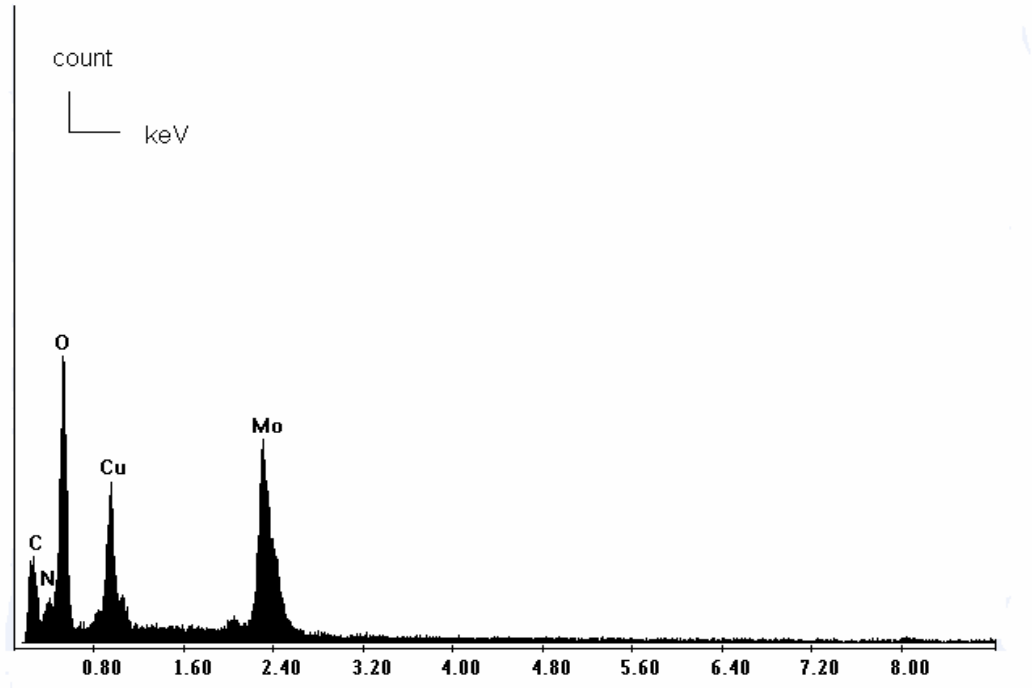

Figure 4.7. SEM EDX peaks of [Cu(en)MoO_4]

The synthesized product was analyzed by powder X-ray diffraction. X-ray powder peaks of the synthesized compound did not matched with any compound in the XRD database.

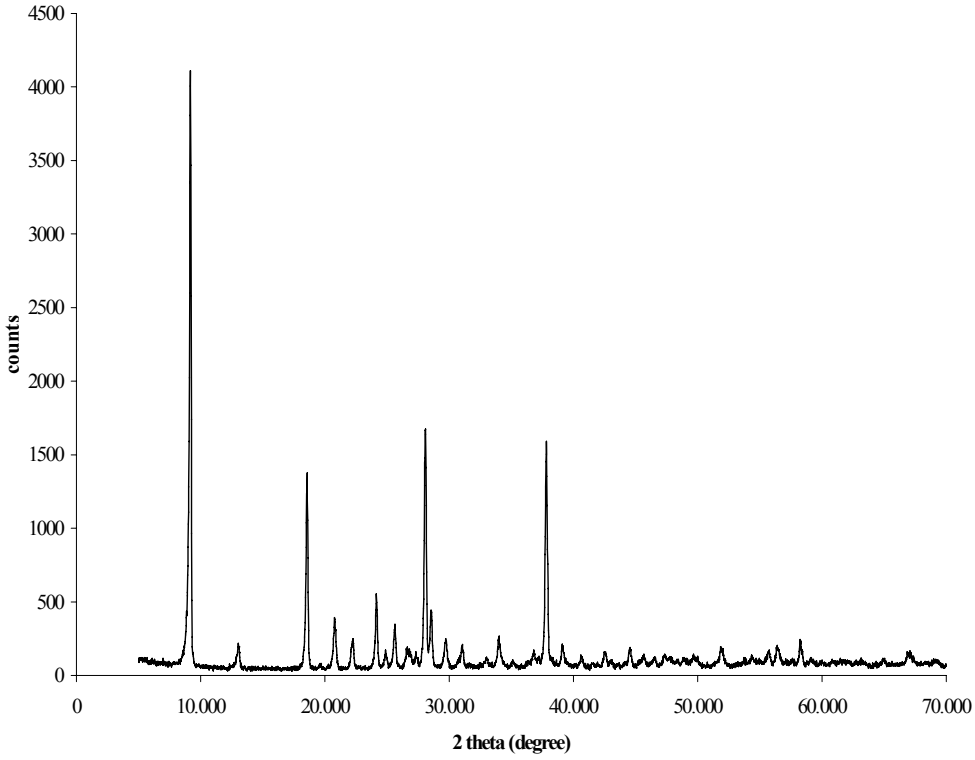

Figure 4.8. Powder patterns of [Cu(en)MoO_4]

4.2.1.2. X-ray Crystallographic Analysis

A single crystal of [Cu(en)MoO_4] with approximate dimensions of 0.41 x 0.06 x 0.02 mm was mounted on a glass fiber with epoxy glue and centered on a Rigaku AFC8 diffractometer equipped with a Mercury CCD area detector. The unit cell parameters and the orientation matrix were based on the centroids of 1345 reflections with I>5 sigma (I) (Steller et al. 1997). Reflection indexing, Lorentz-polarization correction, peak integration, and background determination were performed using the *Crystal Clear* software (Rigaku Corp. 2001).

An empirical absorption correction was applied using a REQABA (Jacobson 1998) routine in the *Crystal Clear* software package. The structure was solved by direct methods with the program SHELXS (Sheldrick 1997) and refined full-matrix least-squares techniques with the program SHELXL (Sheldrick 1997) in the Crystal Structure software.

Crystallographic data are given in Table 4.2. Bond lengths (Å) and bond angles (degree) for [Cu(en)MoO_4] are given in Table 4.3. Final values of the atomic coordinates and isotropic displacement parameters are given in Table 4.4.

Table 4.2. Crystallographic data for $[Cu(en)MoO_4]$

Formula	$[Cu(en)MoO_4]$	
Formula weight	283.58	
Crystal system	monoclinic	
Space group	P2(1)/c	
Cell formula units, Z	4	
Description	Blue rod-like crystal	
Unit cell dimensions	a = 9.9538(2) Å	α = 90°
	b = 9.4364(19) Å	β = 107.734(3)°
	c = 7.6743(15) Å	γ = 90°
Volume ($Å^3$)	686.6 (2)	
Wavelength (Å)	0.71073	
Temperature (K)	293 (2)	
Dcalc, ($g \cdot cm^{-3}$)	2.058	
$R_1(wR_2)$	0.0722(0.0853)	
Limiting indices	$-11 \leq h \leq 12$, $-11 \leq k \leq 11$, $-9 \leq l \leq 9$	
Extinction coefficient	0.0007(5)	
F (000)	411	
Absorption coefficient, μ (mm^{-1})	3.660	
Theta range for data collection	3.05 to 26.02°	

Table 4.3. Bond lengths (Å) and bond angles (degree) for [Cu(en)MoO_4]

Mo(1)-O(2)	1.738(8)	Cu(2)-O(1)	2.575(9)
Mo(1)-O(3)	1.740(8)	Cu(2)-N(2)	2.011(9)
Mo(1)-O(4)	1.786(7)	Cu(2)-N(1)	2.019(9)
Mo(1)-O(1)	1.804(7)	N(1)-C(1)	1.467(13)
Cu(2)-O(1)	1.947(7)	N(2)-C(2)	1.470(13)
Cu(2)-O(4)	1.953(8)	O(4)-Cu(2)	1.953(8)
Cu(2)-O(3)	2.458(8)	C(2)-C(1)	1.508(15)
O(2)-Mo(1)-O(3)	109.1(4)	O(1)-Cu(2)-N(1)	92.9(3)
O(2)-Mo(1)-O(4)	109.3(4)	O(4)-Cu(2)-N(1)	170.3(3)
O(3)-Mo(1)-O(4)	109.4(4)	N(2)-Cu(2)-N(1)	84.8(4)
O(2)-Mo(1)-O(1)	107.8(3)	C(1)-N(1)-Cu(2)	108.0(7)
O(3)-Mo(1)-O(1)	110.8(4)	Mo(1)-O(1)-Cu(2)	130.8(4)
O(4)-Mo(1)-O(1)	110.5(3)	C(2)-N(2)-Cu(2)	107.8(7)
O(1)-Cu(2)-O(4)	88.3(3)	Mo(1)-O(4)-Cu(2)	38.8(4)
O(1)-Cu(2)-N(2)	177.3(3)	N(2)-C(2)-C(1)	106.4(9)
O(4)-Cu(2)-N(2)	94.2(4)	N(1)-C(1)-C(2)	109.3(9)

Table 4.4. Atomic coordinates and equivalent isotropic thermal parameters for [Cu(en)MoO_4]

Atom	**x**	**y**	**z**	**Ueq**
Mo(1)	0.16946(10)	0.89946(10)	0.21945(12)	0.0192(3)
Cu(2)	-0.12238(13)	1.03148(14)	0.30698(18)	0.0209(4)
N(1)	-0.1622(9)	0.8217(9)	0.3084(12)	0.0221(19)
O(1)	0.0784(7)	1.0015(7)	0.3472(9)	0.0212(16)
N(2)	-0.3315(9)	1.0538(10)	0.2589(12)	0.026(2)
O(2)	0.3400(8)	0.8690(9)	0.3609(11)	0.0307(19)
O(3)	0.1772(9)	0.9919(9)	0.0265(11)	0.036(2)
O(4)	0.0830(8)	0.7335(8)	0.1512(10)	0.0265(17)
C(2)	-0.3987(10)	0.9180(11)	0.1886(15)	0.024(2)
C(1)	-0.3092(11)	0.8040(13)	0.3062(17)	0.032(3)

4.2.1.3. Results and Discussion

The title compound, [Cu(en)MoO_4], was hydrothermally synthesized from the reaction of $Na_2MoO_4 \cdot 2H_2O$, $CuCl_2 \cdot 2H_2O$, NaCl and ethylenediamine. The hydrothermal reaction of the reactants led to the formation of the title compound as blue rod-like crystals. Coordination between the atoms is shown in Figure 4.9.

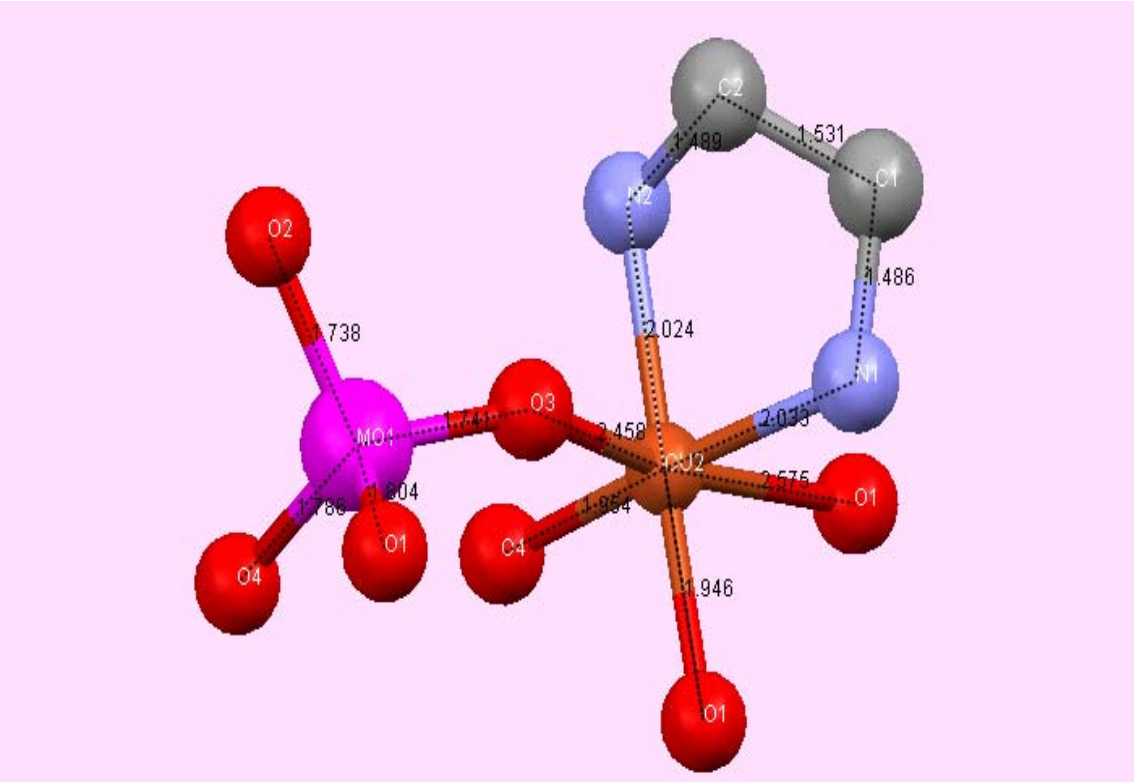

Figure 4.9. Coordination between the atoms

The structure is composed of {CuN_2O_4} octahedra and {MoO_4} tetrahedra. The octahedral coordination environment of Cu(2) atom is defined by 2 nitrogen atoms (N1 and N2) from ethylenediamine ligand with Cu-N distances of 2.019(9) and 2.011(9) Å and four bridging oxygen atoms (O1, O3 and O4) from four adjacent {MoO_4} tetrahedras with Cu-O distances in the range 1.947(7) and 2.575 Å. Mo(1) atom is coordinated by one terminal oxygen atom (O2) with Mo-O bond length of 1.738(8) Å, two doubly bridging (O1 and O4 atoms, μ_2 bridging) and a triply bridging O atom (O1 atom, μ_3 bridging) with Mo-O bond length varying from 1.740(8) to 1.804(7) Å. As expected, all the terminal Mo-O (O2) bond lengths are in the short range, which is

indicative of double bonding (Cui et al. 2005). Each molybdenum atom has one Mo=O double bond and this Mo=O bond length (1.738(8) Å) is comparable to those in molybdenum oxide complexes in the literature(Niven et al. 1991). In Figure 4.10 the connection of $\{MoO_4\}$ tetrahedra and $\{CuN_2O_4\}$ octahedra are shown.

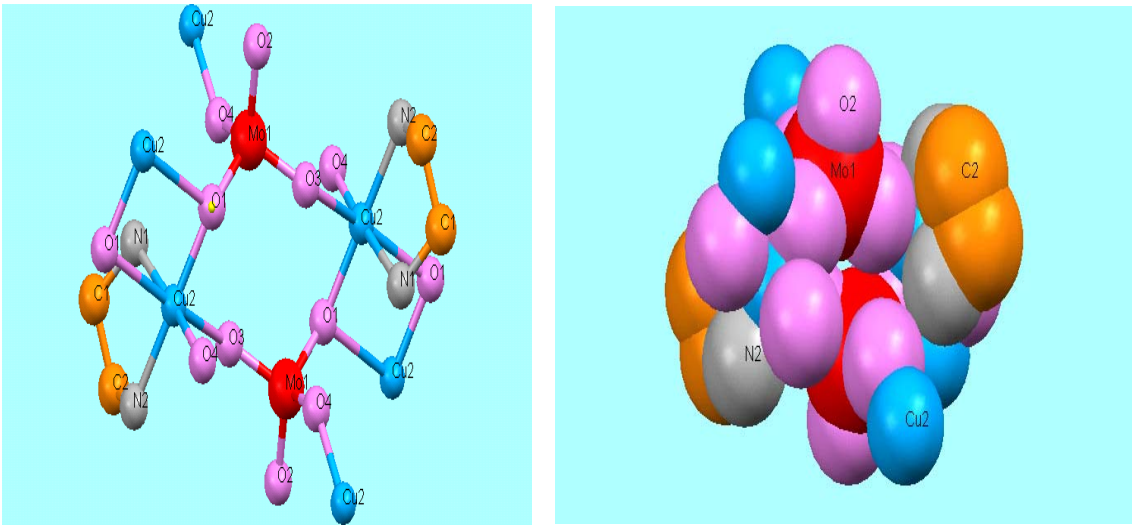

Figure 4.10. Ball and stick and space-filling representations of the connection of MoO_4 tetrahedras and CuN_2O_4 octahedras through b-axis

The extension of the structure can be described as follows: Edge-sharing adjacent $\{CuN_2O_4\}$ octahedras are connected to each other by using O1 atoms and form a binuclear unit through a $\{Cu_2O_2\}$ interaction. These binuclear units are interconnected through bridging $\{MoO_4\}$ tetrahedra to produce a double chain along the c axis. Two adjacent $\{CuN_2O_4\}$ octahedra and two $\{MoO_4\}$ tetrahedra are linked through corner-sharing and form an eight–membered $Cu_2Mo_2O_4$ ring. The 1D chains are linked through bridging O4 atoms, that bind copper and molybdenum atoms, to form 2D layers of the structure.

Consequently, each Cu atom forms three corner-sharing linkages to neighboring Mo atoms of the chain and one to a Mo atom of an adjacent chain, along with one edge-sharing linkage in a Cu binuclear unit. Each Mo atom bridges three Cu binuclear units and a terminal oxo group directed into the interlamellar region. In the $Cu_2Mo_2O_4$ ring of the chains, the two terminal oxo groups of the $\{MoO_4\}$ tetrahedra are oriented toward opposite sides of the plane of the ring defined by the four metal atoms.

The unit cell of the structure is composed of two 2D layers. The shortest distance between two molybdenum atoms which are placed in different layers is 8.471 Å, and that is 8.901 Å for two copper atoms. The layered structure can be seen from b and c directions. Ball and stick representation of the unit cell is shown in Figure 4.11 in which layer structure of the title compound can be seen clearly. In Figure 4.12 polyhedral representation of the unit cell from a direction is illustrated.

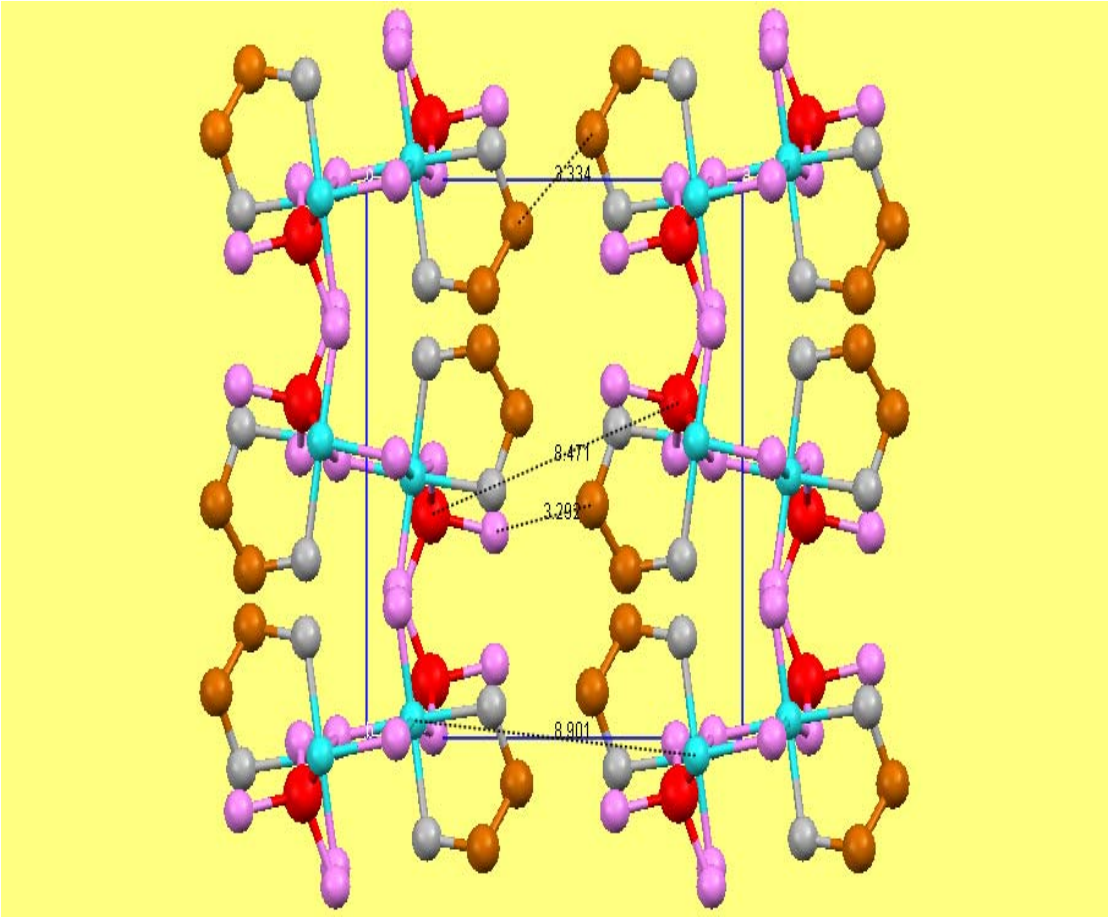

Figure 4.11. Unit cell view of [Cu(en)MoO_4] through c-axis

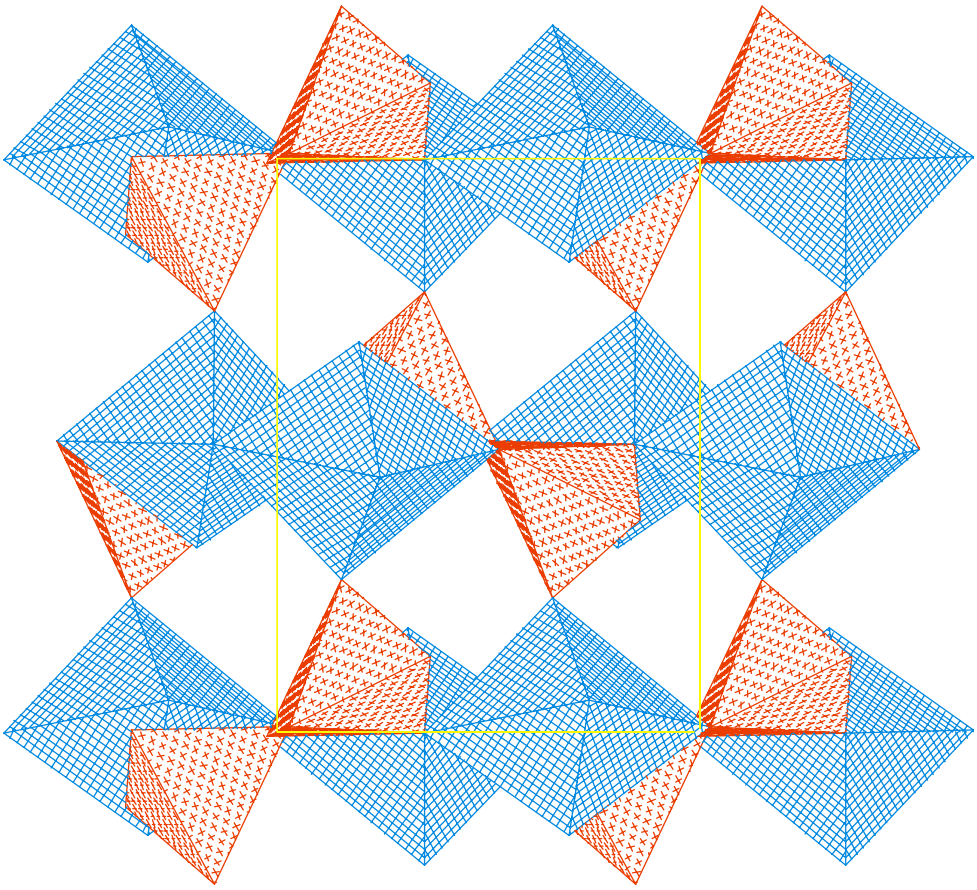

Figure 4.12. Polyhedral representation of [Cu(en)MoO_4] along the a-axis

The +6 oxidation state of the Mo atom is confirmed by bond valance sum calculations ($\sum$ s(M-L) = $\sum$ exp [(r_o-r)/0.37]), where s is defined as the individual bond valance, r_o is the empirically derived single M-L bond distance (r_o=1.907(2) Å for Mo^{6+}-O bond) (Brown and Altermatt 1985) and r represents the bond distances in the structure (Mo-O bond length from Table 4.3). The results showed that the s value for Mo(1) atom is 5.86(11) which was consistent with the formula of the title compound acquired from X-ray analysis.

The +2 oxidation state of the Cu atom is also confirmed by valance sum calculations. Here r_o=1.679(2) Å for Cu^{2+}-O bond and 1.747 Å for Cu^{2+}-N bond. The s value for the Cu atom was found 1.94(4), consistent with the formula of the compound.

The infrared spectrum of [Cu(en)MoO_4], which is shown in Figure 4.13, was recorded as a KBr pellet in the frequency range of 400-4000 cm^{-1}. The IR spectrum of the compound exhibits characteristic bands of the ethylenediamine ligand in the 987-3317 cm^{-1}. Peaks between 3132 and 3317 cm^{-1} are due to υ(N–H), peaks between 2881

and 2982 cm^{-1} are due to υ(C–H), peaks between 1577 and 1651 cm^{-1} are due to δ(N–H), peaks between 1280 and 1458 cm^{-1} are due to δ(C–H) and peaks between 987 and 1234 cm^{-1} are due to δ(C–N) (Millange et al. 2004). The peak in 902 cm^{-1} is attributed to Mo=O stretching, while multiple bands attributed to the bridging (Mo-O-Mo(Cu)) groups' absorptions are found in the 435-864 cm^{-1} region (Wu et al. 2002).

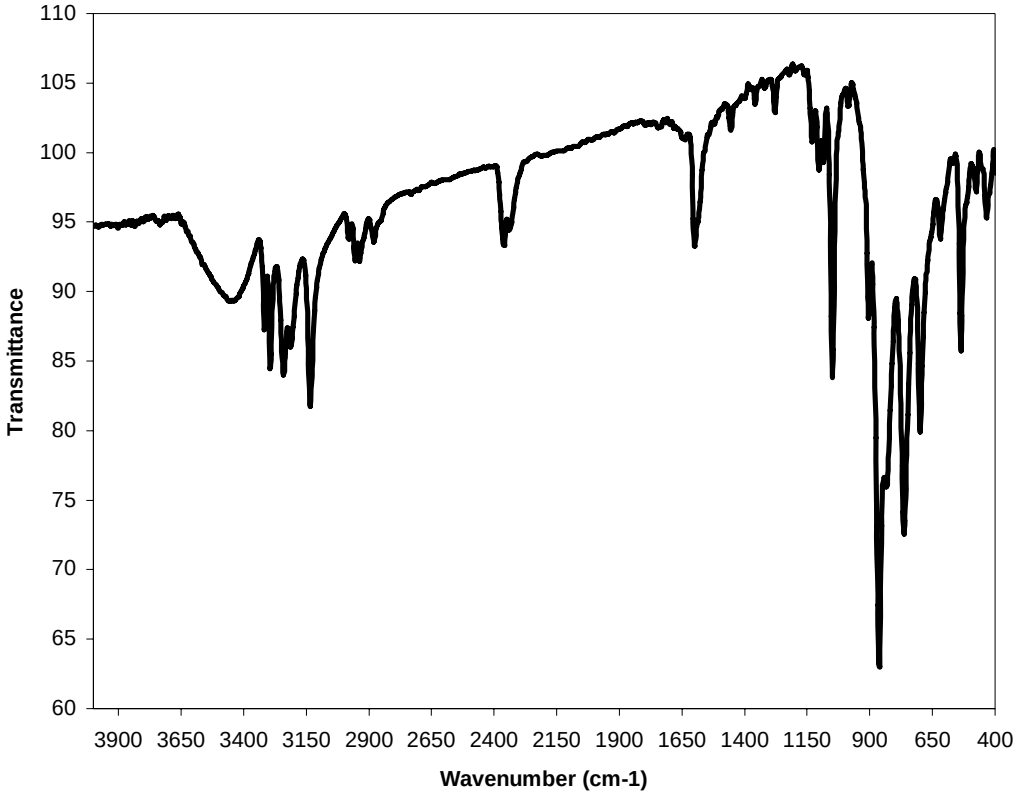

Figure 4.13. Infrared spectrum of [Cu(en)MoO_4]

The thermal behavior of the title compound was studied in the range 25-650°C in nitrogen atmosphere, and the result of the thermogravimetric analysis showed that the compound was stable until 195°C. TG curve exhibited two steps of weight loss. While the first weight loss was 14.61% in the temperature range from 195 to 240°C, the second was 6.78% from 240°C to 450°C (Han et al. 2005). The whole weight loss from 195 to 450°C was summed up to 21.39%, corresponding to removal of the ethylenediamine groups. The observed weight loss (21.39%) was in good agreement with the calculated value (21.15%).

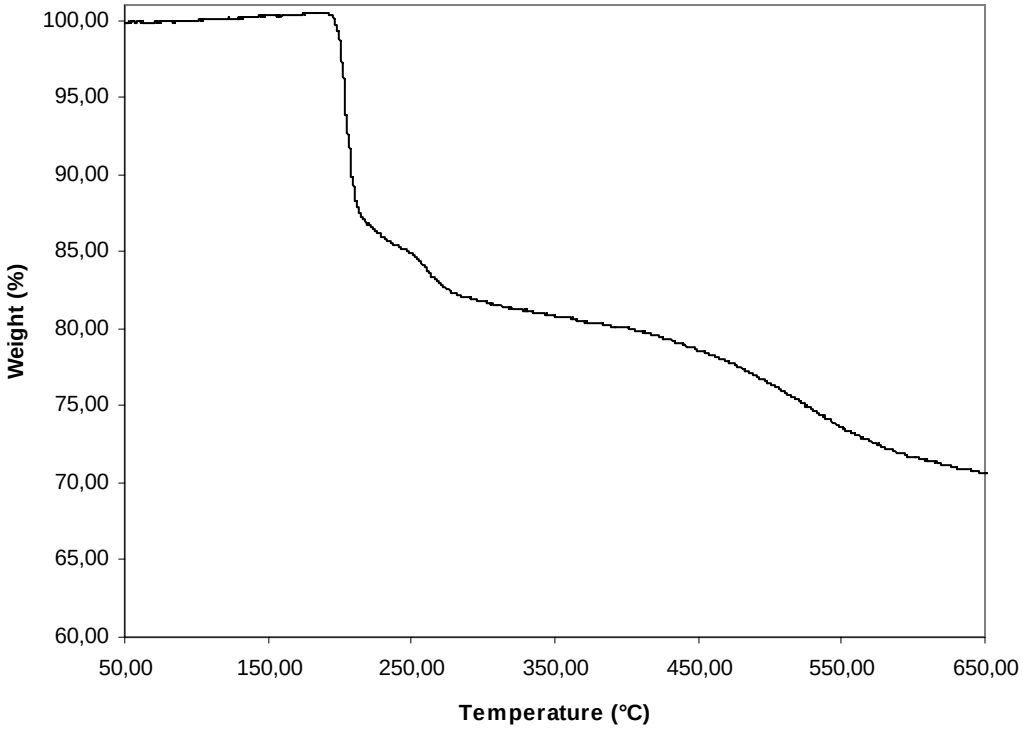

Figure 4.14. TGA curve of [Cu(en)MoO_4]

4.2.2. Synthesis and Characterization of $[Cu(en)_2]_2[Mo_8O_{26}]$

The title compound, $[Cu(en)_2]_2[Mo_8O_{26}]$, has been synthesized by DeBord et al. with different starting materials in 1997 (DeBord et al. 1997). In their work, a mixture of $[Cu(en)_2]Cl_2$, MoO_3 and H_2O in the mol ratio of 1:1:500 was sealed in a borosilicate tube and heated at 150°C for 48 h. Then, shiny purple plates were obtained as reaction product.

In contrast to this work, $[Cu(en)_2]_2[Mo_8O_{26}]$ crystals were synthesized hydrothermally in a Teflon-lined stainless steel autoclave at 170°C for 72 h. in our laboratory and the structure of this compound was solved using SHELX software. In this section the synthesis and structural characterization of this compound are reported.

4.2.2.1. Synthesis of $[Cu(en)_2]_2[Mo_8O_{26}]$

Shiny purple single crystals of $[Cu(en)_2]_2[Mo_8O_{26}]$ were obtained from the reaction of $Na_2MoO_4{\cdot}2H_2O$ (1 mmol, 0.2420 g), $CuCl_2{\cdot}2H_2O$ (2 mmol, 0.3410 g), NH_4Cl (1 mmol, 0.0535 g), ethylenediamine (3 mmol, 0.2 mL) and H_2O (500 mmol, 9 mL). $Na_2MoO_4{\cdot}2H_2O$ (Carlo Erba, 99.5%), $CuCl_2{\cdot}2H_2O$ (Sigma, 99.6%), NH_4Cl (Riedel, >96%) and ethylenediamine (Merck, >99%) were used without further purification.

The reaction mixture was loaded into a 23 mL Teflon-lined autoclave. Nine mL (40% fill) of distilled water was added to the mixture to obtain hydrothermal synthesis conditions. The Teflon-lined autoclave was placed into an acid digestion bomb and then put into the oven. The reaction was heated at 170°C for 3 days and then slowly cooled to room temperature.

After cooling, the product was filtered, washed with distilled water and acetone several times, and then dried in air at room temperature. Shiny purple crystals were obtained as reaction products. The reactants were mixed in a (1:2:1:3:500) mole ratio.

$$Na_2MoO_4{\cdot}2H_2O + CuCl_2{\cdot}2H_2O + NH_4Cl + en + H_2O \xrightarrow[3\ days]{170°C} [Cu(en)_2]_2[Mo_8O_{26}]$$

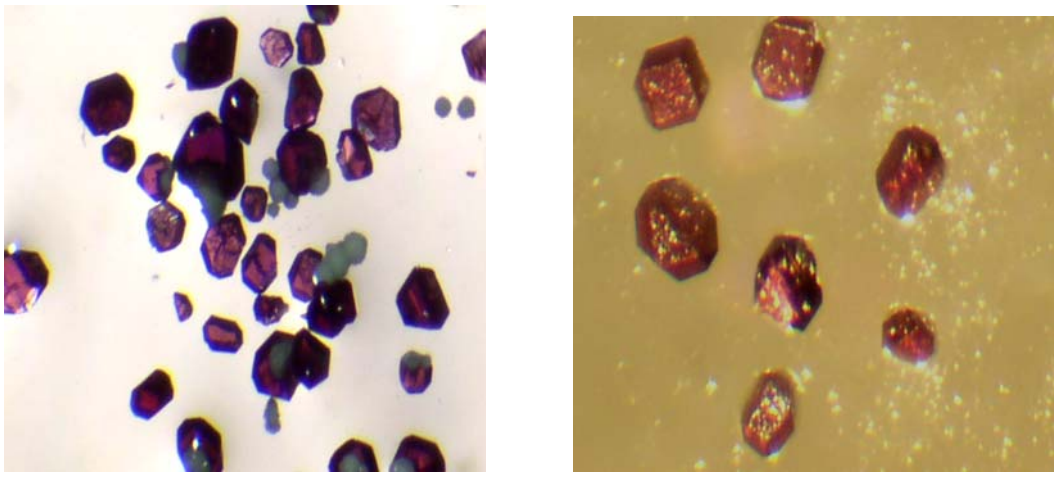

Figure 4.15. Stereomicroscope images of $[Cu(en)_2]_2[Mo_8O_{26}]$

According to SEM EDX analyses, the obtained product contained molybdenum, copper, oxygen, carbon and nitrogen elements in the atomic percentages of 7.43%, 8.17%, 37.92%, 38.71%, and 7.17% respectively. Results of SEM and EDX of the blue rod-like crystals are illustrated in Figure 4.16.

Table 4.5. EDX results of $[Cu(en)_2]_2[Mo_8O_{26}]$

Element	**Weight %**	**Atomic %**
Molybdenum	29.46	7.43
Copper	21.44	8.17
Oxygen	25.06	37.92
Carbon	19.21	38.71
Nitrogen	4.15	7.17

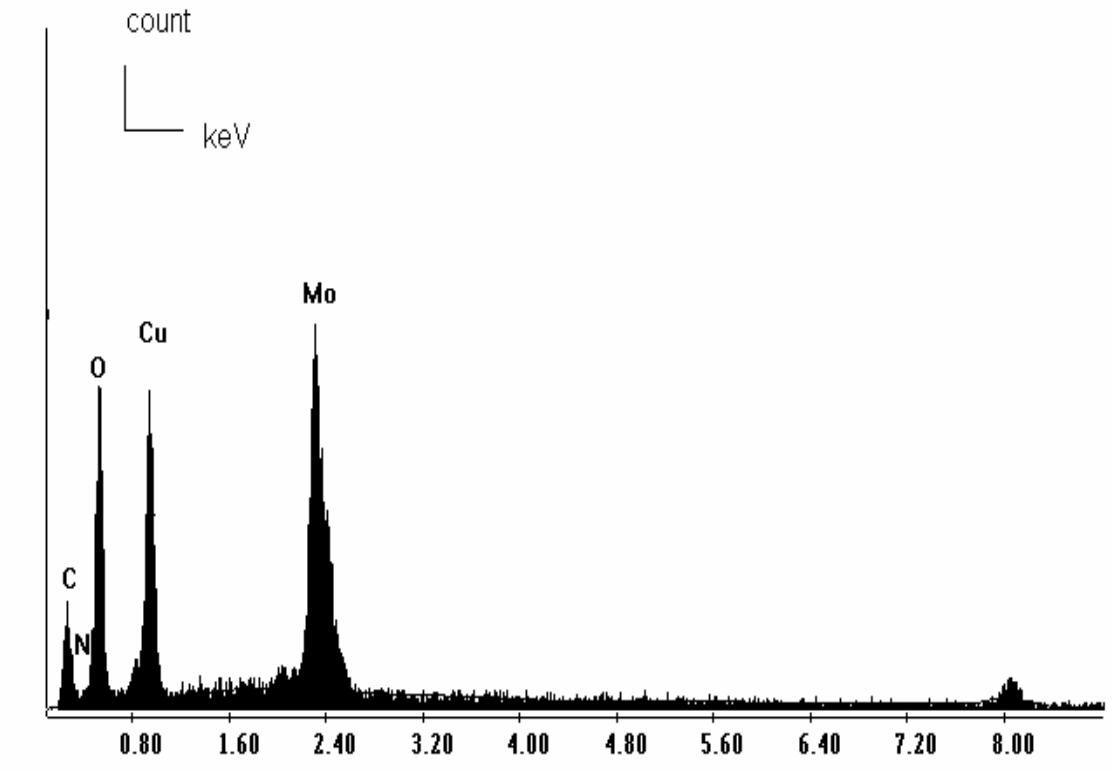

Figure 4.16. SEM EDX peaks of $[Cu(en)_2]_2[Mo_8O_{26}]$

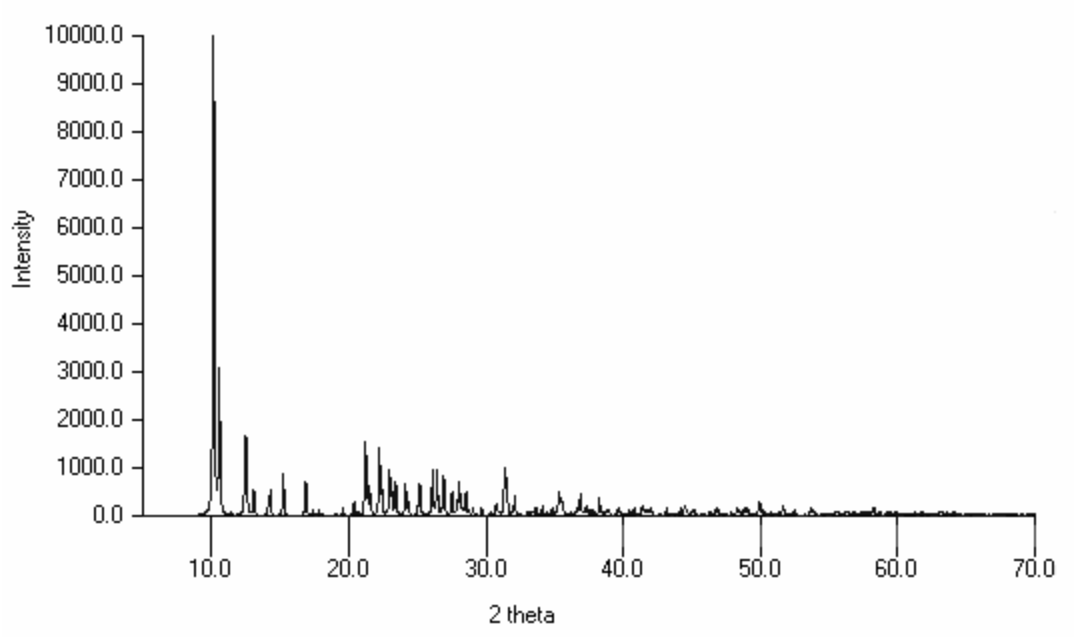

Figure 4.17. Powder patterns of $[Cu(en)_2]_2[Mo_8O_{26}]$

4.2.2.2. X-ray Crystallographic Analysis

A single crystal of $[Cu(en)_2]_2[Mo_8O_{26}]$ was mounted on a glass fiber with epoxy glue and centered on a Rigaku AFC8 diffractometer equipped with a Mercury CCD area detector. The unit cell parameters and the orientation matrix were based on the centroids of 1345 reflections with I>5 sigma (I) (Steller et al. 1997). Reflection indexing, Lorentz-polarization correction, peak integration, and background determination were performed using the *Crystal Clear* software (Rigaku Corp. 2001).

An empirical absorption correction was applied using a REQABA (Jacobson 1998) routine in the *Crystal Clear* software package. The structure was solved by direct methods with the program SHELXS (Sheldrick 1997) and refined full-matrix least-squares techniques with the program SHELXL (Sheldrick 1997) in the Crystal Structure software.

Crystallographic data are given in Table 4.6. Bond lengths (Å) and bond angles (degree) for $[Cu(en)_2]_2[Mo_8O_{26}]$ are given in Table 4.7 and Table 4.8. Final values of the atomic coordinations and isotropic displacement parameters are given in Table 4.9.

Table 4.6. Crystallographic data for $[Cu(en)_2]_2[Mo_8O_{26}]$

Formula	$[Cu(en)_2]_2[Mo_8O_{26}]$
Formula weight	1550.6
Crystal system	orthorhombic
Space group	Pbca
Cell formula units, Z	8
Description	Shiny purple crystals
Unit cell dimensions	a = 13.516(3) Å b = 15.548(3) Å c = 16.725(3) Å
Volume ($Å^3$)	3514.7(12)
Wavelength (Å)	0.71073
Temperature (K)	293 (2)
Dcalc, ($g \cdot cm^{-3}$)	3.046
$R_1(wR_2)$	0.1224 (0.1628)
Limiting indices	$-16 \leq h \leq 16$, $-19 \leq k \leq 19$, $-20 \leq l \leq 20$
F (000)	2944
Absorption coefficient, μ (mm^{-1})	7.505

Table 4.7. Bond lengths (Å) for $[Cu(en)_2]_2[Mo_8O_{26}]$

Mo(1)-O(6)	1.682(13)	Mo(4)-O(1)	1.922(14)
Mo(1)-O(3)	1.726(15)	Mo(4)-O(2)	1.969(16)
Mo(1)-O(4)	1.846(13)	Mo(4)-O(4)	2.194(12)
Mo(1)-O(5)	1.894(13)	Mo(4)-O(5)	2.478(13)
Mo(1)-O(7)	2.277(15)	Cu(5)-N(2)	2.000(18)
Mo(1)-O(5)	2.444(12)	Cu(5)-N(1)	1.988(19)
Mo(2)-O(10)	1.677(13)	Cu(5)-N(3)	2.002(18)
Mo(2)-O(8)	1.709(13)	Cu(5)-N(4)	2.02(2)
Mo(2)-O(1)	1.891(13)	Cu(5)-O(13)	2.436(18)
Mo(2)-O(7)	1.997(13)	O(5)-Mo(2)	2.250(13)
Mo(2)-O(5)	2.250(13)	O(5)-Mo(1)	2.444(12)
Mo(2)-O(3)	2.338(14)	O(5)-Mo(4)	2.478(13)
Mo(3)-O(11)	1.703(14)	N(1)-C(3)	1.49(3)
Mo(3)-O(13)	1.693(17)	N(2)-C(1)	1.51(3)
Mo(3)-O(2)	1.832(15)	N(3)-C(2)	1.47(3)
Mo(3)-O(7)	1.904(13)	N(4)-C(4)	1.51(3)
Mo(3)-O(4)	2.385(14)	C(1)-C(3)	1.49(4)
Mo(4)-O(12)	1.678(16)	C(2)-C(4)	1.56(3)
Mo(4)-O(14)	1.698(15)		

Table 4.8. Bond angles (degree) for $[Cu(en)_2]_2[Mo_8O_{26}]$

O(6) Mo(1) O(3)	105.0(7)	O(14) Mo(4) O(1)	97.9(7)
O(6) Mo(1) O(4)	102.8(6)	O(12) Mo(4) O(2)	93.8(8)
O(3) Mo(1) O(4)	104.6(7)	O(14) Mo(4) O(2)	101.2(7)
O(6) Mo(1) O(5)	105.3(6)	O(1) Mo(4) O(2)	153.4(6)
O(3) Mo(1) O(5)	98.0(7)	O(12) Mo(4) O(4)	154.8(7)
O(4) Mo(1) O(5)	137.7(5)	O(14) Mo(4) O(4)	98.0(7)
O(6) Mo(1) O(7)	93.4(6)	O(1) Mo(4) O(4)	84.6(5)
O(3) Mo(1) O(7)	161.1(6)	O(2) Mo(4) O(4)	74.6(5)
O(4) Mo(1) O(7)	75.1(5)	O(12) Mo(4) O(5)	89.4(7)
O(5) Mo(1) O(7)	72.3(5)	O(14) Mo(4) O(5)	162.8(7)
O(6) Mo(1) O(5)	176.2(6)	O(1) Mo(4) O(5)	72.3(5)
O(3) Mo(1) O(5)	76.1(6)	O(2) Mo(4) O(5)	84.4(5)
O(4) Mo(1) O(5)	73.4(5)	O(4) Mo(4) O(5)	67.6(4)
O(5) Mo(1) O(5)	78.0(5)	N(2) Cu(5) N(1)	85.0(7)
O(7) Mo(1) O(5)	85.8(4)	N(2) Cu(5) N(3)	179.0(8)
O(10) Mo(2) O(8)	105.2(8)	N(1) Cu(5) N(3)	94.7(8)
O(10) Mo(2) O(1)	99.9(7)	N(2) Cu(5) N(4)	94.8(7)
O(8) Mo(2) O(1)	103.7(6)	N(1) Cu(5) N(4)	176.1(8)
O(10) Mo(2) O(7)	95.0(7)	N(3) Cu(5) N(4)	85.4(7)
O(8) Mo(2) O(7)	99.7(6)	Mo(2) O(1) Mo(4)	116.9(7)
O(1) Mo(2) O(7)	147.7(6)	Mo(3) O(2) Mo(4)	120.7(8)
O(10) Mo(2) O(5)	98.3(6)	Mo(1) O(3) Mo(2)	116.8(7)
O(8) Mo(2) O(5)	155.6(6)	Mo(1) O(4) Mo(4)	122.8(7)
O(1) Mo(2) O(5)	78.4(5)	Mo(1) O(4) Mo(3)	105.3(6)
O(7) Mo(2) O(5)	71.2(5)	Mo(4) O(4) Mo(3)	92.3(4)
O(10) Mo(2) O(3)	167.9(7)	Mo(1) O(5) Mo(2)	109.6(6)
O(8) Mo(2) O(3)	86.2(6)	Mo(1) O(5) Mo(1)	102.0(5)
O(1) Mo(2) O(3)	80.7(6)	Mo(2) O(5) Mo(1)	95.5(4)
O(7) Mo(2) O(3)	78.9(5)	Mo(1) O(5) Mo(4)	156.9(6)
O(5) Mo(2) O(3)	70.0(5)	Mo(2) O(5) Mo(4)	86.7(4)
O(11) Mo(3) O(13)	105.5(8)	Mo(1) O(5) Mo(4)	92.3(4)
O(11) Mo(3) O(2)	113.4(7)	Mo(3) O(7) Mo(2)	141.1(8)
O(13) Mo(3) O(2)	103.8(8)	Mo(3) O(7) Mo(1)	107.6(6)
O(11) Mo(3) O(7)	112.7(7)	Mo(2) O(7) Mo(1)	104.8(6)
O(13) Mo(3) O(7)	100.1(7)	C(3) N(1) Cu(5)	108.6(14)
O(2) Mo(3) O(7)	118.9(7)	C(1) N(2) Cu(5)	110.0(14)
O(11) Mo(3) O(4)	88.1(6)	C(2) N(3) Cu(5)	111.7(13)
O(13) Mo(3) O(4)	166.2(7)	C(4) N(4) Cu(5)	109.3(14)
O(2) Mo(3) O(4)	72.4(6)	C(3) C(1) N(2)	107(2)
O(7) Mo(3) O(4)	71.5(5)	N(3) C(2) C(4)	109(2)
O(12) Mo(4) O(14)	106.3(9)	C(1) C(3) N(1)	109.3(18)
O(12) Mo(4) O(1)	98.4(7)	N(4) C(4) C(2)	109(2)

Table 4.9. Atomic coordinates and equivalent isotropic thermal parameters for $[Cu(en)_2]_2[Mo_8O_{26}]$

Atom	x	y	z	Ueq
Mo1	0.44546(11)	0.02659(11)	0.58779(9)	0.0216(4)
Mo2	0.64780(12)	-0.11139(11)	0.58314(10)	0.0232(4)
Mo3	0.52790(12)	0.22687(11)	0.54600(9)	0.0249(4)
Mo4	0.69553(12)	0.09066(12)	0.61414(11)	0.0289(4)
Cu5	0.60755(18)	0.32913(18)	0.34215(15)	0.0308(6)
O1	0.6768(9)	-0.0229(9)	0.6570(8)	0.026(3)
O2	0.6566(11)	0.1901(10)	0.5483(9)	0.037(3)
O3	0.4866(10)	-0.0729(10)	0.6192(9)	0.034(3)
O4	0.5352(9)	0.1035(9)	0.6305(8)	0.026(3)
O5	0.3997(9)	-0.0062(8)	0.4852(7)	0.022(3)
O6	0.3428(10)	0.0454(10)	0.6418(8)	0.031(3)
O7	0.4274(10)	0.1484(9)	0.5137(8)	0.029(3)
O8	0.6312(11)	-0.2000(9)	0.6421(8)	0.031(3)
O10	0.7597(10)	-0.1244(10)	0.5415(9)	0.036(3)
O11	0.4952(12)	0.2856(11)	0.6278(8)	0.036(4)
O12	0.7990(11)	0.0719(12)	0.5615(11)	0.049(4)
O13	0.5250(12)	0.2966(13)	0.4683(10)	0.048(4)
O14	0.7317(13)	0.1400(11)	0.6999(9)	0.047(4)
N1	0.5885(12)	0.2181(12)	0.2853(10)	0.031(4)
N2	0.7365(13)	0.2787(13)	0.3774(12)	0.039(4)
N3	0.4796(12)	0.3799(12)	0.3048(11)	0.035(4)
N4	0.6317(14)	0.4452(14)	0.3934(12)	0.041(5)
C1	0.7409(19)	0.1846(16)	0.3552(15)	0.045(6)
C2	0.4774(16)	0.4736(17)	0.3158(14)	0.041(6)
C3	0.6858(19)	0.1743(18)	0.2787(13)	0.047(6)
C4	0.5367(18)	0.496(2)	0.3928(17)	0.058(8)

4.2.2.3. Results and Discussion

There are five common isomers of $[Mo_8O_{26}]^{4-}$; α, β, γ, δ and ε. The isomer structures of octamolybdates differ in number, types and fusion modes of molybdenum polyhedra. Unfortunately, the occurrence of a particular isomer in hydrothermal syntheses is not predictable (Hagrman P.J. et al. 1999). In Table 4.10 polyhedral subunits and a number of oxo-groups and types of octamolybdates are given.

Table 4.10. Summary of selected structural characteristics of octamolybdate isomers (Source: Allis et al. 2004)

Isomer	Example	Polyhedral subunits	Number of oxo-groups and type				
			O_t	μ_2-O	μ_3-O	μ_4-O	μ_5-O
α	$[Cu_2(tpypz)(H_2O)_2Mo_8O_{26}]$	6 octahedra 2 tetrahedra	14	6	6		
β	$[\{Cu(pca)\}_2(Mo_8O_{26})]$	8 octahedra	14	6	4		2
γ	$[Cu(en)_2]_2[Mo_8O_{26}]$	6 octahedra, 2 square pyramids	14	6	4	2	
δ	$(H_3O)(H_3tptz)[Mo_8O_{26}]$	4 octahedra 4 tetrahedra	14	10	2		
ε	$[\{Ni(H_2O)(4,4'\text{-bpy})_2\}_2M0_8O_{26}]$	2 octahedra, 6 square pyramids	16	4	6		

A two dimensional network of $[Cu(en)_2]_2[Mo_8O_{26}]$ is constructed from γ-$[Mo_8O_{26}]^{4-}$ groups linked through $[Cu(en)_2]^{2+}$ groups. Each $[Mo_8O_{26}]^{4-}$ unit makes strong covalent interactions with two $\{Cu(en)_2\}^{2+}$ groups with Cu-O (O13) distances of 2.436 Å. The molybdate substructure of $[Cu(en)_2]_2[Mo_8O_{26}]$ is the γ-isomer of $[Mo_8O_{26}]^{4-}$, which consists of six $\{MoO_6\}$ octahedra (Mo1, Mo2, Mo4) and two $\{MoO_5\}$ square pyramids (Mo3) linked through corner- and edge-sharing interactions. In Figure 4.18 and 4.19 ball and stick and space-filling representations of $[Cu(en)_2]_2[Mo_8O_{26}]$ are shown.

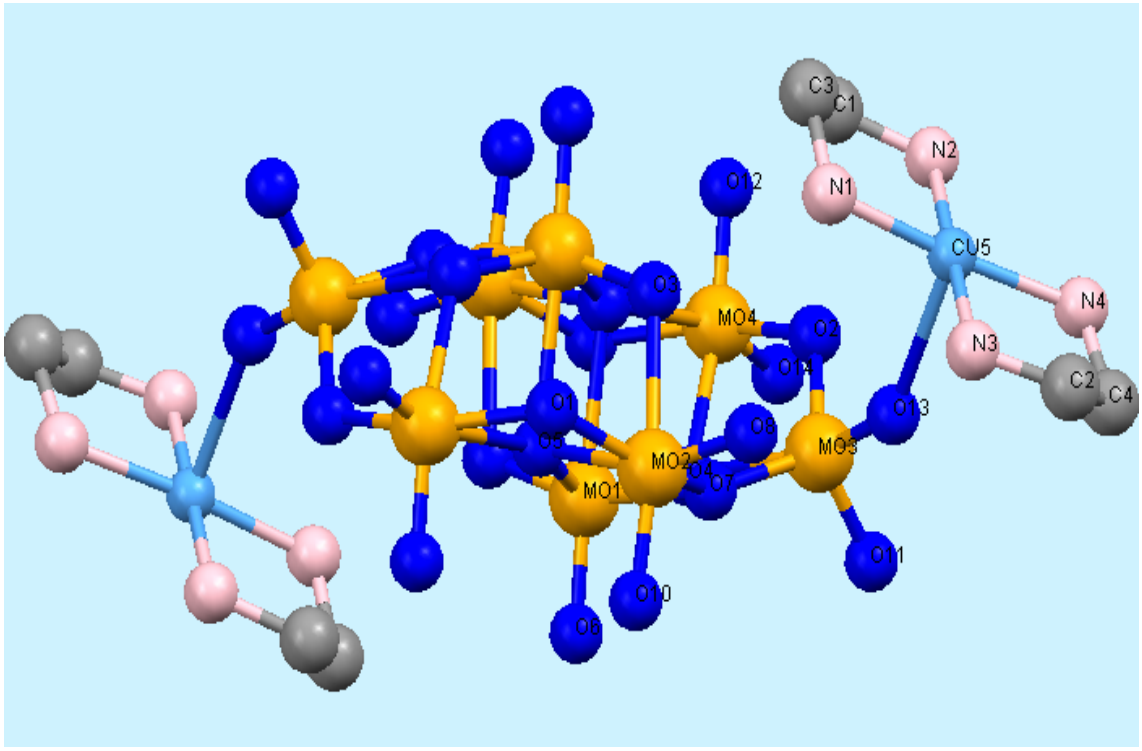

Figure 4.18. Ball and stick representation of $[Cu(en)_2]_2[Mo_8O_{26}]$ through a-axis

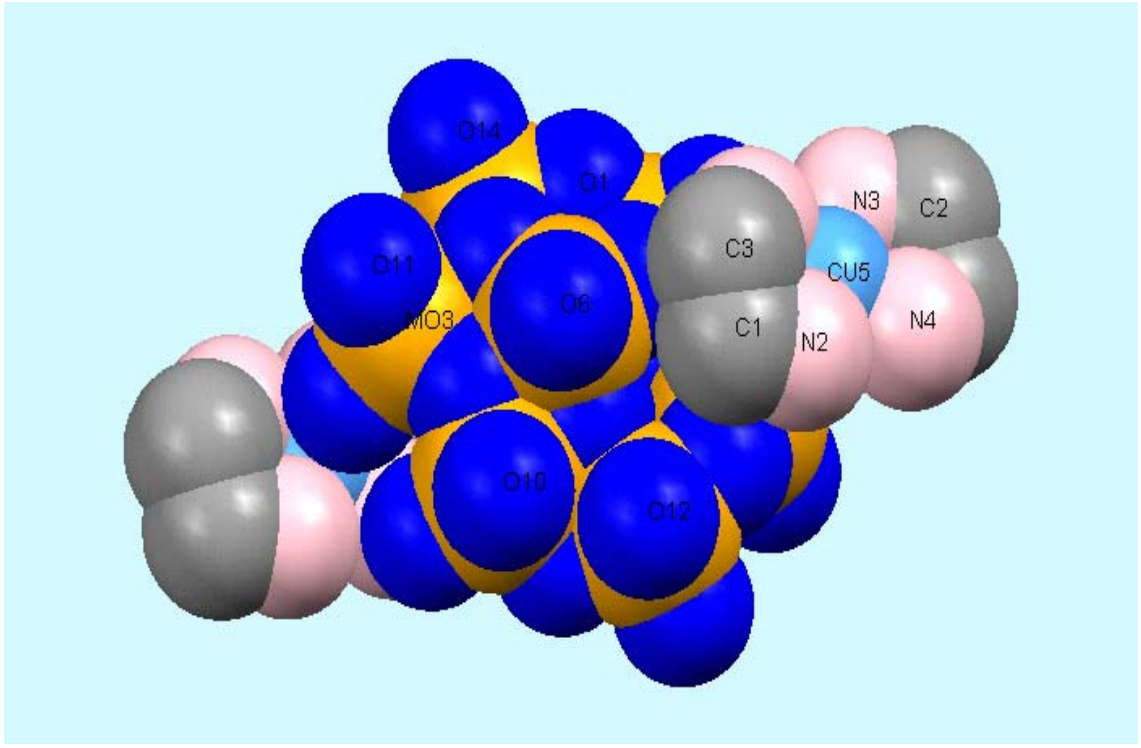

Figure 4.19. Space-filling representation of $[Cu(en)_2]_2[Mo_8O_{26}]$ through a-axis

The Mo-O bonds of each {MoO_6} octahedron (Mo1, Mo2, Mo4) can be divided into three groups depending on the length of the Mo-O bond length: (i) two short Mo-O bonds are between 1.677(13) to 1.726(15) Å; (ii) two medium Mo-O bonds range from 1.846(13) to 1.997(13) Å; (iii) two long Mo-O bonds are in the ranges of 2.194(12)-2.478(13) Å. Each {MoO_5} square pyramid's (Mo3) has 2 short (1.693(17), 1.703(14) Å), two medium (1.832(15), 1.904(13) Å) and one long (2.385(14) Å) Mo-O bond. Terminal Mo-O (O6, O8, O10, O11, O12, O14) bonds are double, bonded having Mo-O bond distances ranging from 1.677 to 1.709 Å. These Mo-O bond lengths are consistent with those in other γ-[Mo_8O_{26}] structures (Niven et al. 1991).

The coordination environment of Cu atom is defined by four nitrogen atoms (N1, N2, N3, N4) from two ethylenediamine ligands with Cu-N distances ranging from 1.988(19) Å to 2.02(2) Å and one oxygen atom(O13) from Mo3 square pyramid with Cu-Mo distance of 2.436 (13) Å. The Cu site of the $[Cu(en)_2]_2[Mo_8O_{26}]$ cluster has only a weak interaction with the adjacent cluster which has a Cu···O distance of 2.98 Å.

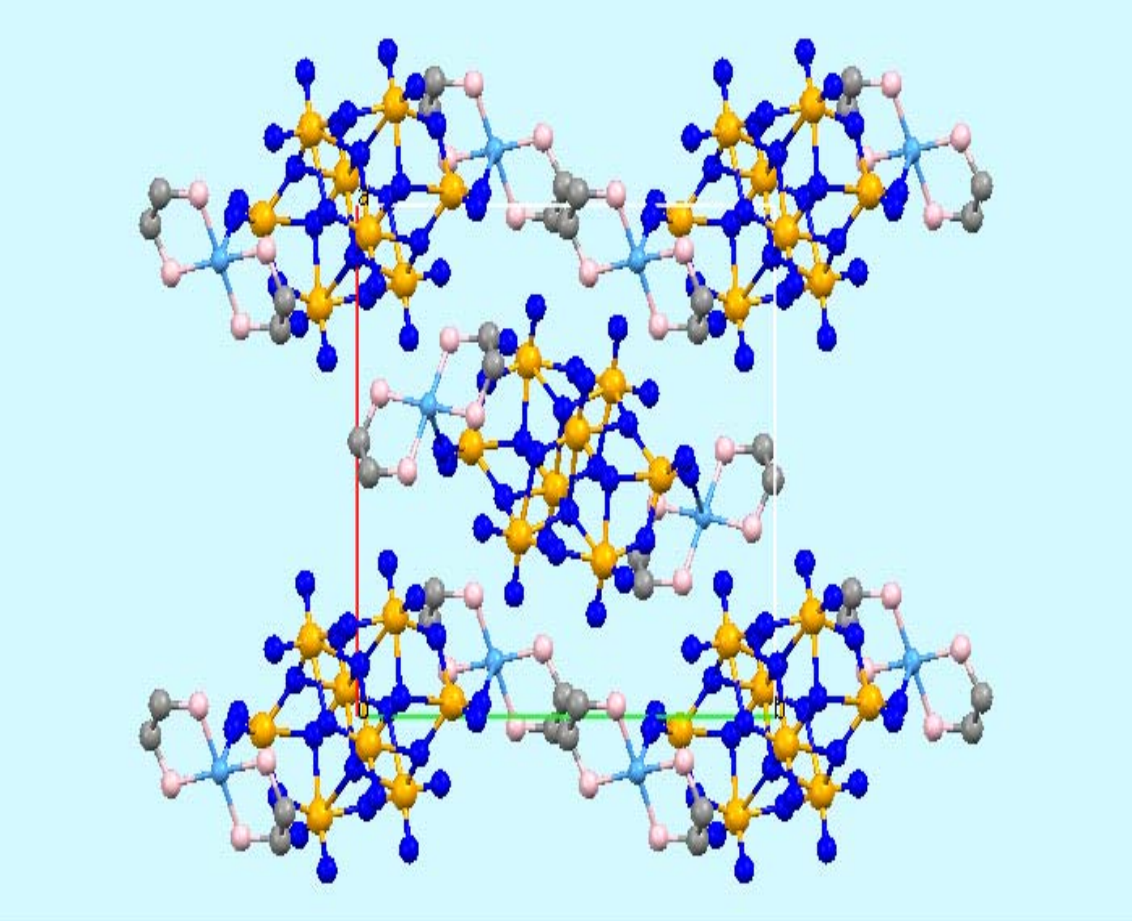

Figure 4.20. Ball and stick representation of two dimensional network through a-axis

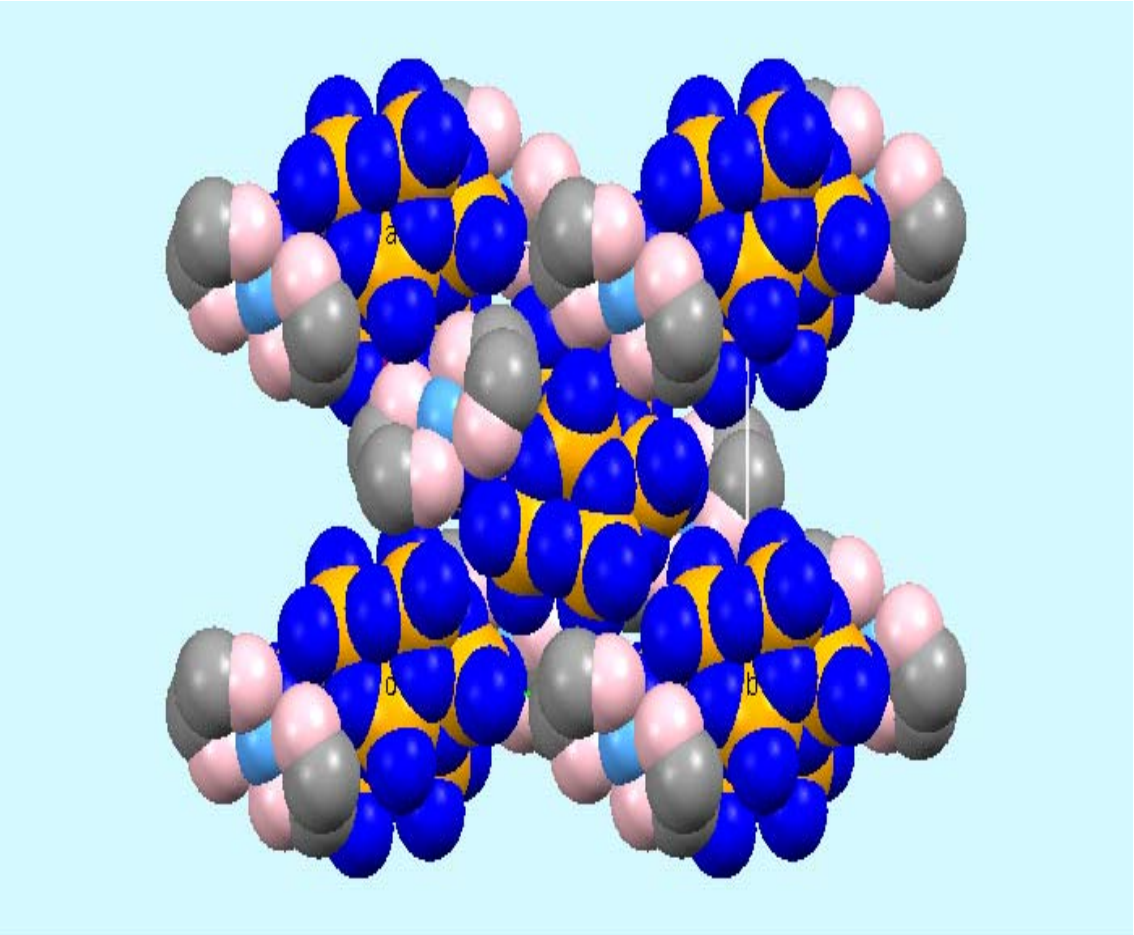

Figure 4.21. Space-filling representation of two dimensional network through a-axis

The +6 oxidation state of the Mo atom is confirmed by bond valance sum calculations ($\sum$ s(M-L) = $\sum$ exp [(r_o-r)/0.37]), where s is defined as the individual bond valance, r_o is the empirically derived single M-L bond distance (r_o=1.907(2) Å for Mo^{6+}-O bond) (Brown and Altermatt 1985), and r represents the bond distances in the structure (Mo-O bond length from Table 4.3). The results showed that the s values for Mo(1), Mo(2), Mo(3), and Mo(4) atoms were 6.285, 6.106, 6.027, and 6.096, respectively. The average value for the calculated oxidation state of Mo atom was 6.129, consistent with the formula of the title compound acquired from X-ray analysis.

The +2 oxidation state of the Cu atom is also confirmed by valance sum calculations. Here r_o=1.679(2) Å for Cu^{2+}-O bond and 1.747 Å for Cu^{2+}-N bond. The s value for the Cu atom is 2.119, consistent with the formula of the compound.

4.2.3. Some Other Synthesized Molybdenum Compounds

Three unidentified molybdenum containing organic-inorganic hybrid compounds, whose structures are not known yet, were synthesized at 170°C for three days. These are green rod-like crystals, black hexagonal shaped crystals and yellow rod-like crystals.

4.2.3.1. Green Rod-like Crystals

A mixture of $(NH_4)_6Mo_7O_{24}\cdot 4H_2O$ (0.1 mmol, 0.1236 g.), $CuCl_2\cdot 2H_2O$ (0.1 mmol, 0.0170 g.), $H_2C_2O_4\cdot 2H_2O$ (0.1 mmol, 0.0126 g.), and H_2O (444 mol, 8 mL) in the mol ratio 1:1:1:4444 was placed in a Teflon-lined acid digestion bomb and heated at 170°C for 72 hours. After slow cooling to room temperature green rod-like crystals were isolated in approximately 90% yield.

$$(NH_4)_6Mo_7O_{24}\cdot 4H_2O + CuCl_2\cdot 2H_2O + H_2C_2O_4\cdot 2H_2O + H_2O \xrightarrow[3\ \text{days}]{170^\circ C} \text{green rod-like crystals}$$

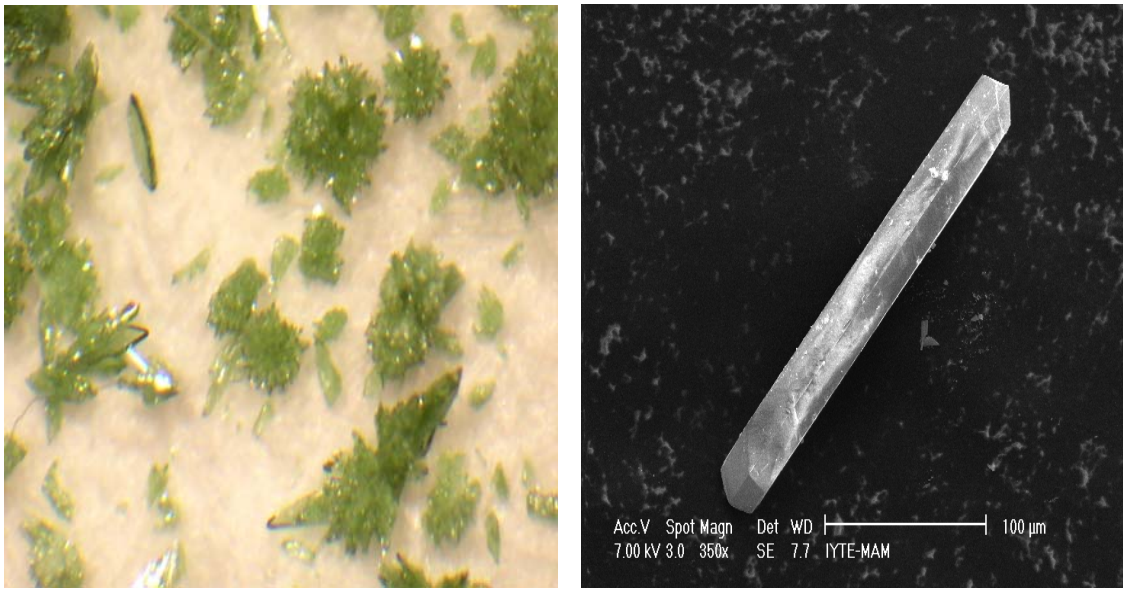

Figure 4.22. Stereomicroscope and SEM images of green rod-like crystals

The SEM EDX results of the green rod-like crystals is illustrated in Figure 4.23 and their X-ray powder pattern which did not match with any compound in the XRD powder database is illustrated in Figure 4.24. SEM/EDX results indicate that the compound includes molybdenum, copper, oxygen, carbon, and nitrogen.

Table 4.11. EDX results of green rod-like crystals

Element	**Weight %**	**Atomic %**
Molybdenum	30.70	9.55
Copper	30.67	14.40
Carbon	5.33	13.24
Nitrogen	3.77	8.02
Oxygen	29.27	54.58

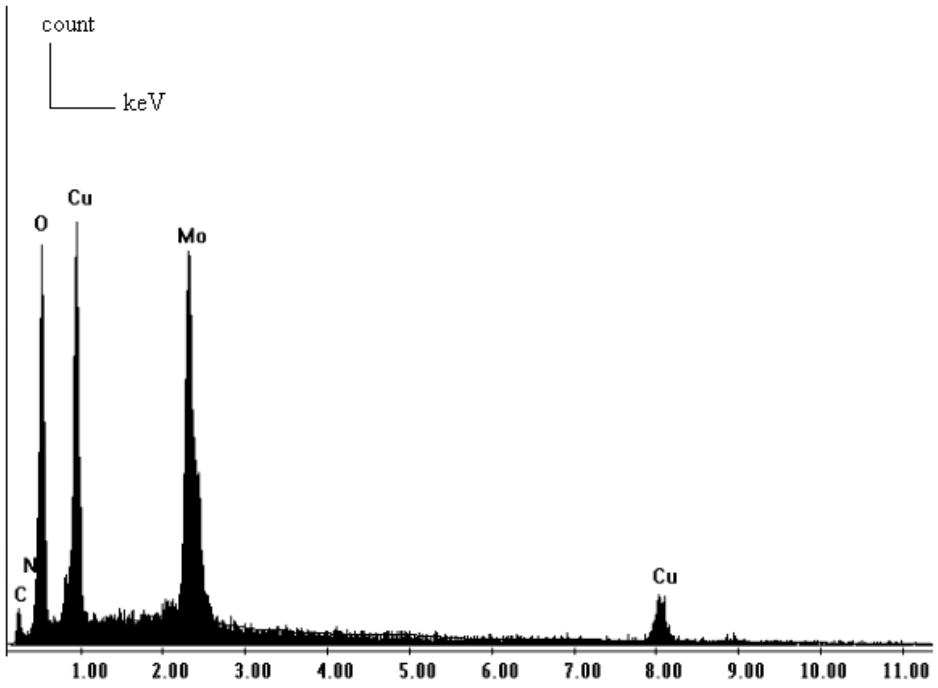

Figure 4.23. SEM EDX peaks of green rod-like crystals

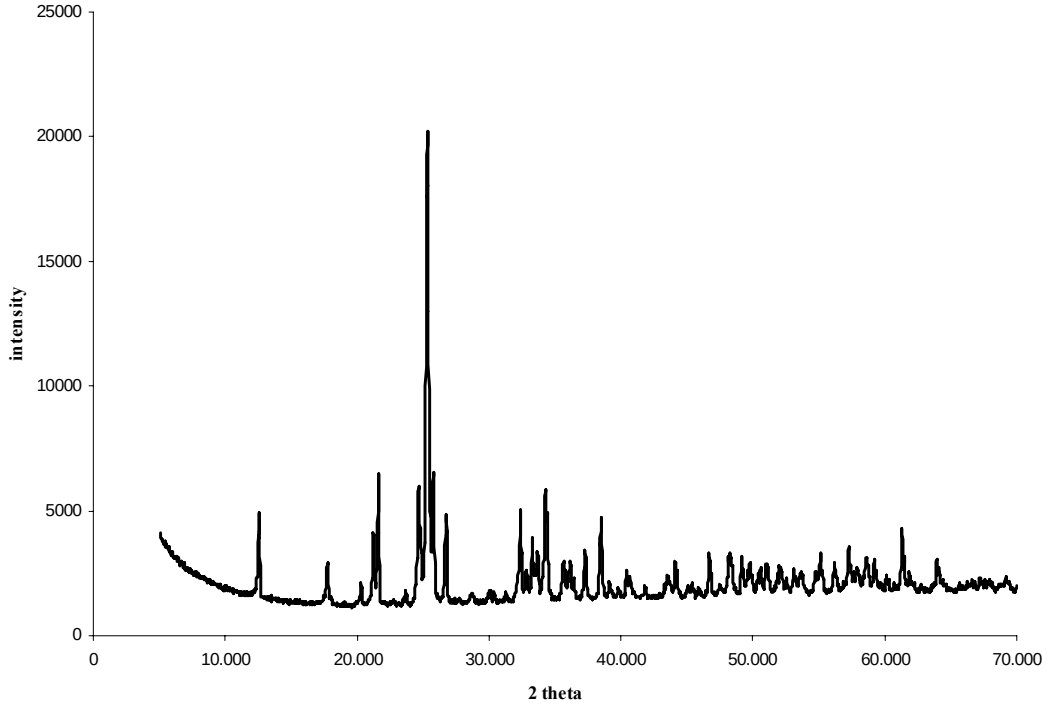

Figure 4.24. Powder patterns of green rod-like crystals

Similar reactions were tried with different reactant ratios, such as 1:1:10:4444. For this reaction the only change was in the ratio of the $H_2C_2O_4 \cdot 2H_2O$ used. When we increased the ratio of $H_2C_2O_4 \cdot 2H_2O$ from 1 to 10, we obtained black hexagonal shaped crystals instead of green rod-like crystals.

4.2.3.2. Black Hexagonal Shaped Crystals

The reaction of $(NH_4)_6Mo_7O_{24} \cdot 4H_2O$ (0.1 mmol, 0.1236 g.), $CuCl_2 \cdot 2H_2O$ (0.1 mmol, 0.0170 g.), $H_2C_2O_4 \cdot 2H_2O$ (1 mmol, 0.126 g.), and H_2O (444 mol, 8 mL) in the mol ratio 1:1:10:4444 at 170°C for 72 hours yielded black hexagonal shaped crystals in approximately 90% yield.

$$(NH_4)_6Mo_7O_{24} \cdot 4H_2O + CuCl_2 \cdot 2H_2O + H_2C_2O_4 \cdot 2H_2O + H_2O \xrightarrow[3\ \text{days}]{170^\circ C} \text{black hexagonal shaped crystals}$$

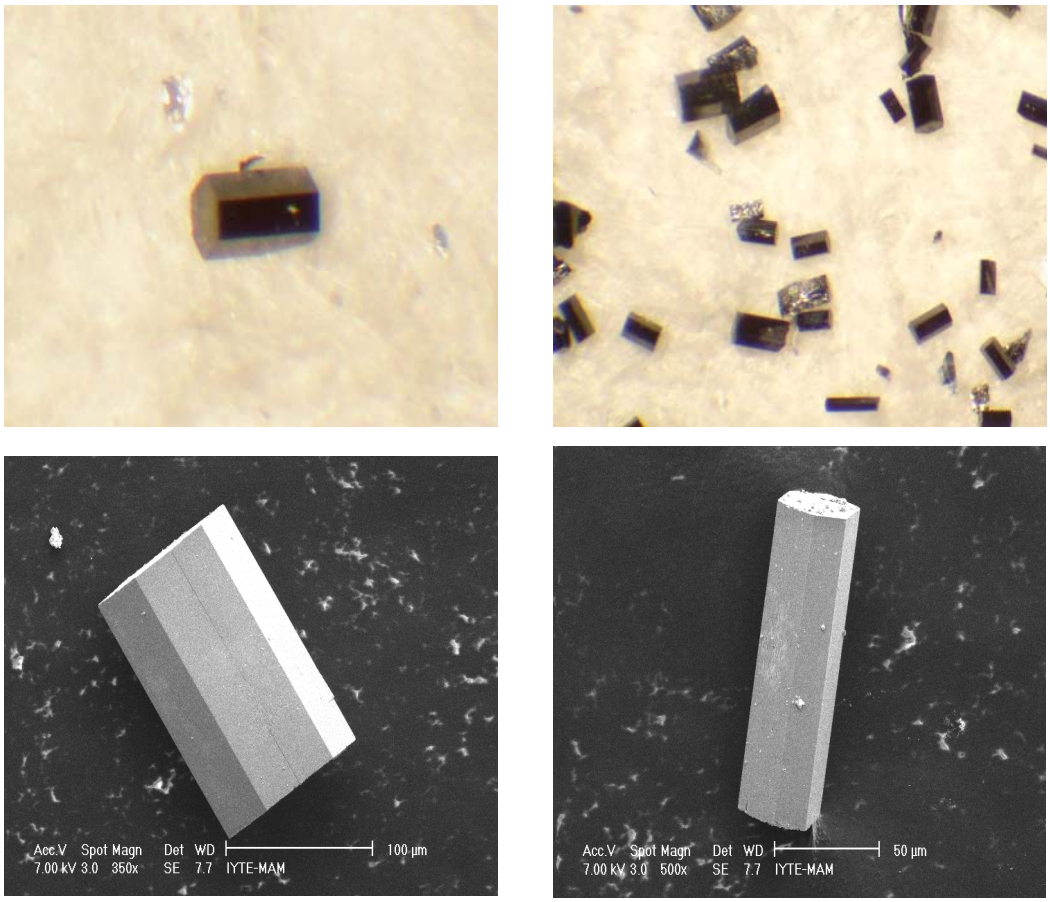

Figure 4.25. Stereomicroscope and SEM images of black hexagonal shaped crystals

The SEM/EDX results of the black hexagonal shaped crystals are shown in Figure 4.26 and their X-ray powder pattern which did not match with any compound in the XRD powder database is illustrated in Figure 4.27. SEM/EDX results indicate that the compound includes molybdenum, oxygen, carbon, and nitrogen.

Table 4.12. EDX results of black hexagonal crystals

Element	**Weight %**	**Atomic %**
Molybdenum	55.07	16.43
Oxygen	29.56	52.89
Carbon	8.32	19.82
Nitrogen	4.75	9.70

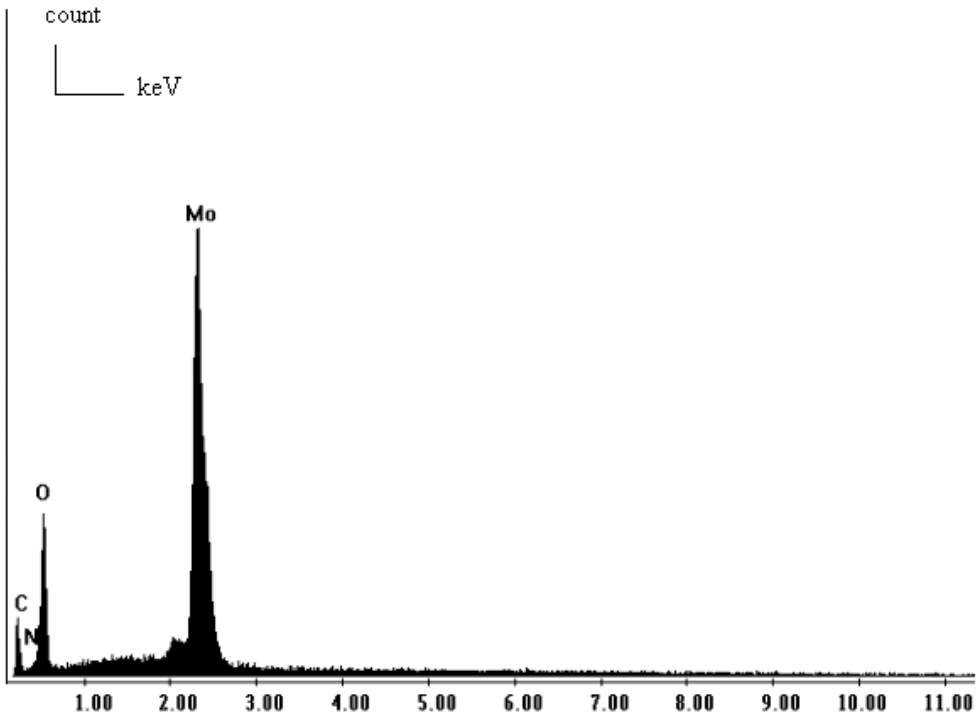

Figure 4.26. SEM EDX peaks of black hexagonal crystals

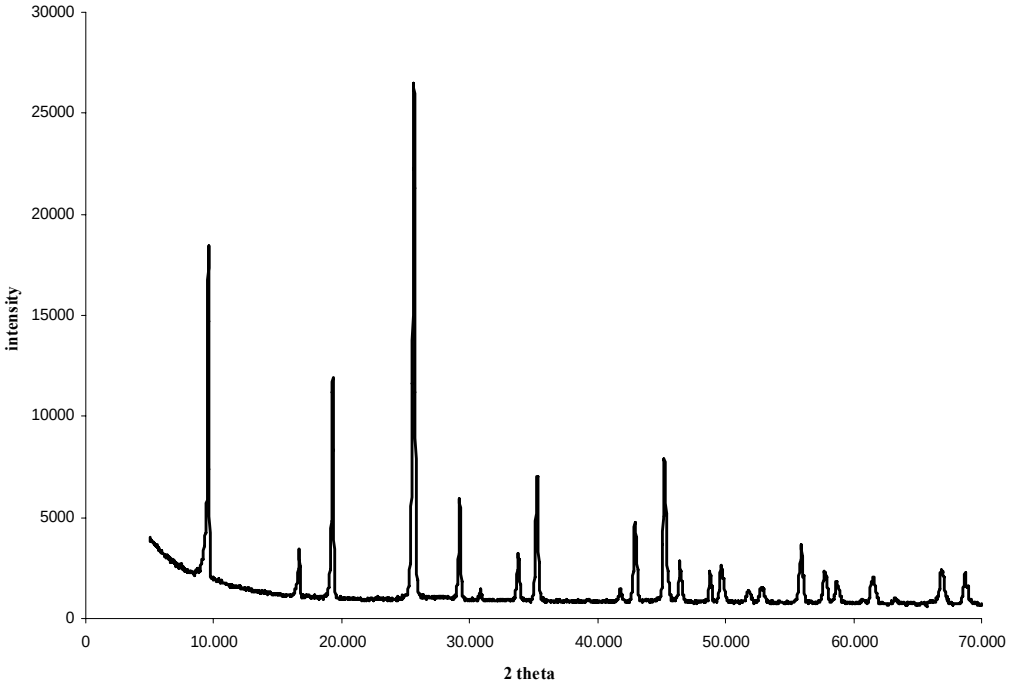

Figure 4.27. Powder patterns of black hexagonal crystals

These two reactions, which produce green rod-like crystals and black hexagonal shaped crystals, are good examples of the effect of mol ratios of the reactants on the reaction products. Interestingly by simply increasing the mol ratio of $H_2C_2O_4 \cdot 2H_2O$ from 1 to 10 different types of products with different colors, shapes and elements were obtained.

4.2.3.3. Yellow Rod-like Crystals

A mixture of $(NH_4)_6Mo_7O_{24} \cdot 4H_2O$ (0.5 mmol, 0.1236 g.), KVO_3 (1 mmol, 0.1380 g.), $Zn(C_2H_3O_2)_2$ (1 mmol, 0.1835 g.), NaCl (1 mmol, 0.0584) and ethylenediamine (1.5 mmol, 0.1 mL) in H_2O (333 mmol, 6 mL) in the mol ratio 1:2:2:2:3:666 was placed in a Teflon-lined acid digestion bomb and heated at 170°C for 72 hours. After the reaction solution was cooled to room temperature yellow rod-like crystals were obtained.

$$(NH_4)_6Mo_7O_{24} \cdot 4H_2O + KVO_3 + Zn(C_2H_3O_2)_2 + NaCl + en + H_2O \xrightarrow[3\ days]{170°C} \text{yellow rod-like crystals}$$

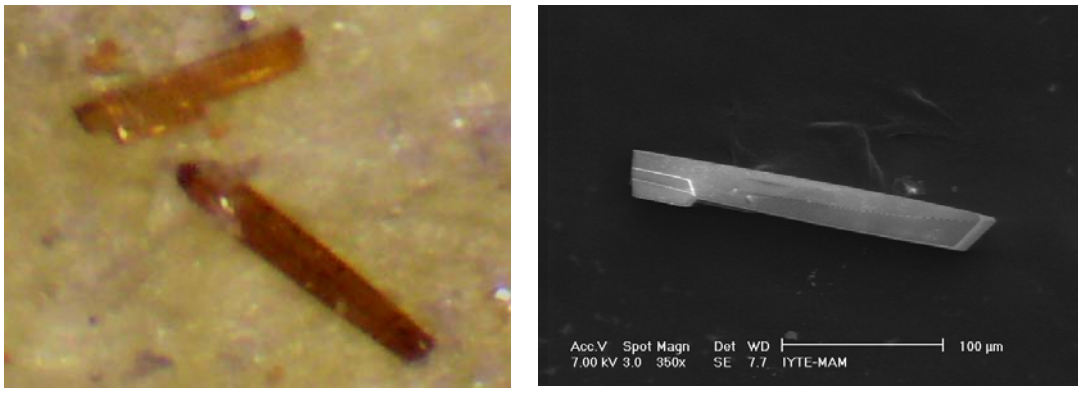

Figure 4.28. Stereomicroscope and SEM images of the yellow rod-like crystal

The SEM/EDX results of the green rod-like crystals are shown in Figure 4.29. Accordingly the compound contains molybdenum, vanadium, oxygen, carbon, and nitrogen.

Table 4.13. EDX results of yellow rod-like crystals

Element	Weight %	Atomic %
Molybdenum	32.39	7.77
Vanadium	12.19	5.51
Carbon	15.65	29.99
Nitrogen	10.08	16.56
Oxygen	26.78	38.53

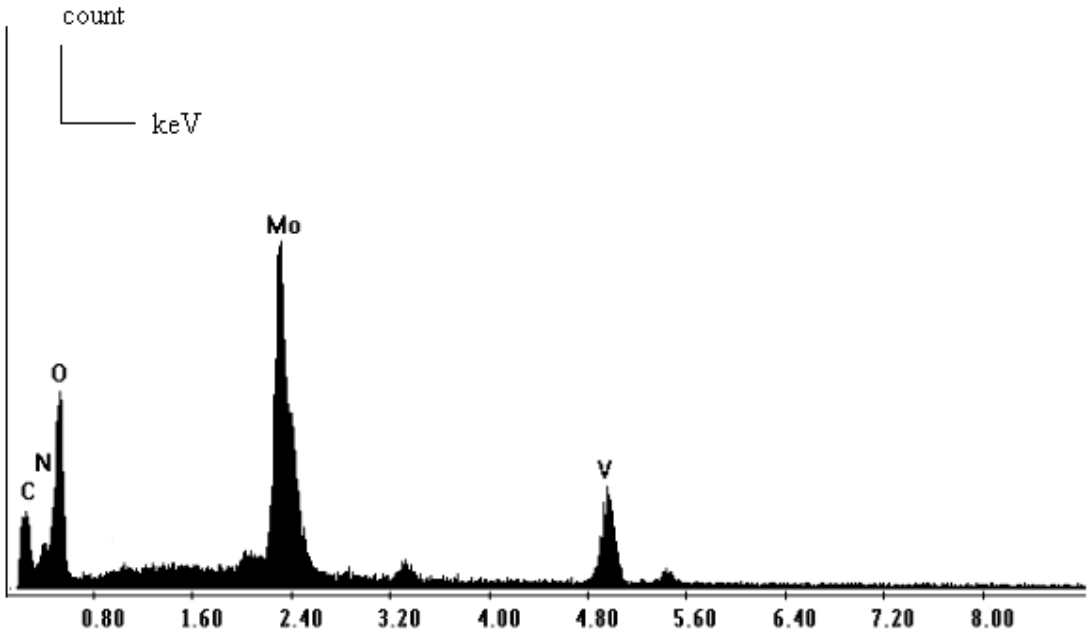

Figure 4.29. SEM EDX peaks of yellow rod-like crystals

CHAPTER 5

CONCLUSION

Recently, the synthesis and characterization of organic-inorganic solid state hybrid materials has attracted great attention due to their chemistry and widely promising potential applications in chemistry, biology and material science (Luo et al. 2003). Recent studies have proven that the hydrothermal synthesis method provides a powerful tool for the synthesis of such materials (Wu et al. 2002).

Our research has focused on the hydrothermal synthesis and structural elucidation of single crystals of copper and molybdenum containing organic-inorganic hybrid compounds. In the literature various types of organodiamine ligands have been introduced into the copper molybdate family, such as 3,3'-bipyridine (3,3'-bpy), 4,4'-bipyridine (4,4'-bpy), 3,4'-bipyridine (3,4'-bpy), o-phenanthroline (o-phen), 1,2-trans-(4-pyridyl)ethene (dpe), bipyridylamine (bpa), and pyrazine (pyz). Ethylenediamine (en) is rarely used as an organic component in the copper molybdate family. To the best of our knowledge $[Cu(en)_2]_2[Mo_8O_{26}]$ (DeBord et al. 1997) is the only reported example which has also been synthesized in our laboratory, and in this study the second example of the ethylenediamine containing layered copper molybdate, $[Cu(en)MoO_4]$, is also reported.

Blue rod-like crystals of a novel organic-inorganic hybrid material, $[Cu(en)MoO_4]$, was synthesized by the hydrothermal method. A solution of $Na_2MoO_4 \cdot 2H_2O$, $CuCl_2 \cdot 2H_2O$, NaCl, ethylenediamine and water in the mol ratio of 1:2:1:3:500 was heated at 170°C for 72 h in a 23 mL Teflon-lined stainless steel autoclave. The compound crystallizes in the space group P2(1)/c of the monoclinic system with four formula units in a cell of dimensions a = 7.6743(15) Å, b = 9.4364(19) Å, c = 9.9538(2) Å, β = 72.266(3)° (T = 293 K), V = 686.6(2) $Å^3$. The structure is composed of layers constructed from $\{MoO_4\}$ tetrahedra and $\{CuN_2O_4\}$ octahedra, with the ethylenediamine ligand coordinated to the Cu atom. Each pair of copper octahedra forms a binuclear edge-sharing unit through a $\{Cu_2O_2\}$ interaction. The binuclear octahedral units are interconnected through the bridging $\{MoO_4\}$ tetrahedra into a layered structure. Layered inorganic oxides are an important subclass of solids due to

their potential applications as ion exchange, ionic conductors and catalysts (Murph et al. 1987). This compound is isostructural to $[Co(en)MoO_4]$ reported by Lin, B.Z (Lin 2002).

A known organic-inorganic hybrid compound of the copper molybdate family, $[Cu(en)_2]_2[Mo_8O_{26}]$, was also synthesized. It has been synthesized by DeBord et al. with different starting materials in 1997 (DeBord et al. 1997). In our study a solution of $Na_2MoO_4{\cdot}2H_2O$, $CuCl_2{\cdot}2H_2O$, NH_4Cl, ethylenediamine and water in the mol ratio of 1:2:1:3:500 was heated at 170°C for 72 h in a 23 mL Teflon-lined stainless steel autoclave. The purple crystals of $[Cu(en)_2]_2[Mo_8O_{26}]$ crystallize in the space group Pbca of the orthorhombic system with eight formula units in a cell of dimensions a = 13.516(3) Å, b = 15.548(3) Å, c = 16.725(3) Å (T = 293 K), V = 3514.7(12) $Å^3$. The structure is composed of γ-$[Mo_8O_{26}]^{4-}$ linked through $[Cu(en)_2]^{2+}$ groups. Each γ-$[Mo_8O_{26}]^{4-}$ unit forms strong covalent interactions with two $[Cu(en)_2]^{2+}$ units. In contrast, there is only a weak interaction between the copper atoms of a given $[Cu(en)_2]_2[Mo_8O_{26}]$ cluster and its neighboring clusters.

Three molybdenum containing organic-inorganic solid state hybrid materials, whose structures are not known yet, were also synthesized at 170°C for three days. Green rod-like single crystals were obtained by the reaction of $(NH_4)_6Mo_7O_{24}{\cdot}4H_2O$, $CuCl_2{\cdot}2H_2O$, $H_2C_2O_4{\cdot}2H_2O$ and H_2O in the mole ratio 1:1:1:4444. According to SEM/EDX results the compound includes molybdenum, copper, oxygen, carbon, and nitrogen atoms in the atomic percentages of 9.55%, 14.40%, 13.24%, 8.02% and 54.58%, respectively.

Black hexagonal shaped crystals formed from the reaction of $(NH_4)_6Mo_7O_{24}{\cdot}4H_2O$, $CuCl_2{\cdot}2H_2O$, $H_2C_2O_4{\cdot}2H_2O$ and H_2O in the mol ratio 1:1:10:4444. SEM/EDX results show that this compound has molybdenum, oxygen, carbon, and nitrogen atoms in the atomic percentages of 16.43%, 52.89%, 19.82% and 9.70%, respectively.

The reaction of $(NH_4)_6Mo_7O_{24}{\cdot}4H_2O$, KVO_3, $Zn(C_2H_3O_2)_2$, NaCl, and ethylenediamine in H_2O in the mol ratio 1:2:2:2:3:666 yielded yellow rod-like crystals. According to the SEM/EDX results, the compound includes molybdenum, vanadium, oxygen, carbon, and nitrogen in the atomic percentages of 7.77%, 5.51%, 29.99%, 16.56% and 38.53%, respectively.

Hydrothermal synthesis has proven to be a powerful method for synthesizing novel copper and molybdenum containing organic-inorganic solid state hybrid

materials. After performing hundreds of reactions, one novel and one known compound were synthesized and their structures were solved and three unidentified compounds were synthesized. By taking the advantage of introducing suitable organic ligands in the synthesis of copper and molybdenum containing organic-inorganic hybrid materials, more and more interesting novel materials may be obtained and studied.

REFERENCES

Allis, D.G., Rarig, R.S., Burkholder, E., and Zubieta, J. 2004. "A Three-Dimensional Bimetallic Oxide Constructed From Octamolybdate Clusters and Copper–Ligand Cation Polymer Subunits. A Comment on the Stability of the Octamolybdate Isomers", *Journal of Molecular Structure*. Vol. 688, pp. 11–31.

Baker, L.C.W. and Glick D.C. 1998. "Present General Status of Understanding of Heteropoly Electrolytes and a Tracing of Some Major Highlights in the History of Their Elucidation", *Chem. Rev*. Vol. 98, pp. 3-49.

Bardin, B.B., Bordawekar, S.V., Neurock, M. and Davis, R.J. 1998. "Acidity of Keggin-Type Heteropolycompounds Evaluated by Catalytic Probe Reactions, Sorption Microcalorimetry, and Density Functional Quantum Chemical Calculations", *J. Phys. Chem*. B Vol.102, pp. 10817-10825.

Barrer, R.M., 1982. *Hydrothermal Chemistry of Zeolites*, (Academic Press, New York).

Brinker, C.J. and Scherer, G.W., 1990. *Sol-Gel Science: The Physics and Chemistry of Sol-Gel Processing*, (Academic, Boston).

Brisdon, A.K., 1998. *Inorganic Spectroscopic Methods*, (Oxford University Press, New York), pp. 10-57.

Brown, G.M., Noe-Spirlet, M.R., Bushing, W.R. and Levy, H.A. 1977. "Dodecatungstophosphoric Acid Hexahydrate, $(H_5O_2^+)_3(PW_{12}O_{40}^{3-})$. The True Structure of Keggin's `Pentahydrate' from Single-Crystal X-ray and Neutron Diffraction Data", *Acta Cryst*. Vol. B33, p. 1038-1046.

Brown, I.D., and Altermatt, D. 1985. "Bond-Valance Parameters Obtained from a Systematic Analysis of the Inorganic Crystal Structure Database", *Acta Cryst*. Vol. B41, pp. 244-247.

Byrappa, K. and Yoshimura, M., 2001. *Handbook of Hydrothermal Technology, A Technology for Crystal Growth and Material Processing*, (Noyes, New Jersey) pp. 1-13.

Chesnut, D.J., Hagrman, D., Zapf, P.J., Hammond, R.P., LaDuca, R., Haushalter, R.C., and Zubieta J. 1999. "Organic/Inorganic Composite Materials: The Roles of Organoamine Ligands in the Design of Inorganic Solids", *Coordination Chemistry Reviews*. Vol.190–192, pp. 737–769.

Cui, X.B., Lü, K., Fana, Y., Xua, J.Q., Yeb, L., Suna, Y.H., Lia, Y., Yua, H.H., and Yi, Z.H. 2005. "A Novel γ-Octamolybdate Supported Transition Metal Complex $[Cu(im)_2]_4[\gamma\text{-}Mo_8O_{26}]$", *Journal of Molecular Structure*. Vol. 743, pp. 151-155.

DeBord, J.R.D., Haushalter, R.C., Meyer, L.M., Rose, D.J., Zapf, P.J., and Zubieta, J. 1997. "New Solids from Old Clusters: Syntheses and Structures of $[Cu(en)_2]_2[Mo_80_{26}]$, $[Cu(enMe)_2]_3[V_{15}O_{36}Cl]\cdot 2.5H_2O$ and

$Cs_{0.5}[Ni(en)_2]_3[V_{18}O_{42}C1]\cdot 2en\cdot 6H_2O$", *Inorganica Chimica Acta*. Vol. 256 pp. 165-168.

Dunitz, J.D. 1964. "The Interpretation of Pseudo-Orthorhombic Diffraction Patterns", *Acta. Cryst*. Vol. 17, pp. 1299-1304.

Eanes, M., 2000. *Synthesis and Characterization of Alkali Silver Chalcogenides and Alkali Rare Earth Germanates by Supercritical Fluids*, Doctor of Philosophy, (Clemson University, USA), pp. 14-19.

Fang, R.Q., Zhao, Y.F., and Zhang, X.M. 2006. "Syntheses and Structures of Two Copper–Molybdate Complexes: The 3-D [Cu(4,4'-bpy)(MoO_4)] and 1-D [Cu_2(HDABCO)$_2$($H_2Mo_8O_{27}$)]$\cdot 4H_2O$", *Inorganica Chimica Acta*. Vol. 359 pp. 2023-2028.

Fournier, M., Feumi-Jantou, C., Rabia, C., Herve, G., and Launau, S. 1992. "Polyoxometalates Catalyst Materials: X-ray Thermal Stability Study of Phosphorus-Containing Heteropolyacids $H_{3+x}PM_{12-x}V_xO_{40}\cdot 13\text{-}14H_2O$ (M=Mo,W; x=0-1)", *J. Mater. Chem*. Vol. 2, p. 971.

Goranson, R.W. 1931. "Solubility of Water in Granite Magmas", *Amer. J. Sci*. Vol. 22, pp. 481-502.

Habashi, F., 1994. *Recent Advances in Pressure Leaching Technology, in*: *Proc. First Intl. Conf. Solvothermal Reactions*, (Takamatsu, Japan) pp. 13-16.

Hagrman, D., Hagrman, P., and Zubieta J. 2000. "Polyoxomolybdate Clusters and Copper–Organonitrogen Complexes as Building Blocks for the Construction of Composite Solids", *Inorganica Chimica Acta*. Vol.300–302, pp. 212–224.

Hagrman, D., Haushalter, R.C., and Zubieta, J. 1998c. "Three-Dimensional Organic/Inorganic Hybrid Materials Constructed from One-Dimensional Copper Daimine Coordination Polymers Linked by Bridging Oxoanion Tetrahedra: [Cu(dpe)(MoO_4)] and [Cu(dpe)(SO_4)(H_2O)] (dpe=1,2-*trans*-(4-pyridyl)ethene)", *Chem. Mater*. Vol.10, pp. 361-365.

Hagrman, D., Warren, C.J., Haushalter, R.C., Rarig, R.S., Johnson, K.M., LaDuca, R.L., and Zubieta, J. 1998a. "Structure-Directing Role of Organoamine Ligands in the Self-Assembly of Novel Bimetallic Oxides", *Chem. Mater*. Vol.10, pp. 3294-3297.

Hagrman, D., Warren, C.J., Haushalter, R.C., Seip, C., O'Connor, C.J., Rarig, R.S., Johnson, K.M., LaDuca, R.L., and Zubieta, J. 1998b. "Structure-Directing Role of Organoamine Ligands in the Self-Assembly of Novel Bimetallic Oxides" *Chem. Mater*. Vol.10, p. 3294-3297.

Hagrman, D., Zubieta, C., Rose, D.J., Zubieta, J., and Haushalter, R.C. 1997. "Composite Solids Constructed From One-Dimensional Coordination Polymer Matrices and Molybdenum Oxide Subunits: Polyoxomolybdate Clusters within [{Cu(4,4'-bpy)}$_4Mo_8O_{26}$] and [{Ni(H_2O)$_2$(4,4'-bpy)$_2$}$_2Mo_8O_{26}$] and One-

Dimensional Oxide Chains in [{Cu(4,4'-bpy)}$_4$Mo$_{15}$O$_{47}$]·8H$_2$O", *J. Angew. Chem, Int. Ed. Engl*. Vol. 36, pp. 873-876.

Hagrman, P.J., and Zubieta, J. 1999. "Solid-State Coordination Chemistry of Metal Oxides: Hydrothermal Synthesis and Structural Characterization of *o*-Phenanthroline-Ligated Copper- and Zinc-Molybdenum Oxides", *Inorg. Chem*. Vol. 38, pp. 4480-4485.

Hagrman, P.J., and Zubieta, J. 2000. "Solid-State Coordination Chemistry: Influences of {M(terpyridyl)} (M=Fe(III), Cu(II), Ni(II)} Subunits on Molybdenum Oxide Structures", *Inorg. Chem*. Vol. 39, pp. 5218-5224.

Hagrman, P.J., Finn, R.C., and Zubieta, J. 2001. "Molecular Manipulation of Solid State Structure: Influences of Organic Components on Vanadium Oxide Architectures", *Solid State Sciences*. Vol. 3, pp. 745-774.

Hagrman, P.J., Hagrman, D., and Zubieta, J. 1999. "Organic-Inorganic Hybrid Materials: From Simple Coordination Polymers to Organodiamine-Templated Molybdenum Oxides", *Angew. Chem. Int. Ed*. Vol. 38, pp. 2638-2684 .

Hagrman, P.J., LaDuca R.L., Koo, H.J., Rarig R., Haushalter, R.C., Whangbo, M.H., and Zubieta, J. 2000. "Ligand Influences on the Structures of Molybdenum Oxide Networks", *Inorg. Chem*. Vol. 39, pp. 4311-4317.

Han, G.H., Lin, B.Z., Li, Z., Sun, D.Y., and Liu P.D. 2005. "Hydrothermal Synthesis and Characterization of a New Hybrid Organic–Inorganic Compound [Cd(en)$_3$]MoO$_4$", *Journal of Molecular Structure*. Vol. 741, pp. 31-35.

Inoue, M., and Yamase, T. 1995. "Synthesis and Crystal Structures of γ-Type Octamolybdates Coordinated by Chiral Lysines", *Bull. Chem. Soc*. *Jpn*. Vol. 68, pp. 3055-3063.

Izumi, Y. 1997. "Hydration/Hydrolysis by Solid Acids", *Catal. Today*. Vol. 33, pp. 371-409.

Izumi, Y., Urabe, K. and Onaka, M., 1992. *Zeolite, Clay and Heteropoly Acid in Organic Reactions*, (Kodansha/VCH, Tokyo), p. 99.

Jacobson, R.A., 1998. *REQABA: REQABA Empirical Absorption Correction, Version 1.1*, (Molecular Structure Corp., The Woodlands, TX).

Janiak, C. 1997. "Functional Organic Analogues of Zeolites Based on Metal-Organic Coordination Frameworks", *Angew. Chem. Int. Ed. Engl*. Vol. 36, pp. 1431-1434.

Kanatzidis, M.G. 1990. "Molten Alkali-Metal Polychalcogenides as Reagents and Solvents for the Synthesis of New Chalcogenide Materials", *Chem. Mater*. Vol. 2, p. 353.

Katsoulis, D.E. 1998. “A Survey of Applications of Polyoxometalates”, *Chem. Rev*. Vol. 98, pp. 359-387.

Kitamura, A., Ozeki, T., and Yagasaki, A. 1997. “Beta-Octamolybdate as a Building Block. Synthesis and Structural Characterization of Rare Earth Molybdate Adducts”, *Inorg. Chem.* Vol. 36, p. 4275-4279.

Klein, L.C., 1988. *Sol-Gel Technology of Thin Films, Fibers, Preforms, Electronics, and Specialty Shapes*, (Park Ridge, NJ.).

Koo, B.K., Bewley, L., Golub, V., Rarig, R.S., Burkholder, E., O’Connor, C. J., and Zubieta, J. 2003. “Anion Influences on the Construction of One-Dimensional Structures of the Cu(II)-bisterpy Family (bisterpy=2,2’:4’,4’’:2’’,2’’’-quarterpyridyl, 6’,6’’-di-2-pyridiine)”, *Inorganica Chimica Acta*. Vol. 351, pp. 167-176.

Kozhevnikov, I.V., 2002. *Catalysis for Fine Chemical Synthesis- Catalysis by Polyoxometalates*, (John Wiley, New York), p, xiii.

Lin, B.Z. 2002. “Layered (Ethylenediamine-κ^2N,N’)- Cobalt(II) Molybdate(VI)” *Acta Cryst*. Vol. C58, pp. 261-263.

Lu, C.Z., Wu, C.D., Zhuang, H.H., and Huang, J.S. 2002. “Three Polymeric Frameworks Constructed from Discrete Molybdenum Oxide Anions and 4,4’-bpy-Bridged Linear Polymeric Copper Cations”, *Chem. Mater*. Vol. 14, pp. 2649-2655.

Luo, J., Hong, M., Wang, R., Shi, Q., Cao, R., Weng, J., Sun, R., and Zhang, H. 2003. “A novel 1D ladder-like organic–inorganic hybrid compound $[(Cu(bIz)_2)]_2[\{Cu(bIz)_2\}_2Mo_8O_{26}]$ (bIz=benzimidazole)”, *Inorganic Chemistry Communications*, Vol. 6, pp. 702–705.

Mamantov, G. and Marassi, R., 1987. *Molten Salt Chemistry: An Introduction and Selected Applications*, (Reidel, Dorrecht).

Mann, S., Burkett, S.L., Davis, S.A., Fowler, C.E., Mendelson, N.H., Sims, S.D., Walsh, D., and Whilton, N.T. 1997. “Sol-Gel Synthesis of Organized Matter”, *Chem. Mater*. Vol. 9, pp. 2300-2310.

Millange, F., Serre, C., Cabourdin, T., Marrot, J., and Férey G. 2004. “Organically Templated Zinc Selenites: MIL-86 or $[H_2N(CH_2)_2NH_2]_2{\cdot}Zn_4(SeO_3)_4$ and MIL-87 or $[H_3N(CH_2)_3NH_3]_4{\cdot}Zn_4(SeO_3)_8$”, *Solid State Sciences* Vol. 6, pp. 229-233.

Misono, M. 2001. “Unique Acid Catalysis of Heteropoly Compounds (Heteropolyoxometalates) in the Solid State”, *Chem. Commun*. Vol. 13, pp. 1141-1152.

Morey, G.W. and Niggli, P. 1913. “The Hydrothermal Formation of Silicates”, *J. Am. Chem. Soc*. Vol. 35, pp. 1086-1130.

Murph, D.W., Sushire, S.A., and Zahurak, S.M., 1987. *Chemical Physics of Interaction*, Nato ASI Series, Series B:Physics, 172, (Plenum, New York), p. 173.

Nacken, R. 1950. "Hydrothermal Synthese als Grundlage fur Zuchtung Von Quarz-Kristallen", *Chem. Z*. Vol. 74, pp. 745-749.

Niven, M.L., Cruywagen, J.J., and Heyns, J.B.B. 1991. "The First Observation of γ-Octamolybdate: Synthesis, Crystal and Molecular Structure of $[Me_3N(CH_2)_6NMe_3]_2[Mo_8O_{26}]\cdot 2H_2O$", *J. Chem. Soc. Dalton Trans*. Vol. 8, pp. 2007-2011.

Noe-Spirlet, M.R. and Bushing, W.R. 1978. "Dodecatungstophosphoric Acid-21-Water by Neutron Diffraction", *Acta Cryst*. Vol. B34, p. 907-910.

O'Donnell, T.A., 1993, *Superacids and Acidic Melts as Inorganic Chemical Reaction Media*, (VCH, New York).

Okuhara, T., Mizuno, N. and Misono, M. 1996. "Catalytic Chemistry of Heteropoly Compounds", *Adv. Catal*. Vol. 41, pp. 113-252.

Parr Instrument Company, 1999. *Operating Instructions; Parr Acid Digestion Bombs*, (Illinois, USA).

Pauling, L. 1929. "The Molecular Structure of the Tungstosilicates and Related Compounds", *J. Am. Chem. Soc*. Vol. 51, No. 225, pp. 2868-2880.

Pope, M.T., 1983. *Heteropoly and Isopoly Oxometalates* (Springer-Verlang, Berlin).

Pope, M.T. and Müller, A., 2001. *Polyoxometalate Chemistry From Topology via Self-Assembly to Applications*, (Kluwer Academic Publishers, The Netherlands), p. 1.

Rabenau, A. 1985. "The Role of Hydrothermal Synthesis in Preparative Chemistry", *Angew. Chem., Int. Eng. Ed*. Vol. 24, pp. 1026-1040.

Rarig, R.S., Lam, R., Zavalij, P.Y., Ngala, J.K., LaDuca, R.L., Greedan, J.E., and Zubieta, J. 2002. "Ligand Influences on Copper Molybdate Networks: The Structures and Magnetism of $[Cu(3,4'\text{-bpy})MoO_4]$, $[Cu(3,3'\text{-bpy})_{0.5}MoO_4]$, and $[Cu(4,4'\text{-bpy})_{0.5}\ MoO_4]\cdot 1.5H_2O$", *Inorg. Chem*. Vol. 41, pp. 2124-2133.

Rarig, R.S., and Zubieta, J. 2002. "Solid-State Coordination Chemistry of Molybdenum Oxides with di-2-Picolylamine (pca): The Hydrothermal Syntheses and Structures of the Molecular Cluster $[\{Ni(pca)(H_2O)\}_2Mo_8O_{26}]$, the Two-Dimensional $[\{Cu(pca)\}_2Mo_8O_{26}]$, and the One-Dimensional [{Cu3(pca)3MoO4}Mo8O26]", *Journal of Solid State Chemistry*, Vol. 167, pp. 370-375.

Reynolds, P.A. 1975. "A Calculation of the Molecular Orientational Disorder in Crystalline Anthrone", *Acta Cryst*. Vol. A31, pp. 80-83.

Rigaku Corp., 2001. *CRYSTAL CLEAR: Crystal Clear Version 1.3*, (Rigaku/Molecular Structure Corp., The Woodlands, TX).

Rosenheim, A., 1921. *Handbuch der Anorganischen Chemie*, (Hirzel Verlag, Leipzich) Vol. 4, Part. 1, pp. 997-1064.

Roy, R. 1994. "Acceleration the Kinetics of Low-Temperature Inorganic Syntheses", *J. Solid State Chem*. Vol. 111, pp. 11-17.

Schubert, U. and Hüsing, N., 2000. *Synthesis of Inorganic Materials*

Sheldrick, G.M., 1997. *SHELXTL-PLUS, Version 6.10*, Bruker AXS, Siemens Analytical X-Ray Instruments, Inc., Madison, WI).

Skoog, D.A. and Leary, J.J., 1992. *Principles of Instrumental Analysis*, (Saunders College Publishing, New York), pp. 568-579.

Smart, L. and Moore, E., 1996. *Solid State Chemistry - An Introduction*, (Stanley Thornes Ltd.).

Souchay, P., 1969. *Ions Mineraux Condenses*, (Masson, Paris).

Steller, I., Bolotovsky, R., and Rossmann, M.G. 1997. "An Algorithm for Automatic Indexing of Oscillation Images using Fourier Analysis", *J. Appl. Cryst*. Vol. 30 pp. 1036-1040.

Stupp, S.I., and Braun, P.V. 1997. "Molecular Manipulation of Microstructures: Biomaterials, Ceramics, and Semiconductors", *Science*. Vol. 277, pp. 1242-1248.

Tao, J., Zhang, X.M., Tong, M.L., and Chen, X.M. 2001. "A Novel Polycatenated Double-Layered Hybrid Organic–Inorganic Material Constructed from $[Zn_2(tp)(4,4'\text{-bpy})]_n^{2n+}$ Layers and $V_4O_{12}^{4-}$ Pillars", *J. Chem. Soc., Dalton Trans.* Vol. 6, pp. 770-771.

Van der Put, P.J., 1998. *The Inorganic Chemistry of Materials-How to Make Things out of Elements*, (Plenum Press, New York and London), pp. 273-316.

West, A.R., 1996. *Solid State Chemistry and its Applications*, (John Wiley and Sons, New York), pp. 4-115.

Wu, C.D., Lu, C.Z., Zhuang, H.H., and Huang J.S. 2002. "Hybrid Coordination Polymer Constructed from *β*-Octamolybdates Linked by Quinoxaline and Its Oxidized Product Benzimidazole Coordinated to Binuclear Copper(I) Fragments", *Inorg.Chem*. Vol. 41, pp. 5636-5637.

Xi, R., Wang, B., Isobe, K., Nishioka, T., Toriumi, K. and Ozawa, T. 1994. "Isolation and X-ray Crystal Structure of a New Octamolybdate: $[(RhCp^*)_2(\mu_2\text{-}SCH_3)_3]_4[Mo_8O_{26}]\cdot 2CH_3CN$ ($CP^* = \eta^5\text{-}C_5Me_5$)", *Inorg. Chem*. Vol. 33, pp. 833-836.

Yuan, M., Li, Y.G., Wang, E.B., Tian, C.G., Wang, L., Hu, C.W., Hu, N.H., and Jia, H.Q. 2003. "Modified Polyoxometalates: Hydrothermal Syntheses and Crystal Structures of Three Novel Reduced and Capped Keggin Derivatives Decorated by Transition Metal Complexes", *Inorg. Chem*. Vol. 42, pp. 3670-3676.

Zapf, P.J., Haushalter, R.C., and Zubieta, J. 1997c. "Crystal Engineering of Inorganic/Organic Composite Solids: the Structure-Directing Role of Aromatic Ammonium Cations in the Synthesis of the "Step"-Layered Molybdenum Oxide Phase [4,4'-H_2bpy][Mo_7O_{22}]·H_2O", *Chem. Commun*. Vol. 3, pp. 321-322.

Zapf, P.J., LaDuca, R.L., Rarig, R.S., Johnson, K.M., and Zubieta, J. 1998b. "A Two-Dimensional Network Constructed via Hydrogen-Bonded Cross-Linkages of Molybdenum Oxide Chains", *Inorg. Chem*. Vol. 37, pp. 3411-3414.

Zapf, P.J., Hammond, R.P., Haushalter, R.C., and Zubieta, J. 1998a. "Variations on a One-Dimensional Theme: The Hydrothermal Syntheses of Inorganic/Organic Composite Solids of the Iron Molybdate Family", *Chem. Mater*. Vol. 10, pp. 1366-1373.

Zapf, P.J., Haushalter, R.C., and Zubieta, J. 1997a. "Hydrothermal Synthesis and Structural Characterization of a Series of One-Dimensional Organic/Inorganic Hybrid Materials of the [$(MoO_3)_n$(2,2'-bipy)$_m$] Family: [MoO_3(2,2'-bipy)], [Mo_2O_6(2,2'-bipy)], and [Mo_3O_9(2,2'-bipy)$_2$]", *Chem. Mater*. Vol. 9, pp. 2019-2024.

Zapf, P.J., Warren, C.J., Haushalter, R.C., and Zubieta, J. 1997b. "One- and Two-Dimensional Organic–Inorganic Composite Solids Constructed from Molybdenum Oxide Clusters and Chains Linked Through $\{M(2,2'\text{-bpy})\}^{2+}$ Fragments (M = Co, Ni, Cu)", *Chem. Commun*. pp. 1543-1544.